Interfacial structure of phospholipids probed by high-resolution, high-repetition-rate broadband vibrational sum-frequency generation spectroscopy

D i s s e r t a t i o n

zur Erlangung des akademischen Grades

d o c t o r r e r u m n a t u r a l i u m

(Dr. rer. nat.)

im Fach Chemie

Spezialisierung Physikalische und Theoretische Chemie

eingereicht an der

Mathematisch-Naturwissenschaftlichen Fakultät der

Humboldt-Universität zu Berlin

Von

M.Sc. Freeda Yesudas

Präsident (komm.) der Humboldt-Universität zu Berlin

Prof. Dr. Peter Frensch

Dekan der Mathematisch-Naturwissenschaftlichen Fakultät

Prof. Dr. Elmar Kulke

Gutachter/in:
1. Prof. Dr. Janina Kneipp
2. Prof. Dr. Ulrich Panne
3. Prof. Dr. Henrike Mueller-Werkmeister

Tag der mündlichen Prüfung: 16.02.2022

Abstract

The label-free characterization of phospholipids is vital for physics, chemistry, biology, and medicine. Due to their wide range of applications, it is important to broaden our knowledge on the interfacial structure of phospholipids at low surface coverages, their heterogeneous mixtures, and the surrounding water molecules. Broadband vibrational sum-frequency generation (BB-VSFG) spectroscopy is a surface-sensitive tool capable of studying the structure of phospholipids at any interface.

This thesis focuses on the applicability of a state-of-the-art 100 kHz BB-VSFG spectrometer recently developed at the SALSA Photonics Lab and on the analysis of the interfacial structure of alkyl chains, surrounding water, and the phosphate head groups of phospholipid layers. First, multi-component phospholipid bilayers were studied at laser repetition rates of 5, 10, 50, and 100 kHz at constant pulse energy. The BB-VSFG spectra suggest that the phospholipid bilayers were stable during the measurements with no heat-induced distortions. Moreover, an increase in the laser repetition rate provided a feasible route to obtain spectra in short data acquisition times without compromising the signal-to-noise ratio. The extremely short acquisition time of 500 ms, the high spectral resolution, and all applied pulse parameters ensured no thermal induced photodamages occur during the measurements under ambient conditions. A systematic study of one- and two-component phospholipid monolayers as a function of surface tension and mixture ratio at different polarization combinations was performed and the dependence of the vibrational spectra was explored. The structure of alkyl chains and surrounding water was analyzed using the same model systems. Vibrational bands that were previously unseen and spectra of monolayers at low surface coverage were reported for the first time with an unprecedented signal-to-noise ratio. The structure of phospholipid monolayers containing identical head groups and different chains was analyzed and compared. The spectra confirmed the presence of water molecules near the phosphate and choline groups of the phospholipid

monolayers. The order of the phospholipid molecules as a function of the composition of the monolayers was inferred from the spectral data. The influence of the hydration and/or changes in the orientation of the phosphate group was visible from the spectra as well. In summary, the work validates the use of high repetition rate BB-VSFG in the analysis of phospholipids at the air-CaF_2 interface and presents suitable experimental conditions that can be employed for more complex biomolecules. This study provides new insight into the molecular-level understanding of the phospholipid monolayers leading to a more detailed understanding of biological processes at the lipid membrane. Besides, the work presented also opens up great perspectives on the application of 100 kHz VSFG spectroscopy for the chemical and structural analysis of complex biological interfaces.

Kurzzusammenfassung

Die markierungsfreie Charakterisierung von Phospholipiden ist von entscheidender Bedeutung für Physik, Chemie, Biologie und Medizin. Aufgrund ihrer breiten Anwendung ist es wichtig, unser Wissen über die Grenzflächenstruktur von Phospholipiden bei geringen Oberflächenbedeckungen, ihre heterogenen Mischungen und die umgebenden Wassermoleküle zu erweitern. Breitband-Schwingungs-Summenfrequenzspektroskopie (engl. *broadband vibrational sum frequency generation*, BB-VSFG) ist eine oberflächenempfindliche Methode, mit der die Struktur von Phospholipiden an jeder Grenzfläche untersucht werden kann.

Diese Arbeit konzentriert sich auf die Anwendbarkeit eines hochmodernen 100 kHz BB-VSFG-Spektrometers, das kürzlich im SALSA Photonics Lab entwickelt wurde, für die Analyse der Grenzflächenstruktur von Alkylketten, des sie umgebenden Wassers und der Phosphatkopfgruppen von Phospholipidschichten. Zunächst wurden Phospholipid-Doppelschichten, die mehrere Komponenten enthalten, bei Laserwiederholraten von 5, 10, 50 und 100 kHz mit konstanter Pulsenergie untersucht. Die BB-VSFG-Spektren legen nahe, dass die Phospholipid-Doppelschichten während der Messungen ohne wärmeinduzierte Veränderungen stabil waren. Darüber hinaus bot die Erhöhung der Laserwiederholungsrate eine praktikable Möglichkeit, Spektren in kurzen Datenerfassungszeiten zu erhalten, ohne dass das Signal-Rausch-Verhältnis beeinträchtigt wurde. Die extrem kurze Aufnahmezeit von 500 ms, die hohe spektrale Auflösung und alle verwendeten Pulsparameter sorgen dafür, dass bei Messungen unter Umgebungsbedingungen keine thermisch bedingten Photoschäden auftreten. Es wurde eine systematische Untersuchung von ein- und zweikomponentigen Phospholipid-Monoschichten in Abhängigkeit von der Oberflächenspannung und dem Mischungsverhältnis für verschiedene Kombinationen an Polarisationen durchgeführt und die Abhängigkeit der Schwingungsspektren untersucht. Die Struktur von Alkylketten und umgebendem Wasser

wurde anhand derselben Modellsystemen analysiert. Bislang nicht beobachtete Schwingungsbanden und Spektren von Monolagen mit geringer Oberflächenbedeckung wurden mit einem bisher nicht erreichten Signal-Rausch-Verhältnis gemessen und beschrieben. Die Struktur von Phospholipid-Monolagen mit identischen Kopfgruppen und unterschiedlichen Ketten wurde analysiert und verglichen. Die Spektren bestätigten die Anwesenheit von Wassermolekülen in der Nähe der Phosphat- und Cholingruppen der Phospholipid-Monolagen. Aus den Daten kann der Ordnungsgrad der Phospholipidmoleküle in Abhängigkeit von der Zusammensetzung der Monolagen abgeleitet werden. Der Einfluss von Hydratation und/oder Orientierungsänderungen auf die Phosphatgruppe war aus den Spektren ebenfalls ersichtlich.

Zusammenfassend kann gesagt werden, dass die Arbeit die Verwendung von BB-VSFG mit hoher Wiederholrate bei der Analyse von Phospholipiden an der Luft-CaF_2-Grenzfläche validiert und geeignete experimentelle Bedingungen, die auch für komplexere Biomoleküle verwendet werden können, vorstellt. Die Dissertation liefert neue Einblicke in das Verständnis von Phospholipid-Monolagen auf molekularer Ebene, was zu einem detaillierteren Verständnis biologischer Prozesse an der Lipidmembran beitragen wird. Darüber hinaus eröffnet die vorgestellte Arbeit auch große Perspektiven für die Anwendung der 100 kHz VSFG-Spektroskopie zur chemischen und strukturellen Analyse komplexer biologischer Grenzflächen.

Table of Contents

1. Introduction

Phospholipids exist as monolayers in the interfacial alveolar region of lungs or tear films. The monolayers present at the air-water interface of the lungs are so-called pulmonary surfactants. They are heterogeneous mixtures of 90 wt% lipids and 10 wt% proteins. The composition of pulmonary surfactants is shown in Figure 1.1. The two main components of these pulmonary surfactants include saturated (~50%) and unsaturated (~20%) phosphatidylcholines (PC) [1]. Other lipids, ~5–10%, such as cholesterol, phosphatidylethanolamine (PE), fatty acids, and lysolipids are also present in small quantities. These phospholipids have important roles in maintaining the structure and stability of the interfacial pulmonary region. They maintain a near-zero surface tension on compression of the air/water interface during exhalation when restricting the increase in surface tension on the expansion of the interface during inhalation [2].

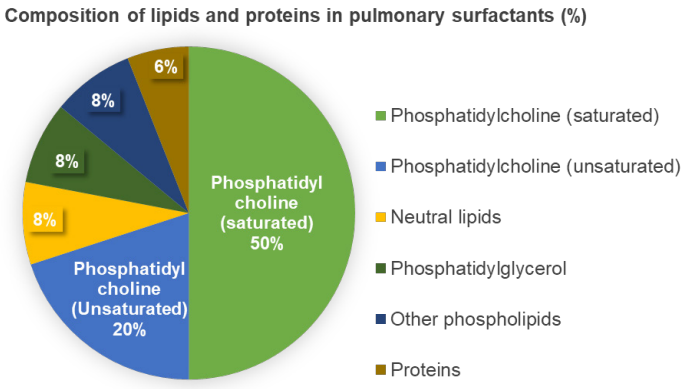

Figure 1.1 Composition of lipids and proteins in the pulmonary surfactants.

A lack of effective pulmonary surfactants in fetuses and newborns leads to pulmonary failure, a defect that is usually treatable. Adults can also suffer from a low concentration of surfactants due to an inherent lack or as a consequence of disease. The low concentration of surfactants causes lung disorders, namely, respiratory distress syndrome. Several treatments are available

for the replacement of surfactants: previously, protein-free synthetic surfactants were applied, which were later on replaced with animal-derived systems. Nonetheless, further investigations of the physicochemical properties of multi-component PC monolayers are required to fully understand their interfacial structure to support the development of new synthetic surfactants. Although many studies discuss the structure of pulmonary surfactants, further label-free investigation of phospholipids at lower surface coverages may reveal more information about their interfacial structure. An in-depth understanding of artificial versus natural lung surfactant is limited by the lack of label-free, sub-monolayer sensitive, real-time analytical tools that are capable of fast data acquisition under ambient conditions.

Broadband vibrational sum-frequency generation spectroscopy is a promising tool that can provide the structure, conformation, orientation, and composition of the molecular layer. Recently, a next-generation, high-repetition-rate BB-VSFG (HRR-BB-VSFG) spectrometer was developed by Heiner et al. in SALSA Photonics Lab, Humboldt Universität zu Berlin, Germany [3, 4]. This thesis focuses on the first application of the HRR-BB-VSFG spectrometer as a bio-analytical tool to study molecules such as phospholipids. A systematic study of one- and two-component phospholipids at different surface coverages revealed the benefits of the spectrometer. This thesis also discusses the interfacial structure of the phospholipids' head and alkyl chains, and the interfacial structure of water molecules near and around the lipid head groups.

2. Motivation and goals

Phospholipids have widespread interest in physics, chemistry, biology, nanotechnology, and biotechnology, their interfacial structure having crucial importance in future technologies. Based on the literature review, there is a plethora of previous work that studied the interfacial structure of phospholipids [5-11]. The structure of phospholipid monolayers and bilayers was previously studied by labeling the molecules, adding probes, or deuterated lipids, however, it was shown that these approaches can alter the physicochemical properties such as structure, conformation, and orientation [12, 13]. The solution for these issues is to implement label-free methods which have monolayer sensitivity. Vibrational spectroscopies such as IR and Raman spectroscopy can help to study the chemical composition and structure of lipids at various microenvironments, however, the lack of sensitivity to discriminate the interfacial signals from the bulk is a limitation of these methods.

Broadband vibrational sum-frequency generation spectroscopy (BB-VSFG) is a nonlinear optical technique, that can be used to study the structure, orientation, and conformation of interfacial molecules. This technique is intrinsically surface-specific due to its unique selection rules. Recently, a next-generation, high-repetition-rate, high-resolution BB-VSFG (HRR-BB-VSFG) spectrometer was developed with two orders of magnitude higher sensitivity compared to typical VSFG spectrometers [3, 4]. The thesis presented here aims to study the applicability of an existing HRR-BB-VSFG spectrometer in bio-analytical chemistry. In order to explore the feasibility of studying biomolecules such as phospholipids using the state-of-the-art spectrometer, phospholipids were selected for this purpose as the structure and interaction of their lipid chain are sensitive to heat-induced processes.

The VSFG measurements were performed in order to explore the experimental conditions for studying biomolecules such as phospholipids. Model systems of multi-component phospholipid bilayers were employed for this purpose. As will be shown by the results, the HRR-BB-VSFG spectrometer has the potential for non-destructive highly sensitive probing of the phospholipids. In particular, the one- and two-component phospholipid monolayers were studied at different surface coverages and compositions. In order to extract the information about the vibrational modes, the fitting was performed. As will be discussed, combining information on the vibrations of the alkyl chains, the head groups as well as the surrounding water molecules, opens new perspectives in characterizing lipid layers as they are abundant in pulmonary surfactants and many other samples.

The thesis is categorized as follows. Chapter 3 introduces the fundamentals of phospholipids and the physical aspects of BB-VSFG and the state-of-the-art of its applications. Chapter 4 contains details on the methods used to obtain the experimental results, which are presented in Chapters 5-7. In particular, Chapter 5 allocates the applicability of the HRR-BB-VSFG spectrometer as a bio-analytical tool for studying multi-component phospholipids, the optimization of experimental conditions, and the stability of phospholipids during the measurements. Chapter 6, presents the HRR-BB-VSFG spectra of one- and two-component phosphatidylcholines and their structural variations at different surface coverages. The chapter also discusses the quantification of the conformational order/disorders in the alkyl chains, the interfacial structure of water molecules between the head group of phosphatidylcholines and the CaF_2 window, and the advantages of using HRR-BB-VSFG spectrometer. Chapter 7 is devoted to the HRR-BB-VSFG spectra of deuterated and non-deuterated phospholipids' head groups at the fingerprint region. This chapter is concerned with the preliminary assignments of vibrational features. Finally, the main conclusions from the results obtained in this doctoral thesis are summarized in Chapter 8 including the future perspectives and an outlook on potential directions.

3. Research background

3.1 Phospholipids

Phospholipids are macromolecules that serve a variety of functions in all organisms. These functions include maintaining the structure of sub- and cellular membranes, acting as metabolic fuels, signaling molecules, and surface wetting agents. Their abundance and importance created a widespread interest in physics [14-16], chemistry [15, 17, 18], biology [17], material science [19], nanotechnology [20-22], biotechnology [17, 23-25], and photonics [26].

3.1.1 Chemical structure

According to the International Committee for the Classification and Nomenclature of Lipids in association with The LIPID MAPS Initiative, lipids are classified into numerous classes and subclasses [27]. The major categories of lipids include fatty alkyls, glycerolipids, and glycerophospholipids [27, 28]. Glycerolipids are lipids made of fatty acid esters of glycerol (alkylglycerols) which are categorized into mono-, di- and tri-substituted glycerols [29]. Glycerophospholipids (also called phospholipids) are the key elements of the plasma membrane, serve as metabolic fuels, and function as signaling molecules. The abundance and importance of phospholipids made them a separate category.

Phospholipids are amphipathic molecules that contain a polar head (phosphorus) and two non-polar tails (alkyl chain) that are linked to two glycerol moieties in their structures. Phospholipids may be subdivided into distinct classes based on the nature of the polar head group. Many lipids have charged head groups which influence the head group's behavior, as it affects repulsion with other molecules and other membrane characteristics. There are positive, negative, and zwitterionic head groups, with negatively charged head groups being the most widespread,

while positively charged ones are much less common. Various head groups include compounds such as glycerophosphocholine (GPC), glycerophosphoethanolamine (GPE), glycerophosphoserine (GPS), glycerophosphoinositol (GPI), glycerophosphoglycerol (GPG), and phosphatidic acid (PA) [28]. These head groups are prepared by esterification of phosphatidic acid. Phosphatidylcholine (PC) has a positively charged choline group. The choline is an N, N, N-tri-methylethanolammonium cation that binds to phosphatidic acid. This process makes the PC a neutral molecule by losing a negative charge on the phosphate group.

The alkyl chain group is characterized by a repeating series of methylene groups that provide the hydrophobic character of phospholipids. The alkyl chain length usually varies from four to thirty-six hydrocarbons (C4-C36) in the tail of a phospholipid. The number of double bonds in the alkyl chain determines the degree of unsaturation. Depending on the degree of unsaturation of the alkyl chain, the phospholipid molecule can be classified as saturated or unsaturated. In saturated phospholipids, all the carbon atoms in the tail groups are hydrogenated while in the unsaturated lipids there will be at least one pair of carbon-carbon double bonds in an extended chain structure. The hydrocarbon tails determine the type of phosphatidylcholine molecule, where one tail is usually an unsaturated hydrocarbon such as oleic acid and the other a fully saturated one. The hydrocarbon chains of the phospholipid have an important role in maintaining the fluidity of the formed monolayers or bilayers. Several factors affect the fluidity of the alkyl chains. The three most important factors that influence membrane fluidity are the number of unsaturated alkyl chains, the concentration of cholesterols, and the temperature. Phospholipid model systems are commonly employed to study the effect of several unsaturated alkyl chains, the concentration of cholesterols, and the temperature on membrane fluidity.

3.1.2 Thermotropic and lyotropic mesomorphism

Studies show that the phospholipids pack mostly as bilayers in all single-crystal structures [30, 31]. Heat or solvent disrupts phospholipids' physical properties, specifically the crystal lattice, and give rise to complex structures or phases [15, 32]. These arising phases have been referred to as mesomorphic or liquid crystalline because they exist in between the crystalline and the liquid state. The phases formed between crystal and isotropic liquid as a result of heat are referred to as thermotropic mesomorphism whereas the phases between crystal and a true solution when interacting with H_2O are termed lyotropic mesomorphism. Lyotropic phases can also exhibit thermotropic mesomorphism: this phenomenon happens when the lipid phases depend on both water content and temperature. There are several lyotropic phases such as

micelles, vesicles, monolayers, and bilayers (see Figure 3.1) [33]. The cubic, hexagonal, or inverted hexagonal and less ordered phases also occur under certain conditions. These phases are formed in a way to adapt to a minimum energy conformation in a water solution.

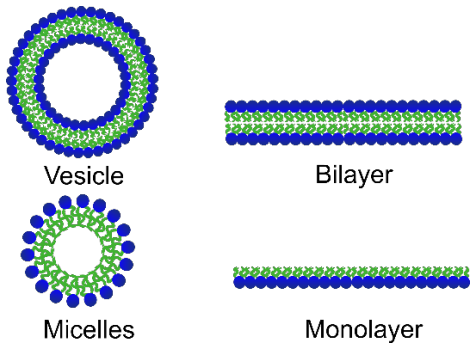

Figure 3.1 The lyotropic mesophases of phospholipids such as vesicles, micelles, bilayer, and monolayer in the aqueous environment are represented as two-dimensional schemes. The blue and green colors represent the head group of the alkyl chain of the phospholipids respectively.

Both polar and non-polar groups associate with each other to form these structures. The shape of a particular phospholipid molecule is an important factor that determines the curvature of the aggregation. Some of these structures have significant biological relevance and are versatile tools for biological functions. Phospholipid bilayers functions include maintaining the structure of the membrane, compartmentalizing cells and organelles from the microenvironment, regulating and controlling the transport of ions and nutrients through channels and pores, and mediating interactions between the internal and external environments of the cells, which involve cellular signaling and energy storage [34]. Phospholipids monolayers act as surface-active wetting agents in the pleura and alveoli of the lung, pericardium, and joints in the human body [35]. The physiochemical properties of the lung surfactants can be understood at various microenvironments when studying the model systems in the laboratory. Various model systems and their preparation are discussed in the following section.

3.1.3 Phospholipid model systems

There are several types of phospholipid model systems such as solid-supported lipid bilayers and monolayers, phospholipid vesicles, polymer cushioned phospholipid bilayers, black lipid membrane, and self-assembled monolayers. Among these model systems, solid-supported bilayers and monolayers have a special interest in spectroscopic and microscopic communities as they are convenient to prepare and measure using several techniques. Therefore, the background and the preparation of planar model systems of phospholipids are discussed in the following section.

I. Phospholipid vesicles

Phospholipids spontaneously form closed structures in aqueous solutions [18]. Lipid vesicles or liposomes are synonymously used terms according to the IUPAC guideline. In general, there are two types of vesicles, multilamellar (MLVs) and unilamellar. MLVs are defined as concentrically arranged, equally spaced, spherical bilayers separated by layers of water, while unilamellar vesicles are defined as spherical structures consisting of a single, closed bilayer that surrounds an aqueous cavity. Unilamellar vesicles are further divided into two classes according to their size. The vesicles larger than ~ 100 nm are referred to as large unilamellar vesicles (LUV), and the vesicles below 100 nm are as small unilamellar vesicles (SUV). Since packing constraints decrease as the vesicle diameter exceeds about 50 nm, some studies refer to the vesicles below 50 nm in diameter as SUVs and above as LUVs [36].

MLVs and LUVs: The procedures for preparing MLVs and LUVs are quick and simple [17]. The preparation of MLVs begins with the selection of neutral phospholipid- first, the phospholipids are dissolved in organic solvents, which is followed by the deposition of the dissolved lipids on a round-bottom flask, and then put up for rotary evaporation under reduced pressure. The resulting film is thoroughly dried under a vacuum. The preparation of LUVs is done with negatively charged phospholipids or lipid mixtures instead of neutral lipids. The term multivesicular vesicle has been proposed for vesicles within a vesicle [37] to distinguish this kind of vesicle from ordinary MLVs. When adding water to the dry lipid film, vesicles are spontaneously formed. The MLVs and LUVs formed after rehydration are heterogeneous in size which is a major drawback of MLVs and LUVs prepared with the above-mentioned procedure.

SUVs: SUVs can be prepared by applying force to the phospholipid dispersions. The external shear force tends to provide energy to disrupt and reseal phospholipid suspensions. High-speed centrifugation [38], ultrasonic irradiation [39], French press extrusion at generally very high pressures [40, 41], and repeated extrusion at low or medium pressures through membrane filters of defined pore size [42] are some of the examples that are commonly employed to prepare unilamellar and oligolamellar vesicles of more homogeneous size distribution. The drawback of high-power sonication is that it can easily lead to the lipid undergoing oxidative and hydrolytic degradation [43]. The bath sonication is milder than probe sonication where the lipid has a minimum risk of degradation. A more homogeneous dispersion of SUVs is obtained by centrifuging the phospholipid dispersion after ultrasonication. Prolonged high-speed centrifugation may be used to improve the homogeneity of the SUV dispersion [38].

Liposomes or lipid vesicles of phospholipids experience both chemical and physical instability. The chemical instability mainly results from the hydrolysis of the ester bonds in phospholipids and the oxidation of their unsaturated alkyl chains. The hydrolysis of phospholipids causes the formation of fatty acids (FA) and lysophospholipids. The presence of these compounds can affect the physical properties of the phospholipid bilayer. The liposomes aggregate and/or fuse to form a larger unit, compromising the structure even more. Several methods have been developed to ensure the physical stability of lipid vesicles on storage, the basis of them being the following: i) The structure of the bilayer can be adjusted for optimum stability. For example, selecting compounds with long and saturated alkyl chains or adding saturated hydrogenated soybean or egg-phosphatidylcholine tends to produce a highly condensed bilayer with low permeability. ii) The aqueous liposomal dispersions can be freeze-dried. Freeze-drying is a logical alternative to achieve long-term stability on the shelf, with most research groups focusing on freezing or freeze-drying as a means of cryo-preservation. The major factors affecting the stability in a freeze-drying and rehydration cycle are the structure of the bilayer, the size of liposomes, and the presence and type of cryo-protectant. The considerable variables during the process include the time of the process, the applied temperature(s), the rate of freezing/drying, and the conditions of rehydration.

II. Phospholipids bilayer and monolayer structures

The deposition of amphipathic molecules on the solid substrate from the air-water interface to form lipid layers dates back to the 1920s [44], however, numerous techniques were employed for layer formation previously to this. Towards the end of the nineteenth century, Lord Rayleigh was working on layer-formation by spreading simple oils over the water surface. He was able to calculate the thickness of the film by measuring the original volume of oil used and the final area it covered. Agnes Pockels observed monolayer thick molecular layers at the air-water interface [45], which were further explored in the 1930s by Irving Langmuir and Katharine B. Blodgett. Langmuir and Blodgett modified the apparatus used by Pockels, which from here on out is referred to as a Langmuir trough. Irving Langmuir received the Nobel Prize for Chemistry in 1932 “for his discoveries and investigations in surface chemistry”. Later on, Gortner and Grendel performed some key experiments using a Langmuir trough on blood cells [30]. They were interested in determining the amount of lipid present in red blood cell membranes by studying the area of lipids using a Langmuir trough. Mueller et al. developed the first planar phospholipid bilayer model system for studying their electrical properties such as electrical capacity, and resistance in the mid-1960s [46]. Later Tamm and McConnell deposited

supported phospholipid bilayers directly onto quartz, glass, and oxidized silicon substrates [47, 48].

There are several methods employed for the formation of phospholipid bilayers or monolayers on solid substrates, such as the vesicle fusion approach [49, 50], Langmuir–Blodgett (LB), and Langmuir–Schaefer (LS) deposition, [51], using self-assembled monolayers (SAM), black lipid membrane, polymer-cushioned lipid bilayers [52-54] or lipid-detergent mixed micelles [55, 56]. Illustrations of bilayer and monolayer formation on hydrophilic solid-substrates are shown in Figure 3.2. Phospholipid bilayers formed on the solid substrate are often named planar-supported lipid bilayers (SLBs) where they mimic intact membranes [49, 50]. The SLBs are ideal for different surface-sensitive spectroscopic techniques and microscopes [53] as they are stable model systems. Vesicle fusion approach and LB-LS deposition of bilayers and monolayer on solid substrates are widely employed due to their ease of preparation [47, 53, 57].

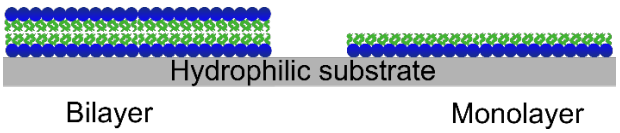

Figure 3.2 The bilayer and monolayer of lipids formed on the hydrophilic substrate.

Planar supported lipid bilayers: The solid-supported lipid bilayers are generally prepared by the vesicle fusion approach, as it is a simple and reliable methodology. SUVs for the vesicle fusion approach can be prepared by a plethora of methods; however, the simplest methodology involves the extrusion of multilamellar vesicles through porous polycarbonate membranes [41-44]. An alternative approach is the sonication and ultracentrifugation of aqueous lipid suspensions where the size distribution of the vesicles depends on the time of sonication, the composition of lipids, charges of lipid, the ionic strength, and screening capability of the buffer [22]. It is worthwhile to use a water bath that reduces the heat produced and keeps the lipids to maintain the temperature for prolonged sonication. The high surface coverage SLBs are formed via the fusion of the prepared vesicles under the right experimental conditions [50]. The asymmetric phospholipid vesicles were studied under various conditions in which SLBs formation can occur with intact vesicles on solid supports [45]. The experimental conditions that determine the quality of the bilayers formed on the substrates include the nature of the lipids, the properties of the buffer solution, and the surface of the substrate. Solid substrates such as glass, silica, mica, or calcium fluoride are commonly used as supports for vesicles. Vesicle fusion on a surface occurs in a two-step process [58]. The process begins with the

adsorption of the SUVs from the buffer solution followed by its fusion onto the surface of the substrate forming planar supported bilayers (see Figure 3.3) [59].

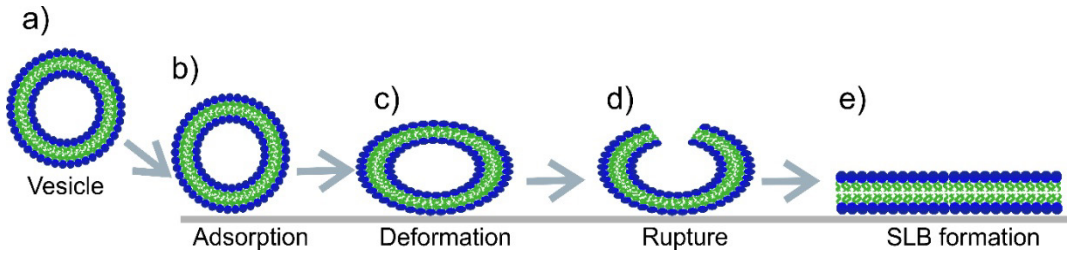

Figure 3.3 Schematic of vesicle fusion on the CaF_2 window a) a vesicle prepared using extrusion method b) adsorption of vesicle on the CaF_2 window and c) deformation of vesicle d) rupture e) supported lipid bilayer formation.

The amphipathic nature of the phospholipids causes the adsorption of vesicles onto the substrate. The hydrophilic head groups of lower lipid leaflets interact with the substrate that encloses a thin water layer, and their hydrophobic alkyl chains interact with the alkyl chains of the upper lipid leaflet. SLB patches form on the substrate by rupturing and fusing surface-adhered vesicles when the concentration of the reaches above a critical value. The process of vesicle rupture may occur via various channels. Lipowsky and Siefert [48] elaborated on the factors that affect the spontaneous rupture and fusion of vesicles. According to them, spontaneous raptures can occur in three distinct ways: i) The main cause for the rupture of adsorbed vesicles is the lipid−substrate interaction. When the lipid-substrate interaction is strong, even at low lipid coverages, the rupture of single vesicles will occur. ii) The rupture may take place upon the incorporation of a newly arriving vesicle into the vesicle overlayer. iii) The vesicle rupture may occur near the boundaries of already formed lipid islands. Several factors affect the adsorption and rupture of SUVs on the substrate: such as the composition, size, osmotic pressure of the vesicles; surface charge, surface roughness, surface cleanliness of the substrate; pH, and ionic strength of the solution [60, 61].

Phospholipid monolayers: A monolayer formed on the surface of the water or any other subphase is not in thermodynamic equilibrium. In general, the equilibrium spreading pressure is a few mN/m. In the case of higher lateral pressures, monolayers prefer to form in a three-dimensional lipid crystal on the water surface. Ordered monolayer phases are metastable: a monolayer may transform spontaneously into a bilayer or collapse into a multilayer film under specific conditions [62, 63], therefore, they may be out of equilibrium in long-range translational order.

Planar supported monolayer: The phospholipid monolayer is the simplest lipid model system. LB deposition permits the creation of monolayers, bilayers, or even multilayers on the solid substrates. The control over the parameters, namely, surface tension, surface pressure, surface area the main advantage of LB depositions. It ensures the high homogeneity of the samples and easy reproducibility. The physicochemical properties of phospholipids can be studied by having control over the lipid monolayer.

3.1.4 Surface pressure – area isotherm (π-A)

Surface tension is the force per unit length (γ=F/L), and its units are N m^{-1} and dyn cm^{-1}. Surface pressure is the difference between the surface tension of pure water (σ_0) and the water covered with a monolayer (σ). The surface pressure of a monolayer can be defined as a function of the area per molecule (A, usually expressed in $Å^2$ or nm^2 $molecule^{-1}$), and the π-A isotherm can be obtained when the total number of molecules and the total area that the monolayer is known. The surface pressure-area isotherm (π-A) provides information on the stability of the monolayer at the water-air interface, conformational changes, and phase transitions [64-66]. The monolayer on the water surface experiences a compression as the barriers move from the initial position, which may also result in a change of surface pressure at the air-water interface. The surface tension is approximately 73 mN/m (20 °C) for the air/water interface. The Langmuir balance and Wilhelmy plate are two main methods that can be used to measure the change π-A during monolayer compression. The continuous monitoring of the π-A isotherm of the monolayer on the surface of the water gives rise to the diagram as shown in Figure 3.4.

In general, the monolayer during compression experiences several phases, namely, gas (G), gas-liquid expanded (G-LE), liquid-expanded (LE), liquid expanded-liquid crystalline (LE-LC), and liquid-crystalline (LC) as demonstrated in Figure 3.4. Initially, when the surfactants are spread on the surface of the water the molecules apply inter and intra-molecular forces to act on each other. They behave as in the 2-dimensional (2D) ideal-gas phase and possess a very low surface pressure (<1 mN/m). When the barriers are moved closer together, the intermolecular distance decreases, the molecules start to interact with each other, and the surface pressure increases. Transition from the "gas" to the "liquid" state occurs, forming the "liquid-expanded" phase. In this phase, the hydrocarbon chains of the surfactants are mostly randomly oriented and may contain *gauche* conformations. Under further compression, the monolayer changes from liquid to the condensed states where condensed lipid domains appear in the expanded phase. As the barriers are moved progressively, the monolayer will have a well-

defined *in-plane* structure in the condensed phase. This phase is named "liquid-crystalline" where the lipid monolayer behaves as a 2D crystal. Further moving the barriers together, the monolayer tends to collapse at smaller surface areas when the compression goes beyond certain limits, forming three-dimensional structures at these collapse points.

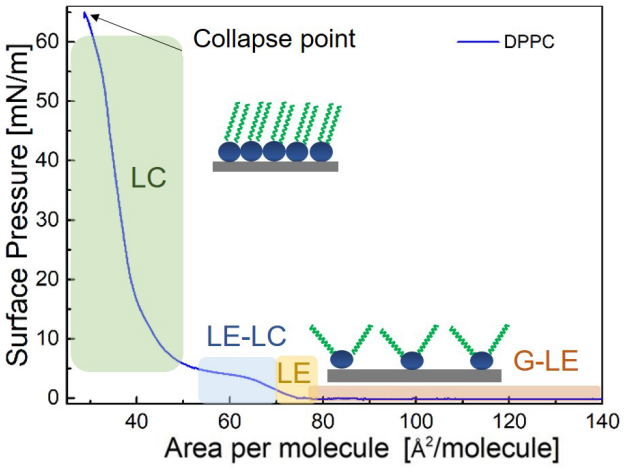

Figure 3.4 Surface pressure - area isotherm of lipid monolayer formed on the surface of the water subphase. The scheme of molecules at the air/water interface was given on the right side. The blue and green colors represent the arrangement of the head group and the tails of the phospholipids in certain phases.

3.2 Structure and dynamic characterization techniques

In the case of phospholipids, the structure and dynamic properties can be measured by several diffraction, spectroscopic and microscopic techniques. An overview of these techniques and their limitations are discussed in this section.

3.2.1 Fluorescence microscopic, and spectroscopic methods

There are several fluorescence measurement approaches such as excitation, emission, time-decay, anisotropy, and microscopy. Some of these techniques relevant for the context of this work are *one*-and *two-photon excitation fluorescence (TPEF) microscopy*, *fluorescence recovery after photobleaching (FRAP*), *fluorescence correlation spectroscopy (FCS), and fluorescence anisotropy.*

The first applications of fluorescence microscopy on lipid monolayers were reported in the 1980s [58, 59]. Phospholipid molecules do not have fluorescing groups, so to emit fluorescence, phospholipids need to be covalently bound with a fluorescent label or a fluorescent probe needs to be introduced into the lipid bilayer. Fluorophores embedded into phospholipid membrane

offer a means to study the dynamics and average orientation of the hydrocarbon chains [67] and also enable the study of properties such as the molecular order [60], domain formation [61, 62], phases, and their co-existence [63-65]. Other properties such as the rotation of molecules, the extent of hydration, polarity, local pH, and lateral diffusion are also extensively studied with fluorescent spectroscopic methods.

The theory of two-photon excitation was proposed in a study of the early 1930s [68], however, the experimental demonstration took almost three decades to implement the theory in experiments [69]. TPEF microscopy was first demonstrated by W. Denk and James Strickler in 1990 [70]. The strength of this approach is that it increased penetration depths for long excitation wavelengths, and also reduced light scattering with two-photon excitation. The method allows the study of structural properties such as domain formation, and molecular order [71].

FRAP exploits the photobleaching property of fluorophores. A region of interest (ROI) is bleached with a high-intensity light beam, which is then followed by the fluorescence recovery of the sample due to diffusion, interactions, or reactions of the surrounding fluorophores. This yields a recovery curve from which the diffusion coefficients, binding rates, or turnover rates can be determined [72]. FCS is a single-molecule method for the characterization of membranes. In this approach, small fluorescence intensity fluctuations are measured in a defined volume, which provides accurate information about diffusion coefficients, concentrations, molecular brightness, intramolecular dynamics, and molecular interactions [72]. Its advantages over FRAP are the improved sensitivity, and the possibility to work at significantly reduced fluorescence labeling densities. Domain-forming - the interaction between lipid and proteins - has long been studied using FCS [73-76]. The challenge of FCS arises during the photobleaching of the applied dye: the loss of fluorescent signal leads to a compromise between the determination of concentrations and diffusion coefficients.

Fluorescence anisotropy or polarization-resolved imaging has been widely used to measure the size of the fluorophore, speed of rotation, and the viscosity of the solvents based on one or two incident polarization states. The idea to investigate a molecular structure by a polarization-resolved fluorescence method was introduced by Perrin in 1926 [77] and developed by Weber in 1953 [78]. Employing this approach, the order, fluidity, orientational order of the lipid molecules are studied using polarization-resolved fluorescence [79, 80].

There are many advantages to using these fluorescence techniques. These benefits include the ability to measure changes in systems, high sensitivity, medium specificity, and non-destructive nature. On the other hand, there are several drawbacks in studying the molecular properties of labeled phospholipids with fluorescent techniques: i) Almost all phospholipid molecules need to be labeled with fluorescent groups. ii) The labeled lipids, as well as the fluorescent probe, have a different molecular shape, and therefore different intermolecular interactions. iii) The probe concentration has to be low otherwise it perturbs the spatial distribution of lipids, their structure, dynamics, and the functioning of the membrane particularly in the ordered phases [81]. iv) A practitioner must handle the data with extreme care when using such probes else misinterpretation can occur.

3.2.2 Nuclear and electronic spectroscopic and microscopic techniques

I. Electron paramagnetic/spin resonance spectroscopy (EPR/ESR)

During this method, a spin probe, namely a nitroxide group, is covalently bound to either the fatty alkyl chains or to the head group of a lipid molecule at a particular position. The spin probe will incorporate lone pair of electrons into the phospholipid structures. These lone pairs of electrons will be then excited with a static external magnetic field, inducing the splitting of spectral lines into several components, which is known as the Zeeman effect. The time-scale of ESR is 10^{-8} s - 10^{-3} s which complements molecular vibrations which are in the order of 10^{-13} s – 10^{-14} s. The order parameter, polarity effect, fluidity, and lateral diffusion of phospholipid mono-and bilayers are usually studied with the help of ESR spectroscopy [13, 82]. The advantage of this technique is its great sensitivity; however, a major disadvantage is that the incorporated spin probes may induce perturbations in the lipid bilayer via the added reporter groups. If the concentration of the spin probes is above a critical value, the properties of the bilayer are altered. Another issue of ESR spectroscopy when studying mixed systems and the liquid crystalline phase is the inhomogeneous distribution of spin probes.

II. Nuclear magnetic resonance (NMR)

The NMR is similar to the ESR spectroscopy in that both techniques are magnetic resonance approaches. During NMR nuclear magnetic resonance arises in an external magnetic field due to the transitions between the Zeeman energy levels of the atomic nuclei [83]. NMR allows the investigation of the lipids in their genuine environments without an external probe molecule, which is an advantage over ESR. Both natural phospholipid bilayers and vesicles can be

investigated with this technique, and it also ables the study of molecular motion in the range of 10^{-12} s - 10^{-1} s. When lipid vesicles or lipid micelles are small, and/or in fluid-phase, simple [84] or multidimensional high-resolution NMR is the preferred method of investigation [85]; while ordered lipid phases and macroscopically oriented lipid samples are investigated using magic-angle spinning. The major drawbacks of NMR are that its measured spectral lines are sensitive to the size of the phospholipid vesicles, to rapid particle tumbling, and molecular diffusion – these dynamic properties cause an isotropic averaging of the NMR lines and this method is not applicable for studying the interaction of model membrane with other molecules in real-time.

III. X-ray diffraction and neutron scattering

The structures of phospholipids and their aggregates can be studied using these scattering techniques [15]. The single-crystal X-ray diffraction techniques are the most promising for investigating phospholipid structure [86, 87], however, complementary information about hydrated phospholipids can also be obtained with neutron diffraction by selective deuteration of the phospholipid layer [88-90]. One of the limitations of these techniques is that it is difficult to obtain suitable single crystals of phospholipids, however, surface-aligned phospholipid bilayers partially solve this problem [91]. Neither of these methods provides information about molecular dynamics, and both techniques lose resolution as the rate of molecular motion increases.

IV. Atomic force microscopy (AFM) and scanning tunneling microscopy (STM)

Phospholipid bilayers have been visualized *in situ* with the electron transmission mode [92], STM [93], and AFM [94], with the AFM and STM methods, also enabling the study of phospholipid structures and their aggregates in water. The sensitivity of these force measurements depends on the strong interaction between the AFM tip or scanning needle and the investigated specimen. The limitation of AFM measurements is the sample distortion from the proximity of a scanning tip, which results in undesired conformational or phase changes. For this reason and because of its chemical sensitivity, the structural identifications are difficult with standard AFM. Additionally, stabilization of monolayers either by a covalent attachment to the substrate or by polymerization is mandatory for this technique.

V. Brewster angle microscopy and autocorrelation spectroscopy

The p-polarized light incident on the air-water interface under the Brewster angle condition is not reflected. The formation of a monolayer on the water surface modifies the Brewster angle

condition, and light reflection is observed at a constant angle of incidence. Both Brewster angle microscopy [95, 96] and Brewster angle autocorrelation spectroscopy [97, 98] work under this method, but the latter additionally involves an autocorrelation technique. This technique provides us a mono-molecular level visualization: we can study the monolayer's morphological features, domain formation, and collapse behavior, however, the application is limited to probing only crystalline samples. Using this technique, the tilt angle of the lipids' alkyl chains can be studied [99, 100].

3.2.3 Vibrational spectroscopy

The vibrational spectroscopy offers a non-destructive and label-free approach to studying the chemical structure, the composition of molecules, and/or complex biomolecules, such as phospholipids. Infrared and Raman spectroscopy are considered two conventional vibrational spectroscopic techniques and will be further detailed below.

I. Infrared spectroscopy (IR)

IR is an absorption spectroscopic technique that can excite molecular vibrations or rotations. The band intensity obtained in the IR spectrum is proportional to the change in the dipole moment of the molecules investigated. This technique has a significant role in the characterization of biomolecules. The physicochemical properties of phospholipids were intensely studied in the 1960s using IR [15, 101], however, the study of phospholipids in their natural aqueous state is limited as the surrounding water strongly absorbs in the mid-infrared region [101-103].

Fourier transform infrared spectroscopy (FTIR) solved this issue, enabling the study of lipid samples in the presence of water, and also provides a higher signal-to-noise ratio compared to classic IR spectroscopy [104]. Several other challenges need to be considered in the case of IR techniques for studying phospholipids. These include phospholipids at high concentrations that cause molecular aggregations that may result in artifacts: when estimating the absorption coefficients, errors may occur when estimating the path length of the cuvette. Additionally, surface-specific techniques are required to study the structure and dynamics at the molecular level, however, IR techniques lack the means to discriminate against bulk signals. This issue is solved by using other label-free optical methods, such as attenuated total internal reflection infrared (ATR-IR) [105, 106] spectroscopy. ATR-IR spectroscopy is sensitive to local structures but is experimentally more demanding, and restricts the choice of substrates. For this reason, more surface-specific spectroscopic methods are required for the investigation of

samples with low surface coverage samples, and to be able to adequately discriminate the vibrational contribution of corresponding molecular species from the signals of the molecules investigated.

Infrared reflection absorption spectroscopy (IRRAS) is another technically improved IR spectroscopic tool with high sensitivity, with which we can study the structure, orientation, and composition of phospholipids [107-109]. The limitations of this method are the choice of substrate and the non-resonant contribution or background (NRB) from the substrate. In the field of advanced IR spectroscopy, nano-FTIR is a relatively new approach becoming popular in the characterization of biomolecules [110-112]. In nano-FTIR, the spectra of absorption, reflection [110], and hyperspectral images of the sample can be obtained by collecting spectra over a 2D array of positions [113]. The main drawback of this approach is the sample distortion because of the measurement tip.

II. Raman microscopy and spectroscopy

Raman scattering is an inelastic scattering process, where an external monochromatic light excites the molecules to a virtual electronic state. The light emitted during relaxation from these virtual electronic states is measured and constitutes the molecule's Raman signal. The effect was first predicted by Adolf Smekal in 1923 [114] which was experimentally proved in 1928 by the Indian scientists C. V. Raman and K. S. Krishnan in liquids [115, 116]. Raman received the Nobel Prize in Physics in 1930 "for his work on the scattering of light and the discovery of the effect named after him". In 1928, the same effect in crystals [117] was reported by G. Landsberg and L. Mandelstam in the Soviet Union. Raman spectroscopy is widely used to characterize molecules to obtain structural, conformational, and compositional information [118-120]. Both Raman and IR provide complementary information on phospholipid molecules. These methods have several advantages over diffraction methods, such as i) that they are extremely fast, cheap, and label-free. ii) Measuring spectra is possible in aqueous media. iii) Being vibrational methods, they are sensitive to structural transitions of phospholipids. iv) The vibrations of individual groups provide structural information on highly localized regions in the phospholipid bilayers. v) Applying it as an imaging technique, Raman microscopy can give sub-micrometer spatial resolution while IR microscopy limited to a few μm, which makes it possible to distinguish the C-H stretching absorptions of the phospholipid alkyl chains from the carbonyl stretching of the interfacial region and the phosphate stretching of the polar head groups. Both for IR and Raman it is challenging to probe thin layers of lipids at the interface. Raman suffers from a very weak scattering cross-section, which is 10^{-12} orders

of magnitude lower than fluorescence, making this spectroscopic technique not widely used for biological samples [121]. The technical limitation of Raman spectroscopy has been overcome with surface-enhanced Raman scattering (SERS) spectroscopy. SERS can be employed to study the structure, composition, and conformation of the molecules adsorbed on a metal substrate [115-117] and because of its compatibility with aqueous samples, its high sensitivity, and narrow linewidth, it is a universally used method for biological applications e.g., in cells and tissues. In SERS, metallic nanoparticles are used to enhance the Raman signals of the molecules via the surface plasmon resonance effect, where it also gives information of molecules at the proximity of the employed nanoparticles. Comparing the relative intensity of certain bands, we can obtain information about molecular orientation [122, 123], however, SERS is limited to the study of molecules adsorbed on metal substrates or nanoparticles in solution. Recently, SERS was employed to study the structure and composition of multilamellar liposomes [124].

3.2.4 Nonlinear spectroscopic techniques

I. Coherent Anti-Stokes Raman Scattering (CARS) and Stimulated Raman scattering (SRS) microscopy

Both these methodologies are advanced coherent nonlinear Raman spectroscopic approaches. CARS is a parametric generation spectroscopic technique without transfer of energy to or from the sample [125, 126], while SRS [127, 128] is a nonlinear dissipative optical method. The benefits of using CARS imaging lie in that no sample preparation is needed beforehand, and the technique enables submicron spatial resolution and chemical imaging. The SRS signal is proportional to the imaginary part of the third-order susceptibility tensor $\chi^{(3)}$. The strength of SRS is its inherently free NRB nature. While using multiplex CARS microscopy [129], the localization of lipid in the sample and the degree of lipid saturation are estimated by probing the entire vibrational spectrum at each spatial point. Phospholipids are probed with a submicron spatial resolution. The ordering of water molecules between the bilayers of phospholipids was reported by employing CARS microscopy [130]. The drawback of CARS is its inability to identify the alkyl chain length, its capability to differentiate between chemically similar head groups such as sphingomyelins and phosphatidylcholines, and it is limited to study the structure and dynamics of lipids with abundant C–H stretching. It also suffers from the NRB generated both by the molecular species and by the surrounding medium.

II. Polarization-resolved SHG, third-harmonic generation, and four-wave mixing microscopy

These approaches are based on nonlinear optical processes that involve two or three photons at the same frequency interacting with a nonlinear material to generate a new photon with twice or thrice the energy of the excitation photons. Polarization resolved SHG (P-SHG) is a second-order non-linear optical process, which inherently promises sufficient surface-specificity, where only non-centrosymmetric media generate the SHG signals. Polarization resolved third-harmonic generation (P-THG) microscopy, a third-order nonlinear optical process, which is sensitive to refractive index mismatch between structures in the focal plane, allowing the imaging of surfaces and interfaces. Because of these methods' surface-specificity, they are both suitable to study lipid order, the surface density of a monolayer, and the orientation of molecules [131-133]. Four-wave mixing (FWM) is a third-order nonlinear optical process. In the case of FWM, three incoming waves generate a fourth signal due to the nonlinear property of the material they cross in. FWM microscopy has the potential to probe the time-resolved dynamics of electronic and vibrational excitations of phospholipids [134, 135].

III. Vibrational sum-frequency generation spectroscopy (VSFG)

VSFG is a second-order nonlinear spectroscopical method, a special case of SHG, where the sum of the two electromagnetic waves generates the so-called sum-frequency signal due to the nonlinear properties of a material present. Similar to other second-order nonlinear processes VSFG signals are inherently surface-specific due to selection rules. Ron Shen and his colleagues established VSFG together with SHG in the 1980s [136]. Employing VSFG, information can be obtained of structure, composition, conformation, and orientation of molecules, with probing their vibrational resonances of molecules at solid-solid, solid-liquid, and solid-gas interfaces [137-141]. Shen et al. pointed out that the VSFG is the only technique that can yield a vibrational spectrum of molecules at a free liquid or liquid mixture interface [143]. The spatial resolution in VSFG is better compared to the resolution achievable in IR microscopy. The spatial resolution of the VSFG can be further improved by focusing the visible (VIS) wavelength laser beam in the sub-μm range [142].

The structural and dynamic properties of phospholipids vary in bulk state and at the interface. To understand the structural properties, tools with high sensitivity and spectral resolution are required. VSFG, an inherently surface-specific, tool is a promising approach that can overcome currently faced challenges in other vibrational spectroscopic methods [133, 134, 136, 141, 142]. While employing VSFG, the structure, orientation, conformation, and composition of the

phospholipids can be studied with sub-monolayer sensitivity. A summary of the above-mentioned structure and dynamic characterization techniques is given in Table 3.1. This summary is prepared with the help of several works reported [17, 72, 134, 143, 144]. From Table 3.1, it is clear that VSFG spectroscopy is a promising tool that can be employed to study phospholipids model systems with sub-monolayer sensitivity. The theory of VSFG spectroscopy is described in detail in the following section.

Table 3.1 The **s**ummary of structural and dynamic characterization techniques and their applications [17, 72, 134, 143, 144] are listed below.

Techniques	**Information obtained**	**Chemical Structure**	**Limitations**
X-Ray and, Neutron reflectometry	Nanostructure of the surface and interface, course of the reaction in the monolayer, monolayer thickness, monolayer**.** counterion interactions	No	Loss of sensitivity at a high rate of molecular motion, lack of molecular dynamics information, samples are measured in ultra-high vacuum chambers, the study of gas/gas, liquid/liquid interfaces is limited
Single-crystal X-Ray diffraction	order, in-plane lattice structure, different phases of the monolayer	No	Single crystals of phospholipids are required, loss of sensitivity at a high rate of molecular motion, and lack molecular dynamics information
Brewster angle microscopy	Morphological features, domain formation, aggregation, monolayer phases, phase-coexistence, collapse behavior, π-T phase diagram	No	Lack of chemical information
AFM STM	Morphological features, domain formation, aggregation	No	Lack of chemical sensitivity (for standard AFM)
NMR	Structure and dynamics	Yes	Low sensitivity and only small lipid vesicles can be used, multilayer vesicles may broaden the NMR lines
ESR	Structure and dynamics	Yes	Spin labeling of lipids is required, misinterpretation of spectra may occur due to the presence of the probe

Techniques	Information obtained	Chemical Structure	Limitations
Fluorescence microscopy	Domain formation, phases, and their coexistence	No	Labeling of lipids with fluorescent dyes is mandatory, misinterpretation of spectra may occur due to the presence of probe, lack of chemical specificity
FRAP	Diffusion coefficients, concentrations, molecular brightness, intramolecular dynamics, and molecular interactions	No	
Fluorescence anisotropy	Orientational order, diffusion	No	
TPEF	Order, domain formation, phases, and their coexistence	No	
FCS	Diffusion coefficients, concentrations, molecular brightness, intramolecular dynamics, and molecular interactions	No	
IR	Structure of the functional groups, degree of ionization, the orientation of alkyl chain and head groups, H-bonding	Yes	Low sensitivity and the application of water and heavy water is limited due to IR absorption
FTIR		Yes	Limited substrates, lipid monolayers/bilayers are challenging to prepare on these substrates
ATR-FTIR		Yes	Limited substrates, lipid monolayers/bilayers are challenging to prepare on these substrates
nano-FTIR		Yes	The measurement tip of the spectrometer can distort the samples
IRRAS		Yes	The choice of substrate is limited, preparation of monolayer on the metal substrate

Techniques	Information obtained	Chemical Structure	Limitations
Raman	Structure of the functional groups, the conformation of alkyl chains, monolayer ordering	Yes	Low sensitivity and efficiency
SERS		Yes	Nanoparticles/ substrates of Ag or Au are required, the monolayers/bilayers are challenging to prepare on these substrates
CARS	Structure of the functional groups, the conformation of alkyl chains, monolayer ordering	Yes	Low sensitivity for the differentiation of the different headgroups of phospholipids, non-resonant background, low
SRS		Yes	Difficult signal isolation from incoming fields
SHG	The surface density of the monolayer, pK_a and the degree of ionization of head groups, the orientation of molecules within the monolayer	No	Low-intensity signal and lack of chemical structural information
THG	Morphology, domain formation, aggregation	No	Lack of chemical information
FWM	Morphology, domain formation, aggregation	No	Lack chemical information
VSFG microscopy and spectroscopy	Orientational and conformational changes, the structure of the interface, phase transitions, surface density of the monolayer	Yes	Interpretation of the spectral information is difficult, heterogeneous samples are difficult to interpret where ordered monolayers are required

3.3 Vibrational sum-frequency generation spectroscopy

A molecule is a combination of bonded atoms where each atom contains a positively charged nucleus surrounded by a negatively charged electron cloud. According to the classical spring model of molecules, nuclei and the bonding forces created by the electron cloud are analog to point masses connected with an ideal spring. Each atom possesses freedom of motion in the X, Y, and Z directions, and thus a molecule of N atoms has 3N degrees of freedom. If we subtract the three translational and the three rotational modes of a whole molecule, we get the molecule's number of internal degrees of freedom. A nonlinear molecule consisting of N number of atoms, therefore, has an internal degree of freedom of 3N-6, while a linear molecule, due to its structure, has 3N-5. The number of vibrational normal modes of a molecule equals the number of its internal degrees of freedom. In vibrational spectroscopy, the frequency of vibrational modes depends on the masses of the involved nuclei and the bonding forces [145]. The information about different molecular properties is acquired by probing the molecular vibrational modes. The symmetry of a molecule or a functional group dictates the selection rules of vibrational spectroscopy, which describe if a particular vibration is active or inactive in IR and/or Raman spectroscopy. Figure 3.5 shows an energy-level diagram of TPEF, SHG, CARS, SRS, and VSFG.

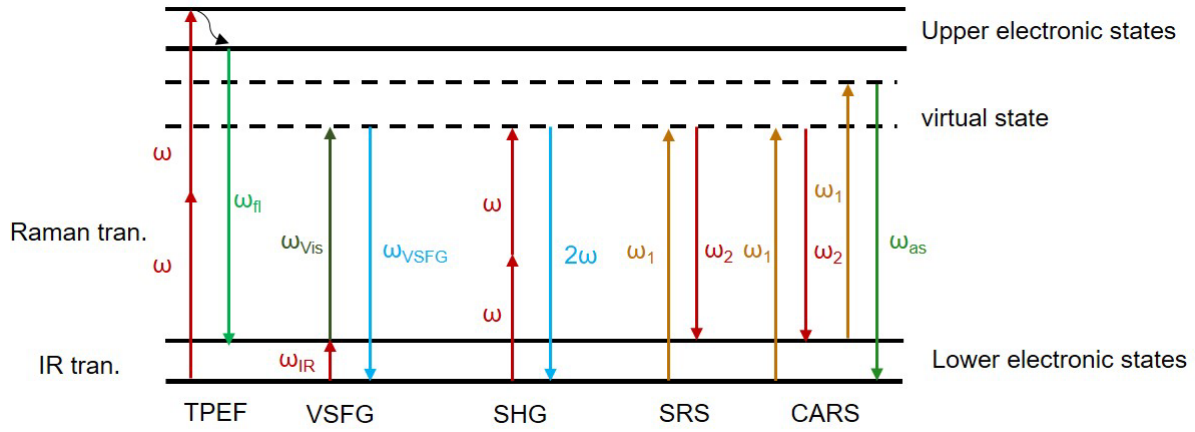

Figure 3.5 Jablonski representation of two-photon excitation fluorescence (TPEF), vibrational sum-frequency generation spectroscopy (VSFG), second harmonic generation spectroscopy (SHG), stimulated Raman scattering (SRS), and coherent anti-Stokes-Raman scattering (CARS). In all the cases, the molecular system absorbs and emits photons where the upward and downward arrows represent the annihilation and emission of the photon, respectively.

The theory of nonlinear second-order optical processes was first described in 1962 by Bloembergen and Pershan [146, 147]. The experimental work was performed after two decades

by Shen et al. in the early 1980s [136, 148, 149] and summarized as follows. The theory of the VSFG is described elsewhere in detail [137, 140, 150-152], but a quick overview of it will be given here. VSFG is a second-order nonlinear optical process that can provide polarization-dependent vibrational information of molecules at the surfaces or interfaces. In VSFG, a broadband mid-infrared (MIR) femtosecond pulse resonantly excites the vibrational transitions in the molecules [153-155]. A non-resonant, narrow-band, picosecond pulse then up-converts the molecular vibrations of the interface excited by the resonant MIR pulse into a second-order signal. The two incoming optical beams of MIR and VIS are spatially and temporally overlapped at the investigating surface to generate a third outgoing VSFG signal. The recorded VSFG spectra represent a convolution of the molecular response function with the visible up-conversion pulse. Since the VSFG process includes both IR and Raman transition (see Fig. 3.5.), only vibrational modes that are both Raman and IR active can be investigated.

When two input laser beams at frequencies of mid-infrared (ω_{MIR}) and visible (ω_{VIS}) overlap in a medium, a sum-frequency of the two incoming laser beams ($\omega_{VSFG} = \omega_{MIR} + \omega_{VIS}$) is generated as an output. The incoming laser beams must be spatially and temporally overlapped at the interface for the generation of the ω_{VSFG} signal. The ω_{VSFG} signal is generated as a result of the sample's absorption of incoming ω_{MIR} and then the up-conversion of its generated vibrational signatures to the lower wavelength range. The scheme of a three-layer model of co-propagating geometry used for the VSFG experimental geometry is shown in Figure 3.6.

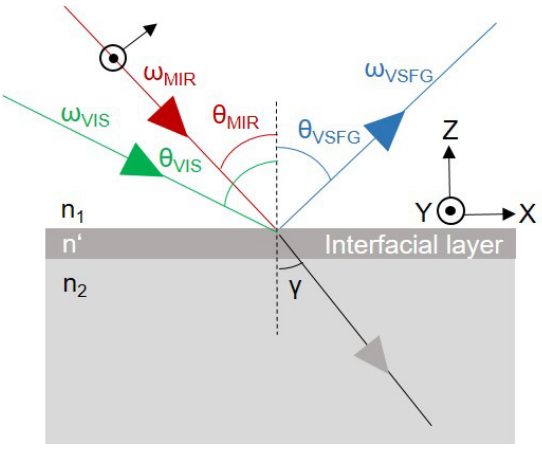

Figure 3.6 Illustration of the three-layer model considered for the co-propagating geometry in VSFG.

In Figure 3.6, ω_{MIR} and ω_{VIS} are the frequencies of incident MIR and VIS beams. The ω_{VSFG} is the frequency of generated VSFG signal, while n_1 and n_2 represent the refractive index of the first and second bulk media. n' is the interfacial refractive index and γ is the refracted angle derived by Snell's law. All the beams lie in the XZ-plane of the laboratory coordinate system

(X, Y, Z) where (i, j, k) is the generic indices. The Z-axis is perpendicular, while the XY plane is parallel to the surface. The θ_{VSFG}, θ_{VIS} and the θ_{MIR} represent the angle between the surface normal and the XZ plane of the corresponding beam. The intensity of the generated VSFG signal, I_{VSFG}, is proportional to the intensities of the incoming electromagnetic beams. The intensity of VSFG can be expressed as equation 3.1 [156]:

$$I_{VSFG} = \frac{8\pi^3 {\omega_{VSFG}}^2 \sec^2 \theta_{VSFG}}{c^3\, n_1(\omega_{VSFG}) n_1(\omega_{VIS}) n_1(\omega_{MIR})} \left|\chi^{(2)}_{eff}\right|^2 I_{VIS} I_{MIR} \qquad 3.1$$

The variables in equation 3.1 correspond to those previously defined. Additionally, I_{VIS} and I_{MIR} represent the intensity of VIS and MIR beams, while $\chi^{(2)}_{eff}$ is the effective second-order susceptibility, which is a macroscopic quantity. Considering the conservation of momentum, the angle at which the VSFG signal is generated can be calculated using the phase-matching condition, which is applicable for all three beams as they are co-propagating at the interface, and can be defined the following way [157]:

$$n_{VSFG}\, \omega_{VSFG} \sin\theta_{VSFG} = n_{VIS}\, \omega_{VIS} \sin\theta_{VIS} \pm n_{MIR}\, \omega_{MIR} \sin\theta_{MIR} \qquad 3.2$$

The positive and negative signs refer to co-propagating and counter-propagating beams, respectively.

The effective second-order susceptibility can be expressed as in equation 3.3 [156]:

$$\chi^{(2)}_{eff} = [\hat{e}(\omega_{VSFG})\boldsymbol{L}(\omega_{VSFG})] \cdot \chi^{(2)} : [\boldsymbol{L}(\omega_{VIS})\hat{e}(\omega_{VIS})][\boldsymbol{L}(\omega_{MIR})\hat{e}(\omega_{MIR})]. \qquad 3.3$$

Here, $\hat{e}(\omega_i)$ are the unit electric field vectors for the corresponding frequencies at the interface and $\boldsymbol{L}(\omega_i)$ are the Fresnel factors, where *i* represent VSFG, VIS, and MIR. A three-layer model is valid at the interface since the molecular layer is thin. The tensorial Fresnel reflection factors $L_{jj}(\omega_i)$ are expressed the following way [156].

$$L_{xx}(\omega_i) = \frac{2n_1(\omega_i)\cos\gamma_i}{n_1(\omega_i)\cos\gamma_i + n_2(\omega_i)\cos\theta_i} \qquad 3.4$$

$$L_{yy}(\omega_i) = \frac{2n_1(\omega_i)\cos\gamma_i}{n_1(\omega_i)\cos\theta_i + n_2(\omega_i)\cos\gamma_i} \qquad 3.5$$

$$L_{zz}(\omega_i) = \frac{2n_1(\omega_i)\cos\theta_i}{n_1(\omega_i)\cos\gamma_i + n_2(\omega_i)\cos\theta_i} \left(\frac{n_1(\omega_i)}{n'(\omega_i)}\right)^2 \qquad 3.6$$

The refractive index of the thin surface, n', is either determined by a series of VSFG measurements at different angles of incidence [158] or estimated from a theoretical model proposed by Y. R Shen [156].

3.3.1 Selection rules

$\chi^{(2)}$ is zero for isotropic and centrosymmetric media where even order nonlinear processes are forbidden. Molecules residing in an ordered fashion at the interfaces break symmetry, thus enabling the generation of VSFG signals. This property makes VSFG intrinsically *surface-specific,* simplifying the need for background subtraction compared to conventional IR and Raman spectroscopy. Figure 3.7 illustrates the scheme of various molecular arrangements in materials and whether the VSFG is applicable or not for said arrangement.

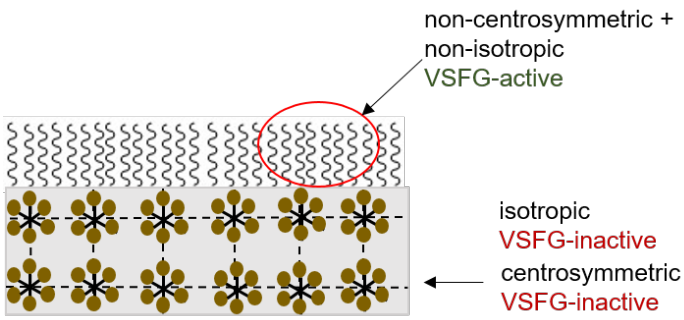

Figure 3.7 Possible molecular arrangements in materials and interfaces. VSFG is inherently surface-sensitive at interfaces where the symmetry is broken.

The macroscopic second-order susceptibility $\chi^{(2)}_{ijk}$ is a third-rank tensor with 27 tensor elements where i, j, and k denote the Cartesian coordinates in the laboratory frame of reference. The procedures for identifying the non-zero tensor elements for different symmetry groups were based on von Neuman's principle [159].

Isotropic achiral surfaces have $C_{v\infty}$ symmetry around the surface normal. For VSFG at achiral isotropic surfaces, all the tensor elements vanish due to symmetry constraints excluding four quadratic terms. These terms only possess either x or y with z and contribute together with the remaining zzz. The tensor elements are listed below in Table 3.2.

Table 3.2 The second-order susceptibility tensor elements are listed below, the non-zero tensor elements are represented in bold letters and the zero tensor elements are crossed out.

xxx	xyx	xzx	yxx	yyx	yzx	zxx	zyx	zzx
xxy	xyy	xzy	yxy	yyy	yzy	zxy	zyy	zzy
xxz	xyz	xzz	yxz	yyz	yzz	zxz	zyz	zzz

The *x* and *y* axes are equivalent while considering an isotropic surface. Among the 7 non-zero tensor elements for an achiral rotationally isotropic interface, the surface with C_∞ symmetry has only four non-zero $\chi_{ijk}^{(2)}$ components. The four non-zero $\chi_{ijk}^{(2)}$ components are:

$$\chi_{xxz}^{(2)}\left(\equiv \chi_{yyz}^{(2)}\right),\ \chi_{xzx}^{(2)}\left(\equiv \chi_{yzy}^{(2)}\right), \chi_{zxx}^{(2)}\left(\equiv \chi_{zyy}^{(2)}\right),\ \chi_{zzz}^{(2)}.$$

$\chi_{eff}^{(2)}$ is a linear combination of four independent experimental polarization combinations, thus it depends on the experimental polarization combinations and the geometries. These polarization combinations are ppp, ssp, sps, and pss, where 'p' denotes the parallel, and 's' to the perpendicular plane of polarization. During VSFG measurements, the parallel (p) and the perpendicular (s) plane of polarization of light can be selected using waveplates for all light beams. The polarization combinations are defined by the individual beams' polarizations, with the characters representing the VSFG, VIS, and MIR polarizations, respectively. For example, the ssp polarization combinations are a representation of s-VSFG, s-VIS, and p-MIR, respectively. Specifically, it is possible to selectively probe the four non-zero susceptibility tensor elements by selecting the plane of polarization of the incident fields and the sum frequency field, respectively. Table 3.3 represents the four different polarization combinations and their non-zero tensor elements. The ppp polarization combination probes an admixture of four tensor elements whereas the other three polarization combinations such as ssp, sps, and pss probe a single $\chi^{(2)}$element.

Table 3.3 Polarization combinations and their corresponding non-zero tensor elements.

Polarization combinations (VSFG, VIS, MIR)	**Constituent $\chi_{ijk}^{(2)}$**

ppp	$\chi^{(2)}_{xxz}, \chi^{(2)}_{xzx}, \chi^{(2)}_{zxx}, \chi^{(2)}_{zzz}$
ssp	$\chi^{(2)}_{yyz}$
sps	$\chi^{(2)}_{yzy}$
pss	$\chi^{(2)}_{zyy}$

Because of the symmetric nature of the Raman tensor [159] and $\chi^{(2)}_{eff}$ being a linear combination of four experimental polarization combinations, the first two indices of the $\chi^{(2)}$elements are interchangeable if the resonance frequencies are far away from electronic transitions. Taking this into consideration, equation 3.3 can be extended for the non-zero tensor elements in the following way:

$$\begin{aligned}&\chi^{(2)}_{eff,ppp} \\ &= -L_{xx}(\omega_{VSFG})L_{xx}(\omega_{VIS})L_{zz}(\omega_{MIR})\cos\theta_{VSFG}\cos\theta_{VIS}\sin\theta_{MIR}\,\chi^{(2)}_{xxz} \\ &- L_{xx}(\omega_{VSFG})L_{zz}(\omega_{VIS})L_{xx}(\omega_{MIR})\cos\theta_{VSFG}\sin\theta_{VIS}\cos\theta_{MIR}\,\chi^{(2)}_{xzx} \\ &+ L_{zz}(\omega_{VSFG})L_{xx}(\omega_{VIS})L_{xx}(\omega_{MIR})\sin\theta_{VSFG}\cos\theta_{VIS}\cos\theta_{MIR}\,\chi^{(2)}_{zxx} \\ &+ L_{zz}(\omega_{VSFG})L_{zz}(\omega_{VIS})L_{zz}(\omega_{MIR})\sin\theta_{VSFG}\sin\theta_{VIS}\sin\theta_{MIR}\,\chi^{(2)}_{zzz}\end{aligned} \quad 3.7$$

$$\chi^{(2)}_{eff,ssp} = L_{yy}(\omega_{VSFG})L_{yy}(\omega_{VIS})L_{zz}(\omega_{MIR})\sin\theta_{MIR}\,\chi^{(2)}_{yyz} \quad 3.8$$

$$\chi^{(2)}_{eff,sps} = L_{yy}(\omega_{VSFG})L_{zz}(\omega_{VIS})L_{yy}(\omega_{MIR})\sin\theta_{VIS}\,\chi^{(2)}_{yzy} \quad 3.9$$

$$\chi^{(2)}_{eff,pss} = L_{zz}(\omega_{VSFG})L_{yy}(\omega_{VIS})L_{yy}(\omega_{MIR})\sin\theta_{VSFG}\,\chi^{(2)}_{zyy} \quad 3.10$$

3.3.2 Second-order susceptibility and hyperpolarizability

Resonant contribution of second-order susceptibility, $\chi^{(2)}_{ijk,R}$ is a macroscopic average of molecular hyperpolarizability, $\beta^{(2)}_{abc,q}$. The i, j, k represent the coordinates of the Cartesian system in the $\chi^{(2)}_{ijk,R}$, which relates to $\beta^{(2)}_{abc,q}$ in molecular coordinate systems (abc) by Euler angle transformation [160]. The relation between the resonant contribution of second-order susceptibility, $\chi^{(2)}_{\mathrm{ijk,R}}$, and the molecular hyperpolarizability $\beta^{(2)}_{abc,q}$ can be written as follows:

$$\chi^{(2)}_{ijk,R} = \frac{N_S}{\varepsilon_0}\sum \langle \boldsymbol{R}(\boldsymbol{\psi})\boldsymbol{R}(\boldsymbol{\theta})\boldsymbol{R}(\boldsymbol{\varphi})\rangle\, \beta^{(2)}_{abc,q} \quad 3.11$$

The term N_S represents the number density of the molecules per unit volume at the surfaces whereas $R(\psi)R(\theta)R(\varphi)$ is the product of three rotation matrices using all three Euler angles to convert from the molecular to the laboratory coordinate systems. The ⟨ ⟩ indicate the orientational averages and ε_0 is the electric permeability in a vacuum. The indices a, b, and c on the β-elements represent the molecular-oriented coordinate system. Equation 3.11 states that the second-order susceptibility, $\chi^{(2)}_{ijk,\mathrm{R}}$, is related to the hyperpolarizability, $\beta^{(2)}_{abc,q}$ of individual molecules averaged over all orientations. The VSFG intensity depends on the order of the molecules at the surfaces, with a highly ordered surface providing high VSFG intensity, while a disordered interface, for instance, a disordered monolayer does not generate any VSFG signal. The expression for the hyperpolarizability is shown in equation 3.12.

$$\beta^{(2)}_{abc,q} = \frac{1}{2\hbar}\frac{A_{ab}B_c}{(\omega_q - \omega_{MIR} - i\Gamma_q)} \qquad 3.12$$

The terms Γ_q, and ω_q are the linewidth and the resonant frequency of the q^{th} molecular vibrational mode, whereas ω_{MIR} is the frequency of the MIR beam. In equation 3.12, the presence of A_{ab} and $B_{\mathbf{c}}$ means that the hyperpolarizability contains both a Raman transition moment and the IR transition moment. In other words, the corresponding vibrational mode must be both Raman and IR active to obtain a VSFG signal. Because of this reason, the VSFG spectrum less number of vibrational modes compared to IR and Raman spectra. The expression 3.12 states that $\beta^{(2)}$ will be negligibly small when the frequencies are far away from the resonance frequency, whereas it increases when the frequency of MIR overlaps with the resonance frequency of the molecules at the interface.

3.3.3 Second-order susceptibility and non-resonant contribution

The effective second-order nonlinear susceptibility ($\chi^{(2)}_{eff}$) has two contributions; one is a resonant contribution that contains the polarization information and the geometrical factors corresponding to the adsorbed molecules with the interacting electromagnetic fields. The other one includes the non-resonant response that will be generated independently of incoming frequencies which depends on the dielectric properties of bulk such as the substrate, water, etc. This can be expressed as equation 3.13.

$$\left|\chi^{(2)}_{eff}\right|^2 = \left|\chi^{(2)}_{NR} + \chi^{(2)}_{R}\right|^2 \qquad 3.13$$

The term $\chi_R^{(2)}$ is the resonant contribution whereas $\chi_{NR}^{(2)}$ is the non-resonant contribution. $\chi_R^{(2)}$ becomes zero when the incoming electromagnetic field of infrared radiation does not match the vibrational excitation of the adsorbed molecules at the surface. The non-resonant background causes several issues such as spectral distortion, or spectral broadening which has previously been reported in [161-163]. The relation between I_{VSFG} and the contribution of both the non-resonant and resonant transitions is given in equation 3.14.

$$I_{VSFG} \propto \left|\chi_{NR}^{(2)} + \sum \frac{A^q}{\omega_{MIR} - \omega_q + i\Gamma_q}\right|^2 I_{VIS} I_{MIR} \qquad 3.14$$

In the equation above, the term $\chi_{NR}^{(2)}$, A^q, Γ_q, ω_q are the non-resonant signal, amplitude, bandwidth, and frequency of the qth vibrational resonance, respectively. Equation 3.14 implies that I_{VSFG} is proportional to $\left|\chi_{eff}^{(2)}\right|^2$.

The spectral width of the visible pulse determines the spectral resolution of the VSFG. The spectral resolution of the VSFG spectra also depends on the interfering NRB of second-order susceptibility. The NRB is an undesired artifact because its amplitude and phase relative to the resonant signal cannot be controlled, however, in some cases, it can enhance the resonant VSFG signal. The interference of NRB to the resonant VSFG can affect the line shapes by making them asymmetric, shifting the peak frequency, and masking the resonant component in conventional VSFG measurements at low monolayer coverage. In certain cases, the NRB impedes the resonant signal, which leads to the misinterpretation of the measured vibrational modes [164-166]. Studies show that an appropriate choice of the shape of the narrow-band visible up-conversion pulse and its temporal delay with respect to the BB-MIR pulse can minimize NRB. The best spectral resolution and highest signal level are both achieved when the non-resonant narrow-band up-conversion pulse arrives with a non-zero time delay after the resonant MIR pulse [167]. However, we must also consider that time delay between MIR and VIS beams can also distort the BB-VSFG spectra [161-163]. To some extent, the contribution of the NRB can be reduced by selecting dielectric materials instead of metals as substrates. Metals and water – which are important materials for biomolecules – have huge non-resonant contributions.

3.3.4 High repetition rate BB-VSFG experimental setup

The VSFG spectrometers can be operated in two modes: i) the scanning-VSFG, and ii) broadband VSFG (BB-VSFG). In both the scanning-VSFG and the BB-VSFG, the incoming VIS beam is fixed to a quasi-monochromatic wavelength. In the case of scanning-VSFG spectroscopy, the narrow bandwidth IR beam is used in the spectral range to obtain a single spectrum. This type of spectrometer was introduced by Shen and co-workers [138, 168]. Many significant improvements were reported in the development of a scanning-VSFG spectrometer [169, 170]. In BB-VSFG spectroscopy, a broad bandwidth mid-infrared (MIR) beam and a narrow bandwidth VIS pulse are focused on the sample to obtain the VSFG spectrum. The unique benefit of the BB-VSFG spectrometer is that a broadband VSFG spectrum is obtained in a single shot acquisition without scanning the MIR frequency. Earlier BB-VSFG systems were built with a free-electron laser as the broad bandwidth MIR source [171, 172]. This system is limited in number across the globe since it requires a synchrotron facility. In 1998, a BB-VSFG system was developed using tabletop Ti: sapphire laser systems by Richter, Petralli-Mallow, and Stephenson [173]. Many advancements in BB-VSFG spectroscopy were reported by improving the stability, repetition rate, and peak intensity of the laser system [174]. In 2017, a new development in the field of BB-VSFG spectrometer driven by a 100 kHz repetition-rate laser system was demonstrated [3]. The two orders of magnitude higher repetition rate and the special scheme for generating narrow bandwidth visible laser pulse reported highly stable optical pulses which improved the sensitivity as well as the spectral resolution of the BB-VSFG setup compared to typical Ti: Sapphire laser systems [151].

3.3.5 Phospholipid model systems studied by VSFG measurements

VSFG measurements of biomolecules, such as proteins [155-161], peptides [162-166], DNA [167], polysaccharides [168], and phospholipids have been reported in the past decades. VSFG spectroscopic studies of phospholipid model systems were preformed previously to investigate domain formations [175], phase transitions [176], transition temperatures [177], membrane potential [138, 178-180], and kinetics of lipid flip-flop [81, 181, 182]. Phospholipid bilayers model systems such as supported lipid bilayer (SLB), [6, 183], black lipid membrane (BLM) [184], polymer-cushioned lipid bilayers [185], the hybrid bilayer with lipids in various compositions [186, 187], and lipid bilayers mixed with cholesterol [181, 187, 188] and engineered nanomaterials [180, 189-192] were studied using VSFG spectroscopy. Phospholipids were studied at different surface platforms. These include solid-water, air-solid, supported lipid bilayers, air-water [7, 193], liquid-liquid, and colloidal surfaces in liquid suspension interfaces. Often solid silica [194, 195], or calcium fluoride [5] were used as the

substrate. The window geometry and the prism geometry were employed usually in the VSFG experimental setup illustrated in Figure 3.8.

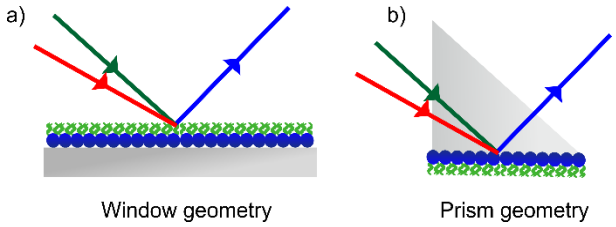

Figure 3.8 Scheme of a) window and b) prism experimental geometry employed in the VSFG setup.

The substrates most commonly employed for collecting VSFG signals are water [96], silica [132], or CaF_2 windows [100] or prisms [133, 134], and metal surfaces [135]. An external reflection such as monolayer on a solvent or window geometry [5, 183, 196], and total-internal or near-total reflection where a monolayer is put on a right-angled prism or a metal surface, is the most commonly employed surface platforms. Many groups employed the prism geometry for obtaining the VSFG spectrum of monolayers [100, 136] or bilayers [137, 138]. Studies show that changing the medium of contact from air to water, phospholipid bilayers or monolayers on prisms can enhance the VSFG resonant signals by tens of times [197].

A bilayer of phospholipids is two monolayers oriented in opposite directions. Symmetric or native bilayers are made of the same type of phospholipids on both leaflets of the bilayer. They are scarcely employed to study the properties of phospholipids as they are chiral and thus generate a low or no VSFG intensity [177, 183]. For this reason, several studies were conducted on asymmetric lipid bilayers. Lipid monolayers aligned at an interface give strong VSFG signals as they have $C_{\infty v}$ symmetry. Bilayers have a reflection plane parallel to the surface and have $D_{\infty h}$ symmetry. The $D_{\infty h}$ symmetry leads to the cancellation of second-order susceptibility [196], where VSFG signals from the upper and lower layer of the leaflets destructively interfere resulting in no VSFG signals [177]. For this reason, asymmetric bilayers with varying densities of deuterated lipids are used in one or both leaflets of the bilayers [81, 181, 198] to enhance VSFG signals. Figure 3.9 represents the symmetric and asymmetric lipid bilayer on the surface of the solid substrate.

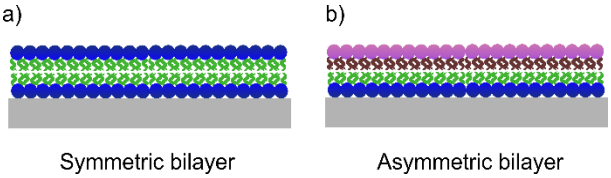

Figure 3.9 Scheme of a) symmetric b) asymmetric lipid bilayer on the surface of the solid substrate.

If we consider the phospholipid bilayer as two monolayers of chiral molecules oriented in opposite directions (see Figure 3.9), the structure's chirality removes the reflection plane and reduces the symmetry from $D_{\infty h}$ to D_{∞} [196]. In this case, the achiral susceptibility elements lead to cancellation and the chiral susceptibility elements do not lead to cancellation. Thus, the chiral elements do not lead to cancellation even if two monolayers are oriented in opposite directions at the interface. In this case, chiral VSFG may not be considered surface-specific if the intrinsic surface-specificity of second-order surface spectroscopy is narrowly defined as the requirement of cancellation in the second-order polarization due to the breakdown of up-versus-down centrosymmetry across an interface.

While employing an advanced BB-VSFG spectrometer to study phospholipids, there are many expectations. These expectations include the improved sensitivity of the spectrometer may allow a practitioner i) to obtain more vibrational modes, ii) better-resolved overtones and combinations of the vibrational resonances, and iii) to probe phospholipids prepared at low surface coverage. Since the repetition rate of the recently developed laser source is tunable up to 100 kHz, the spectral acquisition of the VSFG measurements can be reduced to an optimum time. If this is possible, the risk of phospholipids oxidation or degradation in ambient conditions can be reduced to a large extent. A practitioner should consider minimizing the pulse energy and maximizing the signal-to-noise ratio of the BB-VSFG spectrum while employing a 100 kHz repetition-rate laser-driven BB-VSFG spectrometer for probing biomolecules such as phospholipids. Since high pulse energy can cause photo-damages or chain melting in the phospholipids, optimization of experimental conditions must be performed. The doctoral thesis also focuses on studying the stability of phospholipids at different repetition rates and experimental conditions. The model systems prepared for the investigation are planar-supported lipids bilayers from native phospholipids as it is more realistic, and stable. The simple procedure and the stability of the solid-supported lipid bilayer on the window geometry are considered a factor for the studies. The solid-supported lipid bilayer is prepared on the CaF_2 window, as it is transparent in both MIR and VIS wavelengths of the BB-VSFG spectrometer. Phosphatidylcholine derived from egg-yolk (Egg-PC) is selected for the preparation of the planar-supported lipid bilayers. The heterogeneity of Egg-PC complicates the structural studies at the interface. This issue can be solved by investigating one-component phospholipids and mixing them with another phospholipid of interest which then can be used as a model system for pulmonary surfactants. The BB-VSFG measurements can suggest the interfacial structural changes and lipid chain packing. When there are few molecules at the interface, the structure of the alkyl chain and the phospholipid head groups are challenging to understand. The thesis

also focuses on studying the structure of alkyl chains and head groups of one-and two-component phospholipid monolayer at different surface coverage, and the water molecules entrapped between the CaF_2 and the phospholipid molecules.

4. Materials and Methods

4.1 Materials

The phospholipids 1,2-dipalmitoyl-*sn*-glycero-3-phosphocholine (16:0, DPPC), 1,2-dipalmitoyl-d62-*sn*-glycero-3-phosphocholine (16:0, DPPC-d62), and 1,2-dioleoyl-*sn*-glycero-3-phosphatidylcholine (18:1, DOPC), were purchased as lyophilized powder from Avanti Polar Lipids (Alabaster, AL, USA). 1,2-dialkyl-*sn*-glycero-3-phosphocholine (Egg-PC), phosphate-buffered saline (PBS, pH 7.4), chloroform, and methanol were purchased from Sigma-Aldrich (Germany). The lipids were stored at -20°C since they are sensitive to temperature. All stock solutions were prepared in chloroform:methanol mixtures. Adding a small amount of methanol to chloroform increases the solubility of charged lipids. For all purposes, Millipore water (18.2 MΩ cm) was used. The chloroform dissolves the plastic vails thus the lipid stock solutions were stored in a suitable container made of glass with Teflon sealing.

Numerous calcium fluoride (CaF_2) windows of 25.4 mm diameter were purchased from Korth Kristalle Gmbh. The planar-supported lipid mono-and bilayers were prepared on CaF_2 windows (in 110 orientation). The CaF_2 windows were cleaned using two methods: plasma cleaning and annealing. For plasma cleaning, the CaF_2 (110) windows were initially cleaned with toluene (Merck), ethanol (Merck), followed by Millipore water for 10 min in each solvent. Oxygen plasma cleaning was employed to remove the remaining solvent directly before the preparation of the supported lipid layers. This procedure is known to increase the hydrophilicity of the CaF_2 surface. [199] For the annealing method, initially, the CaF_2 windows were sonicated using ethanol and Millipore water. This was followed by annealing at 500°C for 2 hours, during which nitrogen was applied for 2 minutes in three steps to remove the impurities from the chamber i) at the beginning of annealing, ii) after one hour, and iii) at the end of 2 hours. The plates were

immersed in water for a maximum of 24 hours and isolated from water for the sample preparations.

4.2 Methods

4.2.1 Preparation of planar supported lipid bilayers

Lipid vesicles were prepared according to Ref. [36, 200]. The stock solution of 50 mM was prepared by dissolving the Egg-PC in an organic mixture of chloroform:methanol (1:1, v:v). The solution was dried under the stream of gaseous argon. The flow of argon creates a lipid film on the surface of the apparatus. The lipid film formed after the evaporation of the chloroform: methanol mixture was rehydrated in PBS buffer. The hydration of the lipid film creates vesicles of Egg-PC. Immediately, the vesicles were freeze-thawed seven times in liquid nitrogen at 37 °C, followed by, sonication and extrusion of the vesicles through a polycarbonate membrane. To yield small unilamellar vesicles, a polycarbonate membrane of pore size 100 nm was used. The prepared vesicle solution was passed 17 times through the membrane. The extrusion was performed using the mini extruder (Avanti Polar Lipids, Alabaster, AL, USA) that has several parts: two gas-tight syringes to hold a lipid solution where the parts are sealed to protect the syringe from leakage. The cleaning of all parts except the filter support and polycarbonate membrane is mandatory. A mild detergent followed by, tap water and deionized or distilled water are used for cleaning. The number of passes through the extruder determines the particle size distribution. After the preparation, the vesicles were stored in the refrigerator at -20° C and sonicated before each lipid bilayer preparation. For the preparation of lipid bilayers, the vesicles were diluted in the water (1:9, v:v) and sonicated for 10 min. After sonication, the lipid vesicles were deposited on the surface of the substrate. For all measurements, a CaF_2 window was selected as the solid substrate. The vesicle may undergo several changes on the surface of the substrate, and due to the previously mentioned vesicle fusion, lipid bilayers will form on the surface due to the hydrophilicity of the CaF_2 window. The prepared lipid bilayers adsorbed the solid substrate was gently washed with Millipore water to remove intact vesicles and excess bilayers. The BB-VSFG measurements were conducted immediately after the preparation of solid-supported lipid bilayers.

4.2.2 Preparation of planar supported lipid monolayers

Langmuir-Blodgett (LB) deposition was employed for the preparation of monolayers on the solid substrate. The stock solutions of DPPC, DOPC and its mixtures DOPC: DPPC (9:1, v:v),

DPPC: DOPC (9:1,v:v) dissolved in chloroform: methanol (9:1, v:v) were used for preparation. A few micro-liters of the corresponding phospholipid dissolved in chloroform:methanol mixture was spread on the surface of the water using a Hamilton syringe. Allocating 10 minutes, the organic solvents evaporate i.e., chloroform and methanol from the surface of the water in the LB trough leaving amphipathic phospholipid molecules at the air-water interface. The barriers were moved to the targeted surface pressure with extremely low compression speed (10 mm/s). The barriers were automatically maintained when the target surface pressure was attained. The initially inserted substrate was drawn vertically at a speed of 1 mm/min to transfer the lipid monolayer onto the CaF_2 window. The solid-supported monolayers were measured by using the VSFG spectrometer immediately after preparation.

Extreme care was taken with the cleanliness of the trough and its components before beginning the experiments. The trough and its components were cleaned using methanol or ethanol before preparing the monolayers. Any contaminants on the air-water interface would affect the monolayer ordering, therefore, the cleanliness of the Langmuir trough is vital to maintain stability throughout the experiments. The contaminants present on the trough can be detected on the compression isotherm (surface pressure as a function of area per molecule) as aberrations. Even a slight variation in the surface tension of the meniscus can be measured and displayed on the computer display. If contaminants are present, it is difficult to compress the monolayer more than 35 mN/m - 40 mN/m of surface pressure. After cleaning the trough, the barriers were placed on both edges of the trough and were manually initialized. Figure 4.1 (a-d) shows the scheme of the LB deposition of supported lipid monolayers on a solid substrate (e.g. CaF_2). The LB apparatus consists of several components: i) a trough made of Teflon that holds the sub-phase ii) a dyne probe made of metal iii) a pair of barriers made of Teflon and iv) a dipper that holds the substrate. The lipid molecules form monolayers at the air-water interface due to their hydrophobic nature. The monolayer formed can be transferred either by vertical (LB film) or horizontal dipping (Langmuir-Schaeffer film) onto a solid substrate depending on the hydrophilic-hydrophobic nature of the substrate.

The main purpose of the barriers is to maintain a constant number of molecules at the surface of the sub-phase for a particular surface area. The subphase was poured into the trough. Water was used as a subphase. The Langmuir trough was filled with water and left for a few minutes to stabilize the surface. For calibrating the system, a metallic rod called a dyne probe was used. Besides, the surface tension or surface pressure at interfaces can be measured by using the dyne probe. Before spreading the solution, the dipper holding the CaF_2 window was vertically

inserted into the water for the preparation of the lipid monolayer. All components of the Langmuir trough are computer and software controlled (Kibron, Helsinki). Figure 4.2 shows the Kibron MicroTrough XS apparatus that was used to prepare the solid-supported monolayers.

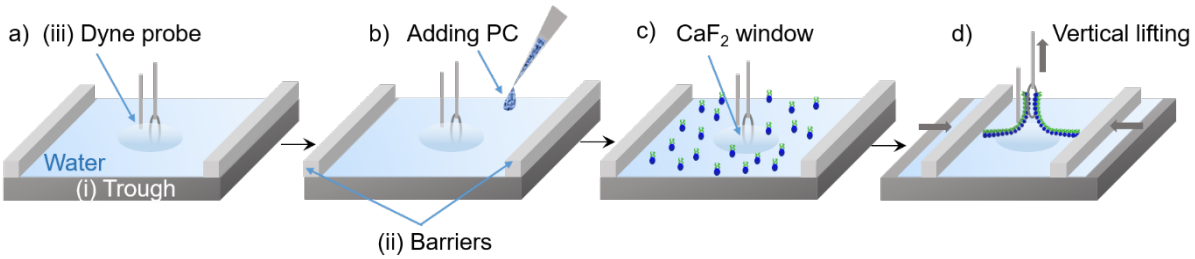

Figure 4.1 a)-d) shows the scheme of Langmuir-Blodgett deposition used for the preparation of solid-supported lipid monolayers. a) LB trough is filled with water and a calcium fluoride window is immersed into the water. b) Lipids in chloroform: methanol was injected into the water surface. c) Lipid molecules are spread at the water surface. d) Monolayer preparation using the vertical lifting of a calcium fluoride window.

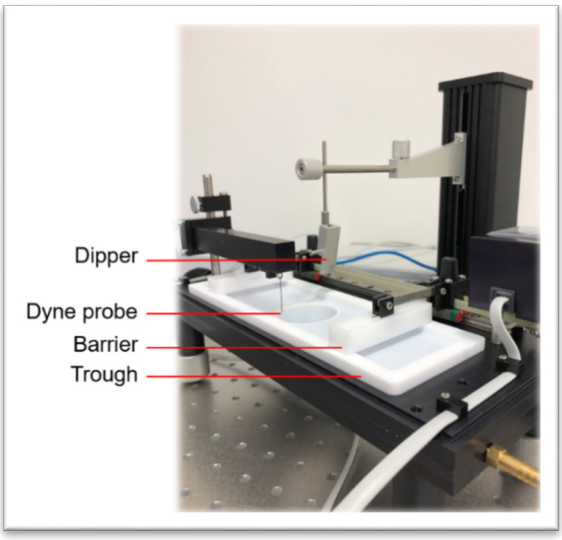

Figure 4.2 Kibron MicroTrough XS apparatus that was used to prepare the solid-supported monolayers.

4.2.3 Broadband vibrational sum-frequency generation spectrometer

Briefly, the whole setup is driven by a compact, turn-key Yb: KGd (WO_4) solid-state laser system (Pharos-SP, Light Conversion Ltd.) operating at a 100 kHz repetition rate. The total pulse energy (E_p), the pulse duration (τ), and the central wavelength of the laser system are 60 µJ and 180 fs, and 1.03 µm, respectively. The 6 W pump pulses from the laser system were split into two parts using a partial reflector.

I. Generation of picosecond visible pulse

From the 6 W laser femtosecond pump laser, a 2 W pump was used to generate narrowband picosecond visible (VIS) pulses. An efficient spectral compression scheme, the chirped sum-frequency mixing was employed to generate the VIS pulses [3, 201, 202]. The 2 W, 20 μJ, 180 fs pump laser beam was equally split into two parts. One part of the laser beam was fed to positive dispersion, and the other was subjected to negative dispersion. After introducing the positive and negative dispersions, the two beams were focused on a 1.5 mm thick, type I BBO crystal generating 5 μJ, transform-limited, 4.5 ps pulses. The pump-to-VIS conversion efficiency was ~50 % and the overall conversion efficiency was ~25 %. The produced 5 μJ VIS picosecond laser pulses were centered ~515 nm with excellent beam quality [3, 4]. The full width at half maximum (FWHM) was about 3 cm^{-1} that determines the spectral resolution in BB-VSFG measurements. For comparison, the typical Ti:sapphire-based BB-VSFG spectrometers have only a 15-30 cm^{-1} spectral resolution [154, 155, 193]. Figure 4.3 shows a schematic of the BB-VSFG experimental setup which was used for all VSFG measurements discussed in this thesis [3, 4].

II. Mid-infrared I beam: 2700 cm^{-1} - 3600 cm^{-1}

The remaining 4 W pump was split into two parts, one part about ~100 mW is used for generating seed pulses and the remaining amount was used for pumping the optical parametric amplifiers (OPA). For seeding the first OPA, supercontinuum pulses were generated in the wavelength range of 1300 nm–1700 nm, and further amplified in two OPA stages (see Figure 4.3 MIR I box). The pre-amplifier and the booster amplifier were based on 5 % MgO-doped, periodically poled Lithium Niobate (PPLN) crystals. Due to the applied collinear OPA geometry, nearly transform-limited, temporally, and spatially clean pulses were obtained in both the 1.52 μm signal and the 3.2 μm idler beamlines at average powers of 460 mW and 180 mW and pulse durations of 32 fs and 63 fs, respectively [3]. The center wavelength of the idler pulses around 3.2 μm was tunable by +/- 0.2 μm. The parameters of mid-infrared beam I (MIR I) which have the spectral full width of 800 cm^{-1}, [3, 4] are summarized in Table 4.1.

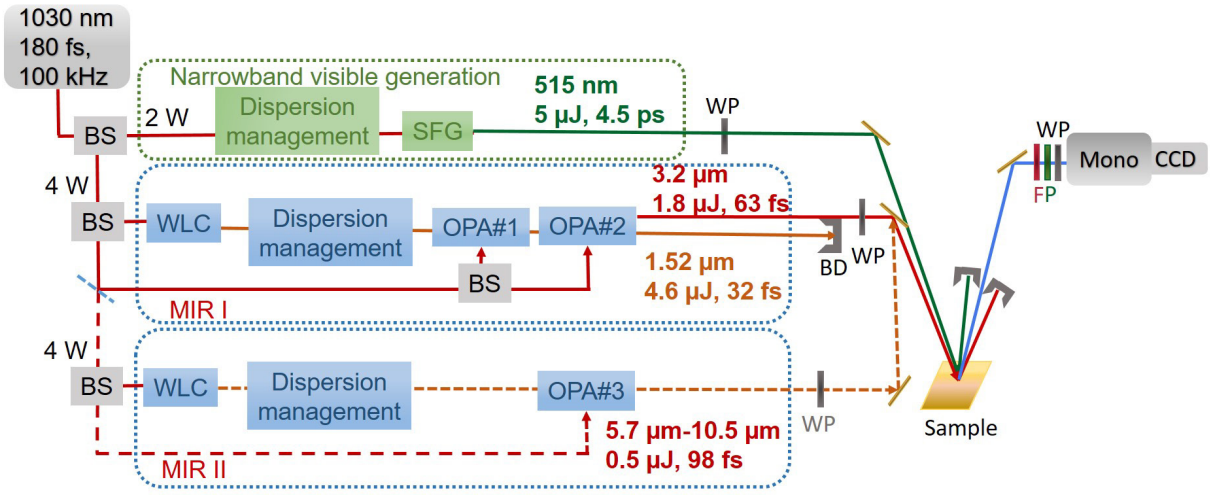

Figure 4.3 Scheme of the 100 kHz broadband vibrational sum-frequency generation spectrometer. BS: beam splitter, MM: magnetic mirror, WLC: white-light continuum generation unit, SFG: sum-frequency generation unit, OPA: optical parametric amplifiers, Mono: monochromator, F: filter, P: polarizer, BD: beam dump, WP: waveplate, CCD: charge-coupled device. MIR I and MIR II denote the two mid-IR beamlines.

III. Mid-infrared II beam: 900 cm^{-1} - 1800 cm^{-1}

Using a magnetic mirror, the switching between the MIR I and MIR II can be easily controlled (see Figure 4.3). The experimental parameters of MIR I and MIR II are summarized in Table 4.1. As discussed above, 4 W was also used to produce sub-100 fs tunable MIR II laser pulses. The MIR II beam was generated with the help of a single-stage OPA where the amplifier was based on $LiGaS_2$ crystal (cf. OPA#3 in Figure 4.3). About 100 mW of 4 W was applied to generate the seed pulse, and the remaining energy was used for pumping the single-stage OPA. Tilting the OPA crystal, the central wavelength of the MIR II laser pulses can be easily adjusted [4]. The generated MIR II beam was tunable in the spectral ranges of 900 cm^{-1}–1800 cm^{-1}. The pulse energies of the MIR II after the pulse compression unit, are measured to be 0.48 µJ at the central frequency of 7.8 µm and decreased to 0.1 µJ at center wavelengths of around 6.5 µm and 8.7 µm. More information about the parameters of the MIR II beam is given in Table 4.1.

IV. VSFG measurements

For BB-VSFG measurements (Figure 4.3), the few-cycle MIR I or MIR II and the 4.5 ps visible laser pulses were spatially and temporally overlapped at an Au (111) surface. The broadband MIR I beam and VIS pulses were focused on the sample using 50 mm and 300 mm focal length lenses at angles of incidence of 57° and 68°, respectively. The broadband MIR II beam between 5.7 µm and 10.5 µm was focused on the sample using a 40 mm focal length lens. The angle of

incidences of both the MIR beams was identical in all the cases. The generated sum-frequency signal was detected using a 320 mm spectrograph equipped with a Peltier-cooled, back-illuminated, deep-depletion CCD. In the experiments conducted with MIR I beamline, the E_p of MIR I and VIS at the sample plane were 0.55 μJ and 4.25 μJ, respectively. Moreover, the E_p of the MIR II and the VIS at the sample plane were 0.06 μJ-0.5 μJ and 4.15 μJ, respectively. The spot size of MIR I and MIR II pulses are 20 μm and 28 μm, respectively. The beam waists for VIS pulses were 150 μm and kept constant in the different spectral window. Both the MIR and the VIS parameters were kept constant for all experiments conducted in the corresponding spectral range.

Table 4.1 Beam parameters applied for the BB-VSFG measurements.

Parameters	VIS	MIR I	MIR II
Central wavelength [μm]	0.515	2.8-3.6	5.7-10.5
E_p [μJ]	4.15-4.25	0.55-2	0.06-0.5
T [fs]	4500	60	100
f [mm]	300	50	40
Spot size [μm]	150	20	28
FWHM [cm^{-1}]	3	800	150-300
OPA crystal		PPLN	$LiGaS_2$
Angle of incidence [deg]	68	57	57

E_p: pulse energy, τ: pulse duration, *f*: focal length, FWHM: full width at half maximum, OPA: optical parametric amplifier.

The BB-VSFG experiments were conducted in the window geometry in reflection mode where both the MIR and the VIS beam come from the same direction of the surface normal i.e., co-propagating geometry. The co-propagating geometry was preferred as there is only a minimal dispersion of the signal [150, 151]. Moreover, in this geometry, the generated VSFG beam and the VIS beam are almost collinear that enabling a straightforward approach to obtain the signal at the detector. In the experimental setup, zero-order half-wave plates were used to control the polarization of the excitation pulses. Additionally, a polarizer and a half-wave plate were employed for selecting the polarization component of the generated VSFG signal with respect to the plane of incidence on the sample where “p” represents the parallel and the “s” stands for the perpendicular polarization. Besides, it can also provide high diffraction efficiency in the grating spectrograph [3, 4]. The window geometry in reflection mode was employed in all the BB-VSFG experiments conducted in this thesis.

4.2.4 Data pre-processing

The calibration spectra were collected by overlapping the MIR and the VIS beams temporally and spatially on the Au (111) surface. The generated BB-VSFG signal from the Au (111) surface was obtained using a monochromator and a CCD camera. Figure 4.4 (a) illustrates the BB-VSFG spectra of Au (111) measured in the C-H, O-H, N-H vibrational stretching range and the fingerprint region. A 50 µm-thick polystyrene film was inserted in the path of the MIR beam while obtaining the BB-VSFG spectra from the Au (111) surface. This procedure was conducted to calibrate the x-axis (i.e., the wavenumber axis) of the BB-VSFG spectra. Figure 4.4 (b) illustrates the BB-VSFG spectra of polystyrene measured in the spectral range of 2700 cm^{-1}-3600 cm^{-1}, and 900 cm^{-1}-1400 cm^{-1}. Table 4.2 represents the polystyrene bands obtained from BB-VSFG spectra measured in the corresponding region. The vibrational modes of polystyrene from the literature were used as a reference to calibrate the x-axis of the collected BB-VSFG spectra [203].

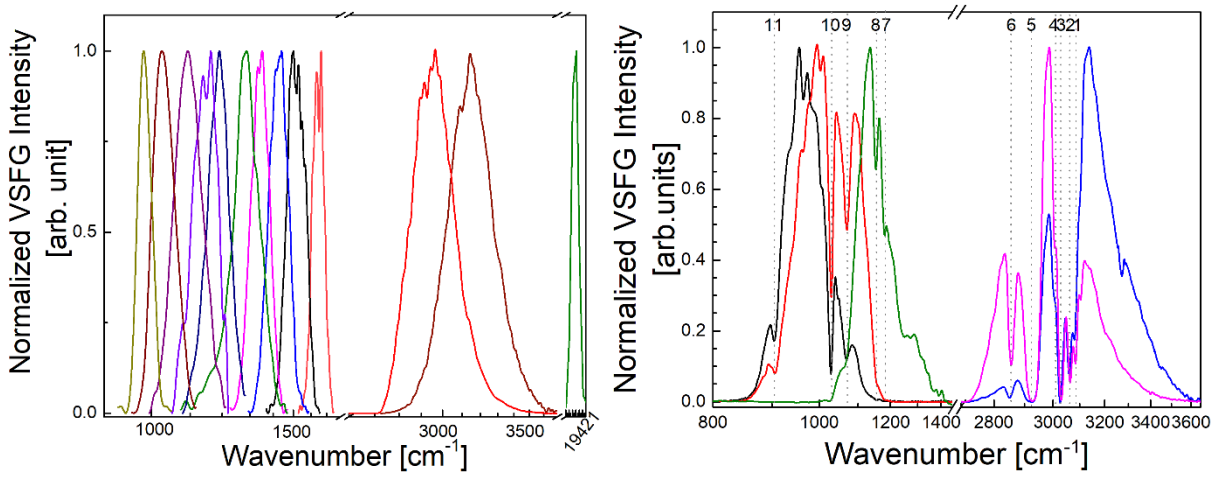

Figure 4.4 a) BB-VSFG spectra of Au (111) surface in the C-H, N-H, O-H i.e., 2700 cm^{-1}-3600 cm^{-1}, and the fingerprint region, 900 cm^{-1}-1400 cm^{-1}. The green spectra centered at 19421 cm^{-1} is the spectrum of the VIS beam. b) BB-VSFG spectra of Au (111) surface obtained while inserting a polystyrene thin film in the MIR beam path in the spectral range of 2700 cm^{-1}-3600 cm^{-1} (C-H, N-H, O-H) and 900 cm^{-1}-1400 cm^{-1} (fingerprint region).

In Figure 4.4 a) the lines with different colors are the Au (111) spectra obtained in different wavelengths. The spectral shape of the Au (111) spectra is identical to that of the MIR beam. The numbers in Figure 4.4 b) corresponds to the absorption bands of polystyrene summarized in Table 4.2. For the calibration of wavenumber, six absorption bands of polystyrene were used, (i.e., 3082 cm^{-1}, 3060 cm^{-1}, 3026 cm^{-1}, 3001 cm^{-1}, 2924 cm^{-1}, and 2850 cm^{-1}) in the C-H, N-H, and O-H vibrational stretching range. Additionally, five vibrational modes were used to

calibrate (i.e., 1181 cm^{-1}, 1154 cm^{-1}, 1069 cm^{-1}, 1028 cm^{-1}, and 905 cm^{-1}) in the fingerprint region (i.e. 900 cm^{-1}-1350 cm^{-1}). The wavenumber calibration was proceeded by the removal of spikes from the BB-VSFG spectra. The background spectra were measured by switching ON the VIS beam alone. The obtained background spectra were subtracted from the raw spectra followed by normalization of the sample spectra using the gold spectrum. Normalization of each spectrum with an Au (111) spectrum is a mandatory procedure that eliminates the shape of the broadband MIR beam to obtain a reliable intensity ratio in the entire spectral range. All the above data pre-processing was performed with the help of home-written MATLAB scripts. Each experiment has been repeated a minimum of three times to ensure similar results in all the cases. The BB-VSFG spectra were fitted with Lorentzian line profiles based on the equation expression 3.14, for more details see section 3.3.3, page 30 in the Research background, using a home-written IGOR Pro8 script.

Table 4.2 Polystyrene bands for wavenumber calibration [203].

No.	ω_v [cm^{-1}]	IUPAC	NBS	NIST	NPL
1	3082		X	X	
2	3060		X	X	X
3	3026	X	X	X	
4	3001		X	X	
5	2924	X	X		
6	2850	X	X	X	X
7	1181	X			X
8	1154	X	X	X	X
9	1069	X	X	X	
10	1028	X	X	X	X
11	905	X	X	X	

IUPAC: International Union of Pure and Applied Chemistry
NBS: National Bureau of Standards
NIST: National Institute of Standards and Technology
NPL: National Physical Laboratory

5. Applicability of high repetition-rate BB-VSFG in bio-analytical chemistry

This chapter is based on the publication *J. Chem. Phys.* 2018, 148, 104702, doi: 10.1063/1.5016629.

Vibrational sum-frequency generation spectroscopy (VSFG) is a surface-specific analytical tool widely used to study the structure, conformation, orientation, and composition of molecules at interfaces. The limitations of the standard broadband VSFG (BB-VSFG) spectrometer are its spectral resolution and sensitivity. Recently, to overcome this challenge, a 100 kHz repetition-rate BB-VSFG spectrometer was developed in SALSA Photonics Lab, Humboldt Universität zu Berlin, Germany [3]. In this chapter, the first application of the state-of-the-art high repetition-rate BB-VSFG (HRR-BB-VSFG) spectrometer was performed. For studying the applicability of the HRR-BB-VSFG spectrometer, a model of the biological membrane such as the multi-component phospholipid bilayer was employed.

The hydrocarbon chains of phospholipids were previously studied by several groups and reported that they exist in either all-trans configurations or packed in near-trans conformations in the crystalline form [15, 103, 175, 204]. The heating of phospholipids causes thermal phase transitions, this includes gel-to-liquid crystalline, sub-transition, pre-transition, and ice-melting induced phase transition. During the phase transitions, the chains undergo large structural rearrangements and disrupt the order in the phospholipid assemblies. This order/disorder is reflected in the vibrational spectrum, which can be in turn correlated to the population of gauche conformers in the hydrocarbon chains. The changes can be observed as variations in the intensities and frequencies of C-H stretching modes in the spectral range between 2800 cm^{-1} and 3000 cm^{-1}. Therefore, the spectrometer was tuned in this spectral range to monitor the

stability of the phospholipid bilayers during the BB-VSFG measurements. The intense laser pulses can cause reorientation, and/or photo-induced damages to the phospholipids. This chapter elaborates on the optimization of experimental conditions for studying the phospholipids, the stability of the phospholipids during the measurements, and the interfacial structure of phospholipid bilayers at the air-CaF_2 interface.

5.1.1 Sample preparation

In this work, phosphatidylcholines (PCs) derived from egg-yolk of chicken (Egg-PC) were used to prepare planar-supported bilayers. They are model systems that were widely employed for investigating the physicochemical properties of biological membranes. Egg-PC is a heterogeneous mixture of different phospholipids, where the composition of fatty acids is represented in Table 5.1.

Table 5.1 The composition of fatty acids in Egg-PC derived from egg-yolk. The parenthesis contains the number of carbon atoms and the pair of unsaturation in their alkyl chains.

Types of fatty acid in Egg-PC	Fatty acid composition (%)
Palmitic (16:0)	32.7
Palmitoleic (16:1)	1.1
Stearic (18:0)	12.3
Oleic (18:1)	32.0
Linoleic (18:2)	17.1
Other	< 2.0

The above Table 5.1 is based on the datasheet provided by Avanti Polar Lipid Inc. This composition of Egg-PC may vary depending on the sources. The major constituents in the Egg-PC mixture are palmitic acid (16:0) and oleic acid (18:1) with the fatty acid chain attached to the *sn*-1 and *sn*-2 positions. The fatty acid chains attached to *sn*-1 are predominantly saturated, and consist of 16-or 18-carbon atoms, and the lipids with higher degrees of unsaturation have their chains attached to the *sn*-2 position, where they consist of 18- or 20-carbon atoms.

The stock solution of Egg-PC was prepared by dissolving their lyophilized powder in the chloroform:methanol mixture. The solution was kept under nitrogen gas flow to evaporate the organic solvents, where a thin film was formed on the bottom of the flask. This film was rehydrated with the PBS buffer solution. After rehydration, the solution was freeze-thawed several times and finally extruded through two polycarbonate membranes to obtain unilamellar vesicles. The detailed protocols for the sample preparation were elaborated in Materials and

Methods (see section 4.2.1, page 38). The schematic of small unilamellar vesicles preparation is shown in Figure 5.1.

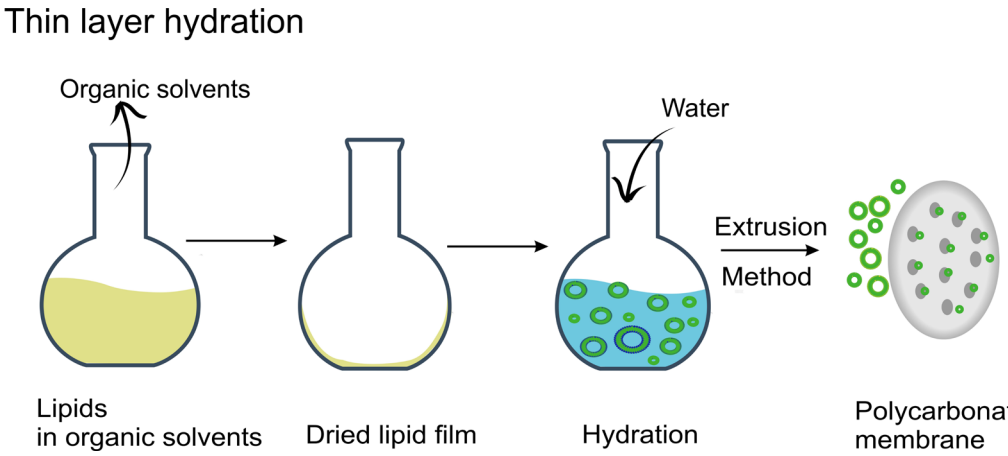

Figure 5.1 The scheme of lipid vesicle preparation: the lipids were dissolved in chloroform:methanol, dried under nitrogen gas, rehydrated with PBS buffer, extruded through polycarbonate membrane to create homogeneous unilamellar vesicles.

A 20µL of unilamellar vesicles prepared by thin layer hydration method was dropped each time on the CaF_2 window to prepare the planar-supported Egg-PC bilayers, where the vesicles adsorb and rupture to form bilayers on the window. This method is the so-called vesicle fusion approach. After the preparation of bilayers, the BB-VSFG spectra were measured as soon as possible.

5.1.2 BB-VSFG measurements and data pre-processing

The spectrometer was adjusted in the spectral range between 2800 cm^{-1} and 3600 cm^{-1} to observe the C-H and O-H vibrational modes. The vibrational spectra were obtained by spatially and temporally overlapping the MIR and VIS beams on the samples, where all the spectra were collected in the reflection mode. Additional details about the setup were given in Materials and Methods (section 4.2.3, page 40). For the experiments, the incident pulse energy of the MIR and VIS pulses was 0.55 µJ and 4.25 µJ, respectively. The measurements were conducted at the air-CaF_2 interface. The spectral resolution of the BB-VSFG spectrometer used for the investigation was ~3 cm^{-1}, and the spectral window was 800 cm^{-1} broad. Briefly, the measurements were carried out as follows. First, the BB-VSFG spectra of polystyrene and Au (111) surface were obtained for calibration of the sample spectra. These absorption bands were obtained by inserting a 50 µm thick polystyrene film in the path of the MIR beam while obtaining the BB-VSFG spectra on an Au (111) surface. Then, the BB-VSFG spectra of Egg-

PC bilayers were obtained by focusing on MIR and VIS beams. Last, the spectra were pre-processed to obtain spectral information. For the pre-processing, the wavenumber axis was initially calculated from the wavelength axis. After calculating the wavenumber axis, the spectra were calibrated with absorption bands of polystyrene, based on the NIST database. As a next step, all spikes were removed from the spectra. This is followed by, subtracting the averaged background spectra from the raw BB-VSFG spectra. These background spectra were obtained by keeping the VIS beam in ON condition. The sample spectra were normalized using gold spectrum, this procedure is mandatory as it provides a reliable intensity ratio in the entire spectral range. All the above-mentioned processes were performed using home-written MATLAB scripts.

The spectral assignments were done after fitting the Lorentzian line profiles on the BB-VSFG spectra. The fitting was performed using IGOR-Pro software.

5.1.3 Optimum time delay for the HRR-BB-VSFG measurements

To find an optimum time delay between MIR and VIS pulses, the BB-VSFG spectra of planar Egg-PC bilayers were measured at four different time delays (0 ps, 0.67 ps, 1.67 ps, 2.67 ps) using ppp polarization combination (see Figure 5.2 dots). This optimum time delay was achieved by delaying VIS pulses after the MIR beam.

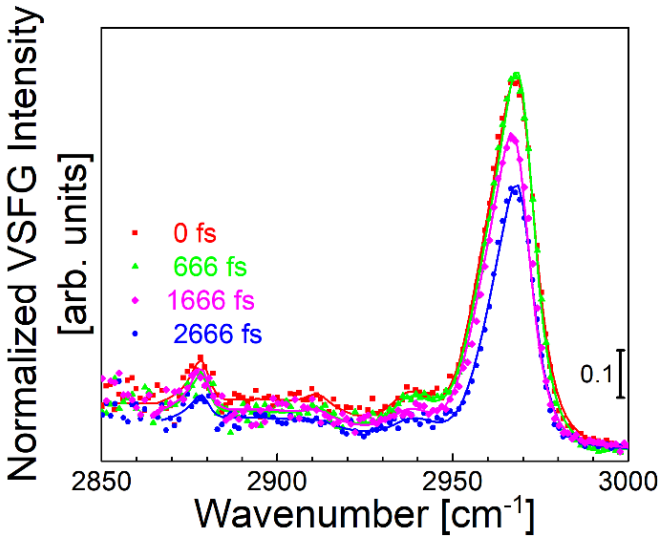

Figure 5.2 Normalized BB-VSFG spectra of Egg-PC bilayers on CaF_2 plate at different time-delays between the MIR-VIS pulses for 0 ps (red), 0.67 ps (green), 1.67 ps (magenta), 2.67 ps (blue) in the C-H stretching vibrational range. The dots and the lines represent the experimentally measured and fitted BB-VSFG spectra, respectively.

The BB-VSFG spectra obtained were fitted with Lorentzian line profiles, according to expression 3.14 (for more details see section 3.3.3, page 30 in the Research background). The sum of six Lorentzian line profiles was fitted to extract the central frequencies, line widths, and amplitudes of the vibrational modes, and the parameters are summarized in Table 5.2. The traces denote the sum of the Lorentzian line profiles (see Figure 5.2).

Table 5.2 Central frequencies, line widths, and amplitudes of the fitted BB-VSFG spectra of Egg-PC at 0 ps, 0.67 ps, 1.67 ps, 2.67 ps time-delays. ω_v, Γ_v, and A_v represent the central frequency, line width, and amplitude of the vth vibrational mode, respectively.

ω_v [cm^{-1}]	Γ_v [cm^{-1}]	A_v [0 ps]	A_v [0.67 ps]	A_v [1.67 ps]	A_v [2.67 ps]
2879±0.2	3.2±1.2	0.4±0.2	0.4±0.2	0.5±0.2	0.3±0.1
2901±0.3	34±2	9.4±0.2	8.6±0.2	8.2±0.2	7.4±0.2
2911±0.9	5±1.5	0.3±0.2	0.3±0.1	0.2±0.1	0.15±0.1
2937±2.9	9±0.1	-4.56±0.5	-4.2±0.6	-4.0 ±0.6	-3.7±0.9
2955±1.2	10.4±0.1	-4.3±0.6	-4.1±0.5	-4.0±0.6	-3.4±0.5
2970±0.5	6.8±0.3	5.8±0.2	5.5±0.1	5.0±0.1	4.6±0.1

From Table 5.2, the absolute values of amplitudes of each spectral band decrease as the time delay between the MIR and the VIS beam increases from 0 ps to 2.67 ps. These observations were in agreement with those reported earlier [164, 166, 205]. The results showed that spectral intensity at 0.67 ps was the highest with a slight reduction in the non-resonant background (NRB). Therefore, 0.67 ps was considered as an optimum time delay for all measurements conducted in this chapter.

The VIS pulse shape, duration, and timing can significantly affect the spectral resolution of BB-VSFG spectra [151, 163]. When the delay between the MIR and VIS pulses is zero (the τ=0) in the BB-VSFG measurement, the non-resonant contribution is fully up-converted, where half of the VIS pulse is utilized to up-convert the resonant contribution of the response. The truncation of the resonant part results in i) spectral broadening, ii) decreased BB-VSFG signals, and iii) strong non-resonant signals that can distort and even overwhelm the resonant signal of interest. This is because the non-resonant part is up-converted by the strongest portion of the VIS pulse, whereas the resonant part is up-converted by the decaying tail. Previous studies have shown that introducing a positive time delay between the VIS pulse to the resonant MIR pulse is an appropriate strategy to enhance the resonant signals [165, 167]. The delay between the VIS and MIR pulses leads to increases in the overall BB-VSFG signal level. In this case, a larger portion of the VIS pulse is used for up-conversion, where the truncation of the resonant

signal is minimized. Meanwhile, the non-resonant part of the response is minimized as it is up-converted by the weaker leading edge of the VIS pulse.

The lineshape broadening and phase flipping are the artifacts caused by the time delay between the VIS and MIR pulses [161, 162]. The signs of the amplitude remain constant, indicating that no phase flipping was observed between the neighboring bands at different time delays (see Table 5.2). In this work, this result was only achieved as a result of the high resolution (3 cm^{-1}), transform-limited VIS pulses [3]. Shalhout et al. demonstrated experimentally and theoretically the effect of the time delay on the broadband VSFG spectra with two nearby vibrational modes [161]. The studies showed that the relative phase between the two coherently excited vibrational modes flips at a certain time delay. Lagutchev et al. reported that the asymmetric shape of the VIS pulse can suppress the NRB and improve the VSFG signal by a factor of 20 [166]. Curtis et al. reported that suppression of the NRB signal leads to other distortions in the VSFG signal, which can complicate the analysis of the VSFG spectra [165]. Wang et al. estimated the broadening of the spectral lineshapes by the Gaussian VIS pulse of linewidths from 0.6-15 cm^{-1} [151, 163]. A ps VIS probe pulse with our spectral FWHM causes less than 1 cm^{-1} broadening for our extracted Lorentzian vibrational spectral bands.

5.1.4 Signal to noise ratio of HRR-BB-VSFG spectrum

As this is the first application of HRR-BB-VSFG spectroscopy, it is crucial to study the signal-to-noise ratio (SNR) of the spectrum. To investigate the SNR, the spectra of planar Egg-PC bilayers on CaF_2 substrate were collected at different acquisition times and averaged. The measurements were collected using a ppp polarization combination (see Figure 5.3). The single, 10, and 100 times averaged BB-VSFG spectrum obtained with an integration time of 10 s and 30 s, 60 s, 100 s, and 200 s are shown in Figure 5.3 a and b. The BB-VSFG spectra shown below were obtained at the 100 kHz laser repetition rate and 800 cm^{-1} broad.

The SNR values calculated for different integration times are summarized in Table 5.3. The peak at 2965 cm^{-1} was selected to estimate the SNR because of its minimum overlap with the neighboring modes. The root-mean-square (RMS) noise was obtained from the standard deviation of the baseline value between the range of 3000 cm^{-1} and 3100 cm^{-1} of the spectra. The low SNR at the edges of the single spectrum is due to the low energy density of the MIR beam (Figure 5.3 a, blue).

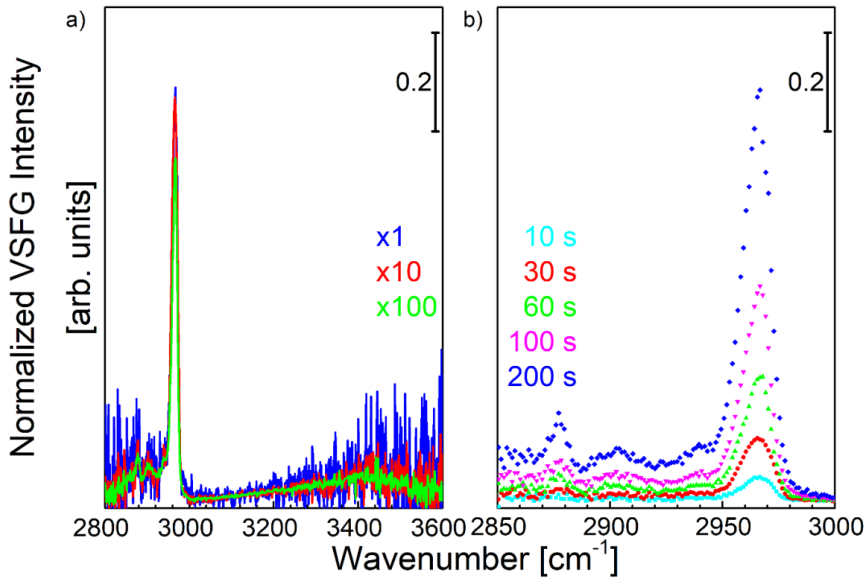

Figure 5.3 Normalized 100 kHz BB-VSFG spectra of the planar Egg-PC bilayers at the air-CaF_2 interface: a) single spectrum (blue), 10 (red), and 100 (green) times averaged spectra b) obtained at the integration times of 10 s (cyan), 30 s (red), 60 s (green); 100 s (magenta), 200 s (blue).

Table 5.3 Calculated signal-to-noise-ratio (SNR) for different spectral acquisition conditions of Egg-PC bilayer BB-VSFG spectra are listed below.

Acquisition time [s]	10 s	30 s	60 s	100 s	200 s	10 s ×10	10 s ×100
SNR	80	154	231	275	283	190	500

The increase in the integration time improved the SNR of the spectra (see Figure 5.3b) [206]. The BB-VSFG spectra of Egg-PC revealed that the SNR could be improved by a few orders of magnitude while employing a 100 kHz BB-VSFG spectrometer compared to standard VSFG spectrometers, which is the limitation of conventional BB-VSFG spectrometer [207]. Our results also revealed that the BB-VSFG spectra can be collected using low (second to the millisecond) integration times without compromising the SNR of the spectra. The high SNR obtained from the phospholipids bilayers was surprising because of three reasons: the experimental geometry used, the bilayers symmetry, and the phospholipid composition.

As explained in the Research background, the window geometry was selected over the prism geometry for the measurements. The results presented in this work revealed that it is possible to achieve high SNR spectra even at the air-CaF_2 interface. In a more general sense, the result revealed that the geometry of surface platforms does not limit the phospholipid studies using

BB-VSFG spectroscopy. In earlier studies, phospholipid bilayers were prepared either on prism geometry and/or immersed in water to improve the signal-to-noise ratio of the VSFG spectra [183, 194]. Zhan Chen et al. found that the VSFG signal intensity of the phospholipid bilayer in contact with water is around 34 times stronger compared to that in the air [197]. They found that the main reason for the signal enhancement is the increased Fresnel coefficients of the water-lipid interface, rather than the changes in the molecular orientation, which only slightly changes the VSFG signal. Their results revealed that the contact medium can greatly influence the VSFG signal intensity. Xiaolin Lu et al. noticed that the VSFG signal of phospholipid bilayer/monolayer obtained using prism and window geometry are very different [194]. They found that the reason for different VSFG spectra at different polarization combinations is the combined effect of interfacial Fresnel coefficients and the second-order nonlinear susceptibility tensor components [194]. In the ssp polarization combination, the absolute value of the Fresnel coefficient for the window geometry is much smaller than that for the prism geometry. In the case of the ppp polarization combination, the total internal reflection changes the spectral feature as a result of Fresnel coefficients and the interplay between the different χ_{ijk} tensor terms.

Based on the literature review, the intensity of VSFG spectra of the planar bilayer reported was either very low [183] or without any signal [177]. The asymmetric bilayers are generally used to improve the SNR [177]. As elaborated in the Research background, this is because the intensities from the upper and lower leaflets of the symmetric phospholipid cancel each other which may lead to destructive interference, due to the symmetry conditions of the BB-VSFG. The phospholipid bilayers used in this work were PCs consisting of different chain lengths and identical head groups, as discussed at the beginning of this chapter. Our results proved that the Egg-PC bilayers are a good model system for HRR-BB-VSFG spectroscopy. The high SNR of the BB-VSFG spectra indicate that the bilayers were asymmetric at the interface. Recently, Olenick and coworkers [183] reported the VSFG spectra of the symmetric lipid bilayer with both scanning and for a 1 kHz spectrometer. The spectral acquisition time they used to obtain the VSFG spectra was ~120 minutes using either of the spectrometers. They reduced the integration time to 20 minutes where an average of 5 spectra was integrated over 4 minutes. Comparing the spectra in this work to theirs [183], our spectra have high SNR. In conclusion, the BB-VSFG spectra can be collected with high SNR from a heterogeneous, planar-supported Egg-PC bilayer on CaF_2 window geometry at the air interface irrespective of all these factors. These results pointed out that the BB-VSFG employed for the measurements has high sensitivity while the acquisition time of the measurements were also significantly reduced compared to a typical VSFG spectrometer.

5.2 BB-VSFG spectra of Egg-PC bilayer at different laser repetition rates and illumination conditions

To study the stability of phospholipids, the measurements were performed at different laser repetition rates. The BB-VSFG spectra were obtained in four polarization combinations such as ppp, ssp, pss, sps at repetition rates of 5 kHz, 10 kHz, 50 kHz, and 100 kHz. The acquisition time for collecting BB-VSFG spectra was varied accordingly with the repetition rate (see Figure 5.4). The desired repetition rate was achieved by adjusting the repetition rate of the pump laser with the integrated pulse picker and maintaining constant pulse energy. That is, a constant number of laser pulses were ensured on the sample at all the employed laser repetition rates.

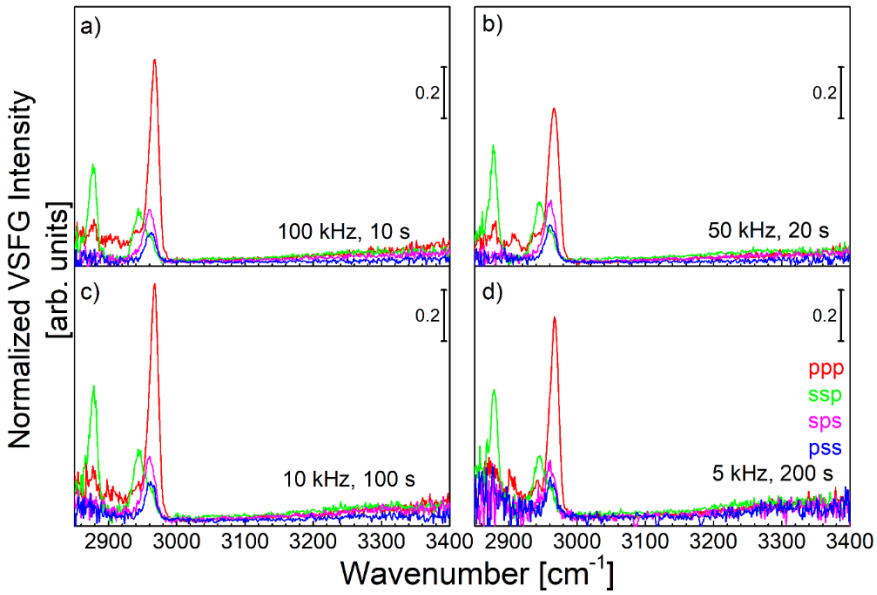

Figure 5.4 Normalized BB-VSFG spectra of the planar supported bilayers of Egg-PC on a CaF_2 plate measured at ppp, ssp, sps, and pss polarization combinations at different laser repetition rates and acquisition times: a) 100 kHz, 10 s; b) 50 kHz, 20 s; c) 10 kHz, 100 s; d) 5 kHz, 200 s. The acquisition time was adjusted to ensure a constant number of laser pulses.

The SNR of a single BB-VSFG spectrum obtained at laser pulse repetition rates of 100 kHz, 50 kHz, 10 kHz, and 5 kHz were calculated in the same way as it was discussed in the 100 kHz measurements and the results were summarized in Table 5.4.

Table 5.4 Calculated signal-to-noise-ratio (SNR) of single BB-VSFG spectrum obtained at 100 kHz, 50 kHz, 10 kHz, and 5 kHz laser repetition rates are listed below.

Repetition-rates	100 kHz	50 kHz	10 kHz	5 kHz
Acquisition time [s]	10	20	100	200
SNR	76	55	50	37

From Table 5.4, the SNR calculated for a BB-VSFG spectrum obtained at 200 s integration time and of 5 kHz laser repetition rate was 37 (see Table 5.4). Besides, the SNR for the average of ten spectra is 129 which was measured by applying two orders of magnitude lower average power with shorter integration times compared to typical 1-5 kHz BB-VSFG spectrometers. The results showed that the SNR of ten times averaged spectra are similar to the values found in the literature and these results were achieved by an order of magnitude lower average power and integration time. The 100 kHz laser repetition-rate provides the highest value of SNR (see Table 5.4). The result showed that the SNR of the BB-VSFG spectra increases with the laser repetition rate at a constant number of laser pulses and pulse energies incident on the sample. There is a trade-off between laser repetition rate, average power, and thermal damages.

Several studies showed that the photo-damage and higher-order processes occur at high excitation intensity [208-210]. Considering VSFG, the photo-damage mechanisms could be different as it has two optical pulses of femtosecond (fs) and picosecond (ps). The ps pulses in the VIS spectral range match the Raman energy levels. The fs pulses in the MIR spectral range initiate vibrational absorption through IR processes, which contribute to additional damage to the sample. The intense laser pulses at the focal point may generate plasma through multiphoton processes and destruct the biological sample [211, 212]. In general, lasers with low repetition rate, high pulse energy, and low average power were used in the experiments to obtain efficient signals and to potentially reduce thermal effects. Based on the literature review, the laser parameters generally employed by several research groups for the experiments are listed in Table 5.5. In our case, ultrashort laser pulses with a 100 kHz laser repetition rate were employed for VSFG signal generation. To secure the advantage of a high repetition rate we should remain below any possible nonlinear photo-damage threshold. So far, no 100 kHz laser repetition rate study has been reported for VSFG spectroscopy.

The pulse energies of both MIR and VIS pulses listed above were used for measuring molecules that have no absorption in the VIS range of the spectrometer (see Table 5.5). In order to study photosensitive chromophores, doubly resonant VSFG spectroscopy is used, where the power of the VIS was kept as low as possible to minimize photo-degradation. The VIS and MIR powers measured on the sample are generally 0.14-2 mW and 3-4 mW, respectively [213-215]. The pulse energies used in typical VSFG experiments were in the range of 2 to10 mW and 4 to 425 mW for MIR and VIS pulses, respectively. In the case of the 100-kHz setup, the pulse energies were much less but the average powers were higher than the typically applied parameters because of the applied high laser repetition rate (see Table 5.5).

Table 5.5 VSFG experimental setup developments and the laser parameters used for the measurements in the spectral range of 2800-3600 cm^{-1}.

Timeline	Laser [kHz]	Pulse energy IR [μJ/pulse]	Pulse energy VIS [μJ/pulse]	References
1987	-	-	-	[216]
1996	5 Hz	10	8	[172]
1998	1 kHz	3	4	[173]
2001	1 kHz	7.7	240	[154]
2004	1 kHz	1-3	425	[169]
2007	1 kHz	10	20	[166]
2008	1 kHz	2-3	10-15	[217]
2009	5 kHz	2.3-4	43	[155]
2017	100 kHz	0.55-2	4.15-4.25	[3, 4]

We attribute the higher SNR at higher repetition rates to the lower accumulated dark noise of the CCD camera used at shorter integration times. We also noted that the accumulated dark noise can be reduced by using other types of CCD cameras i.e., iCCD, iEMCCD. The average background intensity measured was 1.5×10^3 counts at repetition rates of 5 kHz and 10 kHz (see Figure 5.4 c-d), where it was ~ 10^3 counts at 100 kHz (see Figure 5.4 a). The total noise, dark current noise, and readout noise added in quadrature were about 5.5 e^- per pixel RMS over a 200 s integration time at 5 kHz laser repetition rate and decreased to 4.057 e^- per pixel over a 10 s integration time at 100 kHz (see Figure 5.3 a versus d). The average powers generally applied were 20 mW / 215 mW (MIR / VIS) whereas the SNR for the 5 kHz laser repetition rate was 110-170 [154, 155, 196]. The measured average power for different laser pulse repetition rates keeping the pulse energy constant is shown in Table 5.6, where the pulse energy is simply the average power measured per laser repetition rate of the pulses.

Table 5.6 Applied pulse energies and average powers at different laser repetition rates in the HRR-BB-VSFG measurements.

Repetition rate [kHz]	AP_{VIS} [mW]	AP_{IR} [mW]	PE_{VIS} [μJ]	PE_{IR} [μJ]
100	425	55	4.25	0.55
50	213	28	4.25	0.55
10	43	6	4.25	0.55
5	21	3	4.25	0.55

It should be noted that the average power on the phospholipid bilayers decreases proportionally with a decrease in laser repetition rate as summarized in Table 5.6. Our BB-VSFG spectra were obtained only with an average power of 2.75 mW / 21 mW (MIR / VIS) at a 5 kHz repetition

rate where typically 20 mW/ 215 mW (MIR / VIS) were used at the same repetition rate, respectively [154, 155]. It should be noted that in the present experiments the applied average power at 100 kHz is a few times higher than the typical values applied in 1-5 kHz laser repetition rates [196]. Another point of discussion is the time for the acquisition of a vibrational spectrum. Here, the time for obtaining the BB-VSFG spectra of all the polarization combinations was about 20 to 30 min. Only a single spectrum can be collected in the case of scanning-VSFG during this acquisition time. While employing such low repetition rate spectrometers, studies show that the VSFG spectra of unsaturated lipids in ambient conditions change over time [218]. For this reason, the application of the high repetition rate of VSFG spectrometers helps to investigate molecular layers at interfaces that change their structure over time.

5.2.1 Stability of Egg-PC bilayer at different laser repetition rate

To investigate systematically the influence of the laser repetition rate on the phospholipids, the BB-VSFG spectra of Egg-PC were measured at 5 kHz, 10 kHz, 50 kHz, 100 kHz. The ppp polarization combination spectra were selected for the analysis and fitted using the sum of six Lorentzian line profiles (see Figure 5.5). The central frequencies, the amplitudes, and the line widths of the four laser repetition rates such as 5 kHz, 10 kHz, 50 kHz, 100 kHz are given in Table 5.7.

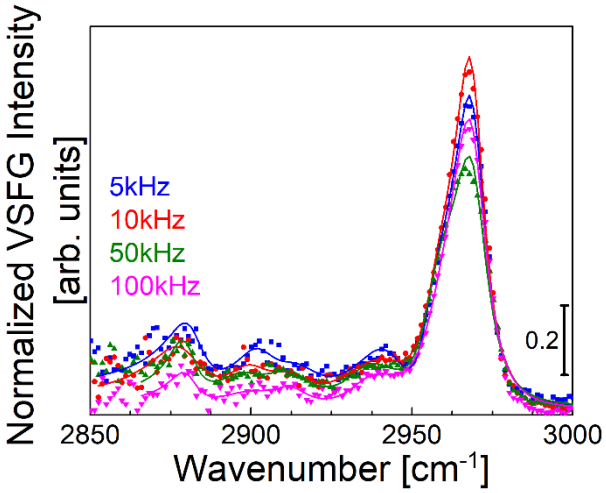

Figure 5.5 BB-VSFG spectra of planar supported bilayers of Egg-PC were collected using ppp polarization combination at 5 kHz, 10 kHz, 50 kHz, and 100 kHz.

Table 5.7 Fit parameters for Lorentzian line profiles in ppp polarization combination as a function of laser repetition rate, where ω_v Γ_v and A_v represent the central frequency, line width, and the amplitude of the vth vibrational mode, respectively.

ω_v [cm^{-1}]	Γ_v [cm^{-1}]	A_v [100 kHz]	A_v [50 kHz]	A_v [10 kHz]	A_v [5 kHz]
2880.0±1.2	8±2	1.1±0.2	1.4±0.1	2.4±0.1	1.7±0.1
2901.5±1.9	10±1.9	1.5±0.2	1.4±0.2	1.1±0.1	1.3±0.1
2914.0±1.3	5±1.5	0.9±0.1	1.5±0.4	1.2±0.1	1.4±0.1
2938.0±2.0	11±1.4	3.0±1.1	2.6±1.2	4.4±0.1	5.2±0.1
2956.0±1.1	7.9±1.4	-5.7±0.7	-5.7±2.2	-7.0±0.1	-6.3±0.1
2969.3±0.2	6.5±0.2	7.2±0.2	5.4±0.5	5.8±0.1	5.4±0.1

The values of wavenumbers and linewidths shown in Table 5.7 are the averages obtained from the four laser repetition rates. The position of the central frequency remains the same in all the BB-VSFG spectra. The parameters of the Lorentzian line profiles provide accurate values of vibrational modes than the features from the BB-VSFG spectra. It can be visible from the spectra that the NRB of 100 kHz laser repetition rate spectra was minimal (see, Figure 5.5, magenta). The highest amplitude at 2969 cm^{-1} was observed for a 100 kHz repetition rate indicate that this repetition rate provides better resolved spectral features compared to the standard VSFG spectra. The amplitudes of vibrational modes also suggest that the Egg-PC bilayers were stable during the measurements (see Table 5.7)

5.2.2 Stability of Egg-PC bilayers at different illumination conditions

The BB-VSFG spectra of the bilayers were recorded with an integration time of 10 s at 100 kHz over a time interval of 20 min (see Figure 5.6 and Figure 5.7). Three cases were considered: i) the VIS beam always ON and MIR switched ON and OFF ii) the MIR beam always switched ON and VIS switched ON and OFF, and iii) the VIS and MIR beams simultaneously ON and OFF during all the measurements (i-iii). The spectral intensity of vibrational modes was monitored over time to examine the changes in the BB-VSFG spectra of the bilayer.

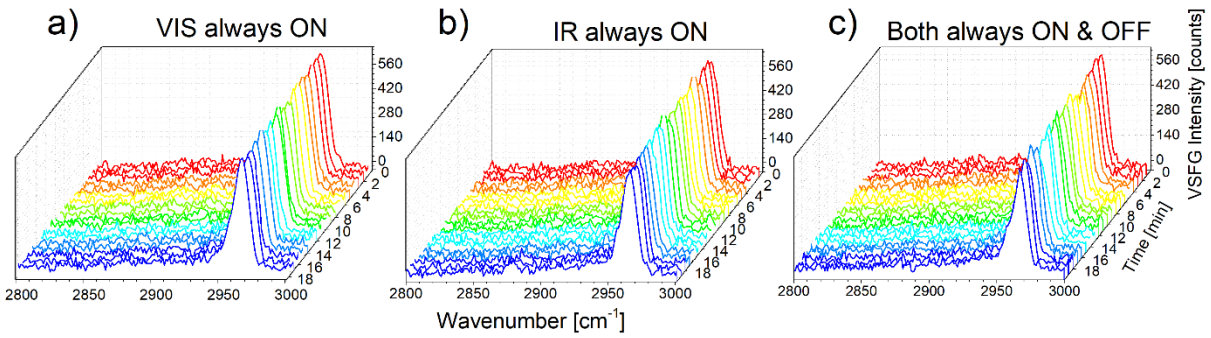

Figure 5.6 BB-VSFG spectra of Egg-PC were measured in the ppp polarization with a) VIS beam always turned ON, b) IR beam always turned ON, and c) both beams simultaneously switched ON and OFF.

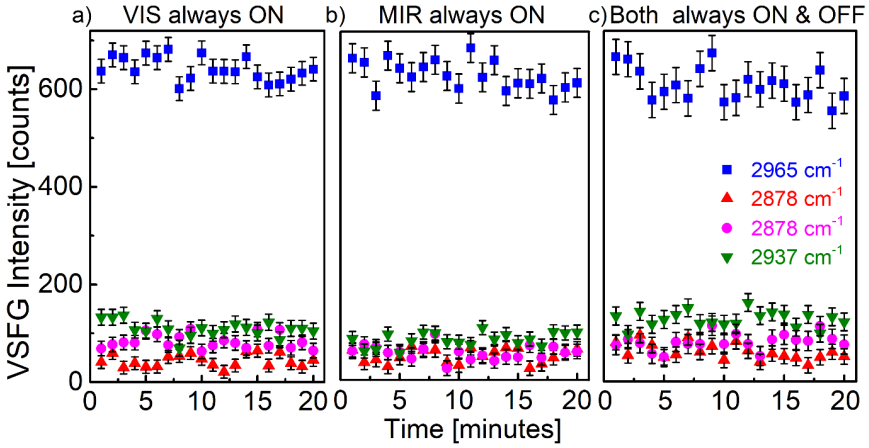

Figure 5.7 The spectral intensity fluctuation of BB-VSFG spectra of planar Egg-PC bilayer at the air-CaF_2 interface at 100 kHz over time in the ppp polarization combination. The vibrational modes of 2965 cm^{-1}, blue; 2937 cm^{-1}, green; 2878 cm^{-1}, magenta; and 2878 cm^{-1}, red; obtained by using ppp and ssp polarization combinations were recorded over time. The error bars were calculated from the root-mean-square fluctuation of the peak intensity over 20 min.

The spectral intensity was observed as constant during the experiments in all three cases (see Figure 5.7). The vibrational features of phospholipids here were in good agreement with those reported previously [5]. In the case of any thermal induced structural rearrangement, the vibrational features of methylene modes appear intense around 2850 cm^{-1}, which was not observed in our spectra [219, 220]. It is observed that there was neither a correlation between different radiance conditions nor the fluctuation in maximal intensities as well as spectral positions (see Figure 5.7). Our result suggests that there is no or negligible laser-induced thermal damage to the sample. The BB-VSFG spectral intensity over time infers that the planar supported bilayers at the applied average powers/pulse energies were stable in the air during the experiments. This result is in agreement with the simple 3-dimensional analytical heat diffusion model. The modeling was conducted in collaboration with Dr. Mark Mero from Max-

Born-Institut für Nichtlineare Optik und Kurzzeitspektroskopie im Forschungsverbund Berlin and summarized in ref. [221].

5.3 Interfacial structure and order of alkyl chains of Egg-PC bilayers

As elaborated in section 3.3 (page 27-28), the achiral molecules at the interface have four non-vanishing polarization combinations as ppp (p-VSFG, p-VIS, p-IR), ssp, sps, and pss. The planar-supported bilayers were measured at ppp, ssp, pss, and sps polarization combinations by applying a time delay of 0.67 ps between VIS and MIR beams for the polarization combination (see Figure 5.8). The above-mentioned four polarization combinations were carefully adjusted on the polarizers for the measurements.

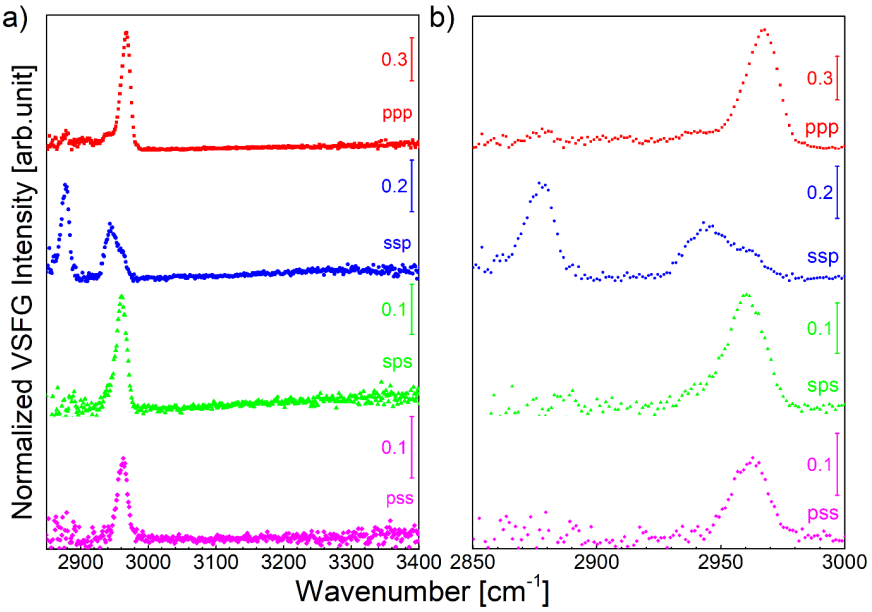

Figure 5.8 Normalized BB-VSFG spectra of Egg-PC bilayer at air-CaF_2 interface collected using ppp, ssp, sps, and pss polarization combinations a) in the C-H and O-H vibrational stretching region from 2800 cm^{-1} to 3400 cm^{-1} and b) the spectra between 2800 cm^{-1} and 3000 cm^{-1}. Experimental parameters: acquisition time 10 s, pulse energy of MIR and VIS were 0.55 µJ and 4.25 µJ, respectively.

Different colors of BB-VSFG spectra represent the different polarization combinations used for collecting the spectra (see Figure 5.8). Figure 5.8 b shows the spectral range between 2800 cm^{-1} and 3000 cm^{-1} of each polarization combination. Briefly, the band around 2969 cm^{-1} in ppp, sps, and pss is the strongest in the BB-VSFG spectra. The bands at 2878 cm^{-1} and 2937 cm^{-1} were the two dominating features in ssp polarization combinations (see Figure 5.8, blue dots). The amplitudes, the peak positions, and the line widths of the vibrational modes were unambiguous from the experimental BB-VSFG spectrum. Therefore, fitting with Lorentzian line profiles is required to extract this information of the vibrational modes.

To obtain more information regarding the C-H stretching vibrational mode of methyl and methylene groups, the BB-VSFG spectra obtained at ppp and ssp polarization combinations were fitted to the sum of six Lorentzian line profiles based on equation 3.14, page 29. The spectral intensity depends on the polarization of the incident electromagnetic fields which have the field vectors in many directions. The obtained BB-VSFG spectra together with the fitted Lorentzian line profiles are shown in Figure 5.9. The center frequencies, amplitudes, and the line widths of vibrational modes of the planar Egg-PC bilayer obtained by fitting the Lorentzian line profile on the measured BB-VSFG are summarized in Table 5.8. The summary of vibrational mode assignments in the C-H stretching region is given in Table 5.9.

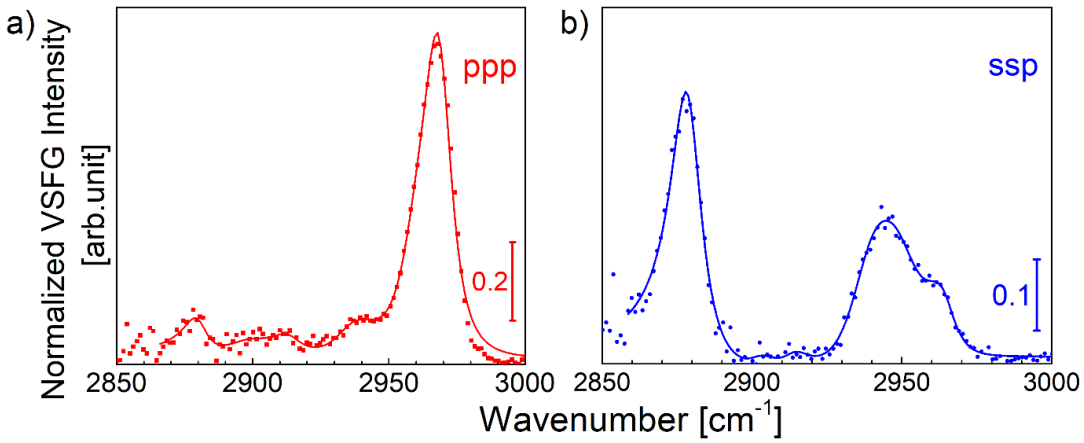

Figure 5.9 BB-VSFG spectra of Egg-PC on CaF_2 plate measured (dots) at 10 s using a) ppp and b) ssp polarization combinations and fitted as a sum of six Lorentzian lines profiles (lines).

The bands at 2879 cm^{-1}, 2902 cm^{-1}, 2914 cm^{-1}, 2938 cm^{-1}, 2954 cm^{-1}, and 2969 cm^{-1} were extracted by fitting Lorentzian line profiles on the measured BB-VSFG spectra. These bands were assigned to vibrational modes of methyl and methylene stretching in the hydrocarbon chains. The vibrational modes observed in the current study were in good agreement with the spectra of lipid monolayers reported before [5, 157, 222, 223]. A strong band at 2879 cm^{-1} observed in the ssp polarization combination was assigned to methyl symmetric stretching mode, $CH_{3\text{-}S}$. This vibrational mode was observed and reported earlier [5, 198, 224]. A sharp band appeared at 2969 cm^{-1} in the ppp polarization combination, which was assigned to methyl asymmetric stretching mode, $CH_{3\text{-}AS}$. The intensity of the 2969 cm^{-1} band was markedly decreased and blue-shifted to 2964 cm^{-1} in the ssp polarization combination. The band at 2964/2969 cm^{-1} is the in-plane component of the methyl asymmetric stretching. This band was observed as the intense spectral feature in the VSFG spectra [5, 7, 198, 224]. The spectral feature at 2954 cm^{-1} was assigned to the out-of-plane methyl asymmetric stretching. This band at 2954 cm^{-1} was difficult to assign as several assignments were existing in the VSFG

community. The assignment in this work was in agreement with ref. [225]. The vibrational mode at 2954/2964 cm^{-1} was reported earlier in *n*-alkyl chains by R. Snyder et al. [225]. Conboy et al. reported that this vibrational band at 2954 cm^{-1} was the combination of Fermi resonance of the methyl stretching at 2938 cm^{-1}, and the asymmetric methyl stretching at 2969 cm^{-1} [198]. Recently, this band was assigned to the methylene symmetric stretching coming from the glycerol moiety of the phospholipids' head group [226].

Table 5.8 The central frequencies, line widths, and amplitudes of the Lorentzian line profiles fitted on the measured BB-VSFG spectra of Egg-PC in ppp and ssp polarization combinations, where ω_v Γ_v and A_v represent the central frequency, line width, and the amplitude of the vth vibrational mode, respectively.

ω_v [cm^{-1}]	Γ_v [cm^{-1}]	A_v [ppp]	A_v [ssp]
2879±0.2	6±1	1.6±0.2	4.4±0.1
2902±0.9	7±1	1.3±0.2	0.5±0.2
2914±1.7	5±1.5	0.2±0.1	0.6±0.4
2938±1.9	9±2	-2.7±1.1	5.2±1.2
2954±1.9	10±0.6	-4.4±0.7	-1.8±2.2
2969 (ppp)/2964 (ssp)	6.4±1.9	6.7±0.2	-1.3±0.5

Table 5.9 The vibrational mode assignments of phospholipids obtained by the BB-VSFG spectrometer in the C-H stretching region are presented below.

ω_v [cm^{-1}]	Assignments	References
2879	CH_3 sym. str.	[157, 198, 227]
2902	CH_2 asym. str.	[5, 223]
2914	CH_2 FR (C-H stretching + H-C-H)	[5, 223, 228]
2938	CH_3 FR	[5, 157, 223]
2954	CH_3 out-of-plane asym. str.	[225]
2969 (ppp)/2964 (ssp)	CH_3 in-plane asym. str.	[5, 157, 198, 224, 225]

sym. : symmetric stretching, asym: asymmetric stretching, FR: Fermi Resonance

The band at 2938 cm^{-1} that appeared as a shoulder was assigned to the components arising from the Fermi resonance of methyl symmetric stretching mode which was visible in the ssp polarization combination (see Figure 5.9). This band appeared due to the energy level splitting of the methyl symmetric stretching and the overtones of asymmetric bending modes of the methyl groups near 1450 cm^{-1}; this resonance splitting is referred to as Fermi resonance (FR).

The largest fraction and complementary components of the fundamental vibration were designated as the fundamental and FR. The methyl FR was observed by employing VSFG spectroscopy [6, 198, 227, 229, 230].

The broadband features centered at 2902 cm^{-1} and 2914 cm^{-1} were assigned to methylene asymmetric stretching, $CH_{2\text{-}AS}$, and the Fermi resonance between the C-H stretching and the H-C-H bending overtone, $CH_{2\text{-}FR}$, respectively. The observations were in agreement with the reported vibrational bands [5, 157, 198, 225]. Snyder et al. predicted these FR components for the first time in the polyethylene chains [228]. Wang et al. pointed out that the methylene asymmetric and their Fermi resonance components are misinterpreted in the VSFG literature [222, 223]. The result obtained showed that these bands at 2902 cm^{-1}, 2914 cm^{-1}, and 2938 cm^{-1} were distinguishable by employing the HRR-BB-VSFG spectrometer.

Since the VSFG spectral intensity depends on the number density of the molecules, conformation, and orientation at the interface, the amplitudes of the methyl asymmetric stretching at 2969 cm^{-1} and the asymmetric methylene stretching at 2902 cm^{-1} indicate that the bilayers were well-ordered or slightly disordered on the surface of the CaF_2 window. These results suggest the methyl groups in the hydrocarbon chains were tilted with an angle between 20° and 30° with respect to the surface normal [106]. The small spectral amplitude of methylene symmetric $CH_{2\text{-}S}$ and asymmetric $CH_{2\text{-}AS}$ modes indicates that the alkyl chains were near all-*trans* conformation [157]. In the case of disordered bilayers, the methyl vibrational modes have low or no contributions in the BB-VSFG spectra [157]. The spectra of phospholipid bilayer show that the vibrational feature at 2914 cm^{-1} and 2938 cm^{-1} in ppp polarization combination, can be discriminated by using HRR-BB-VSFG spectrometer, which was one of the limitations in BB-VSFG.

5.4 Conclusions

The work presented in this chapter studied the applicability and experimental conditions of high-repetition-rate laser-driven BB-VSFG spectrometers for investigating interfacial bio-molecular layers. The model system made of Egg-PC bilayer was used for this purpose. The results obtained were discussed in many aspects including the potential of the HRR-BB-VSFG spectroscopy and the interfacial structure of the phospholipids.

The VSFG measurements at different time delays between VIS and MIR pulses provided the optimum delay at 0.67ps with minimal NRB and high SNR. The spectra of Egg-PC measured at different laser repetition rates were reported for the first time. The spectra obtained at

100 kHz showed the highest SNR compared to the other repetition rates. The high SNR of the bilayer spectra was surprising considering the properties of the model membrane and the interface. The high SNR indicates that the phospholipid is a good model system that can be studied in its natural form without introducing asymmetries in ambient conditions.

The intensity of the BB-VSFG spectral features monitored over time suggests that there were neither photo-induced effects nor any structural rearrangement at different experimental conditions. The BB-VSFG spectra also indicate that the phospholipid bilayers were stable under different laser repetition rates, pulse energies, average powers, and acquisition times. Thus, the 100 kHz laser repetition rate-driven BB-VSFG can be employed to study biomolecules such as phospholipids with no thermal damage or disorders.

The fast measurements ca. 10 s for each spectrum reduced the chances of lipid degradation or oxidation in ambient conditions. Therefore, in the future, this technique can be employed to study and follow real-time fast kinetic changes that occur within 20 min.

The result revealed that the vibrational bands at 2879 cm^{-1} were better resolved with our BB-VSFG compared to the standard VSFG spectra obtained with a low repetition rate spectrometer. The vibrational spectra obtained also revealed that the vibrational modes at 2914 cm^{-1} and 2938 cm^{-1} were distinguishable using HRR-BB-VSFG, which was challenging to observe using a typical VSFG spectrometer. These results were achieved because of 3 cm^{-1} FWHM transform-limited ps visible pulses of the BB-VSFG spectrometer. The experiments here demonstrate that the HRR-BB-VSFG spectrometer can be used to probe structural changes occurring at interfaces with better SNR compared to conventional BB-VSFG spectrometers. In conclusion, this work shows the applicability of the HRR-BB-VSFG spectrometer and its potential to study a variety of biomolecules to study the interfacial structural information which can be further studied.

6. Interfacial structure of one-and two-component phosphatidylcholines studied by HRR-BB-VSFG spectroscopy

This chapter is based on the publication of *Anal. and Bioanal. Chem*. 2019, 411, 4861–4871, doi: 10.1007/s00216-019-01690-9.

Phospholipids exist as monolayers in the interior walls of alveoli and have many roles such as primary defense barrier, maintaining the structure and fluidity, and lowering the surface tension during the exhalation [231, 232]. The interfacial properties such as structure, order, and orientation of the phospholipid molecules are different compared to their bulk. An in-depth understanding of these properties of phospholipids can help in developing new drugs for diseases such as respiratory distress syndromes in newborns.

The interfacial structure of phospholipids was previously studied with and without adding fluorescent dyes, spin labels, and/or probes [5, 7, 183, 198, 224]. However, investigating the phospholipids using high resolution, high sensitivity analytical tools can provide further interfacial structural information. The BB-VSFG can provide the interfacial structure of native phospholipids, but one of the drawbacks is the sensitivity of the spectrometer that limits the investigation at low number densities. The intensity of the spectra depends on the number density of the molecules at the interface. Another drawback is the integration time for collecting a single spectrum, which restricts the studies of unsaturated phospholipids as they oxidize in the air within 20 minutes. The HRR-BB-VSFG spectrometer intuitively provides an opportunity to solve these issues in a better fashion compared to a typical BB-VSFG spectrometer.

In this work, the HRR-BB-VSFG spectra of saturated and unsaturated PCs, and their heterogeneous mixtures were studied at different surface pressures and concentrations. The structural variations are discussed for the one and two-component and the interfacial water molecules around and between the phospholipid head groups at different surface pressures. The results were elaborated in the perspectives of HRR-BB-VSFG and the interfacial structure of phospholipids. The conformational order/disorder of the one- and two-component monolayers was also discussed in this chapter. The vibrations displayed by the fatty acid hydrocarbon chains were used to obtain the conformational changes, which can further reveal the fluidity of monolayer assemblies.

6.1.1 Sample preparation

One and two-component model systems were prepared for investigating the structural variations and their related phenomena in detail. For the sample preparation, Langmuir-Blodgett deposition was employed to prepare solid-supported monolayers to mimic the lung surfactants. The monolayer formed on the surface of the water due to the amphipathic nature of the phospholipids was transferred to the calcium fluoride (CaF_2) window. Four monolayers of phosphatidylcholine (PC) were prepared for the measurements. The monolayers include 1,2-dipalmitoyl-sn-glycero-3-phosphocholine (16:0 PC, DPPC), and 1,2-dioleoyl-sn-glycero-3-phosphocholine (18:1 Δ9-*cis* PC, DOPC) and their different mixtures were prepared as listed in Table 6.1. The structure and name of the phospholipids are illustrated in Figure 6.1. The stock solutions of both PCs were prepared in chloroform:methanol (9:1, v: v) mixture. The phospholipid solutions were handled with care to prevent contamination, degradation, and to maintain a stable concentration. The lipids were stored in the freezer (i.e., -20°C) as it is sensitive to the temperature. The lipid stock solutions were stored in glass containers with Teflon sealing since the chloroform dissolves the plastic vails.

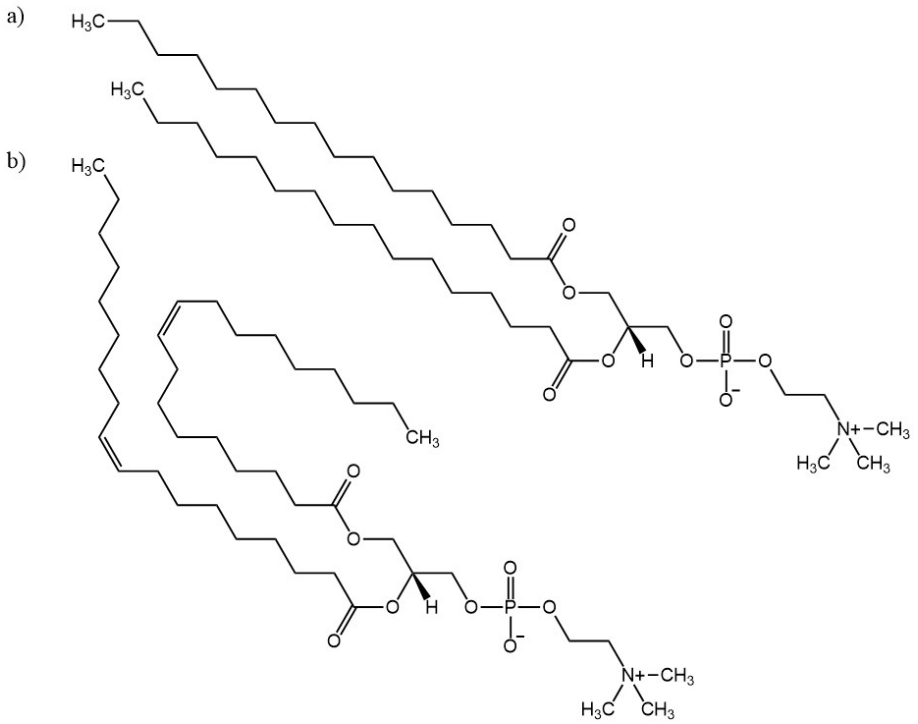

Figure 6.1 The phospholipids used in this study: a) 1,2-dimitoyl-sn-glycero-3-phosphocholine (16:0 PC, DPPC), b) 1,2-dioleoyl-sn-glycero-3-phosphocholine (18:1 PC, DOPC).

The chemical structure of phospholipid molecules is classified into three key components: i) a hydrophilic head group, ii) two hydrophobic alkyl tails, and iii) two glycerol linkage that connect the head group to the alkyl chains. Depending on the degree of saturation of the alkyl tails, the lipid molecule is further classified as saturated and unsaturated molecules. The molecules employed in this investigation were saturated DPPC and unsaturated DOPC phospholipids. The saturated DPPC has 16 hydrogenated carbon atom tails while the unsaturated DOPC has 18 carbon atom tails with a pair of carbon double bonds in the Δ9-cis position of the alkyl chain (see Figure 6.1). Both lipids are zwitterionic, containing positively charged choline and negatively charged phosphate groups. The fluidity of the monolayer and bilayer are maintained by the alkyl chain-chain interaction.

Before the measurements, the CaF_2 plates were cleaned to avoid any contamination on the surface. For cleaning the CaF_2 surface, the plates were initially sonicated for 20 min with ethanol and Millipore water followed by annealing at 500°C for 2 hours. The plates were placed in a quartz chamber lifted by quartz plates. A flux of nitrogen was applied for 2 min in three steps initially at the start of annealing, then after 1 hour, and finally after 2 hours till the temperature of the plates was reduced to the minimum, to eliminate impurities from the surface of the plates. The plates were dipped in water directly after the cleaning procedure until the measurements.

Table 6.1 The representation of samples prepared for the investigation in this chapter.

DPPC($\boldsymbol{v}$ %)	**DOPC** ($\boldsymbol{v}$ %)	**Representations**
0	100	DOPC
10	90	DOPC:DPPC (9:1)
90	10	DPPC:DOPC (9:1)
100	0	DPPC

$\boldsymbol{v}$: volume in percent, **DPPC:** 1,2-dipalmitoyl-sn-glycero-3-phosphocholine, **DOPC:** 1,2-dioleoyl-sn-glycero-3-phosphocholine

It should be noted from Table 6.1 that the component with the higher volume content is written first to simplify notations in tables and figures. To prepare solid-supported phosphatidylcholine monolayers, Kibron MicroTrough XS apparatus and Filmware X 4.0 software (Kibron, Helsinki, Finland) were employed [64, 65, 233]. The Langmuir-Blodgett trough and the two barriers were thoroughly cleaned with ethanol and Millipore water before the experiments. A 1 mg/ml stock solution of both DOPC and DPPC was prepared by dissolving the powders in chloroform: methanol (9:1, v/v). The CaF_2 window was clamped to the dip coater and immersed into the water (see section 4.2.2). After that, the stock solution was gently spread on the subphase in the LB trough. From the stock solution of the corresponding lipid, a volume of 20 µl was spread on the water surface using a Hamilton syringe, and a time of 15 min was permitted for the complete evaporation of the solvent before the compression. The monolayer formed at the air-water interface was compressed to 30 mN/m, 18 mN/m (the LC phase), and 5 mN/m surface pressures. Finally, the CaF_2 window was lifted at a rate of 1 mm/m to yield solid-supported monolayers.

6.1.2 Surface pressure-area (π - A) isotherm of one- and two-component phosphatidylcholine monolayers on the water surface

The surface pressure-area (π-A) isotherms of one- and two-component lipid monolayers on the water surface namely, DPPC, DOPC, DPPC:DOPC (9:1, v: v), and DOPC:DPPC (9:1, v: v), were measured to investigate the thermodynamic properties are shown in Figure 6.2. The isotherms were obtained by compressing the monolayers formed on the water surface with the barriers at a constant speed of 5 mm/min.

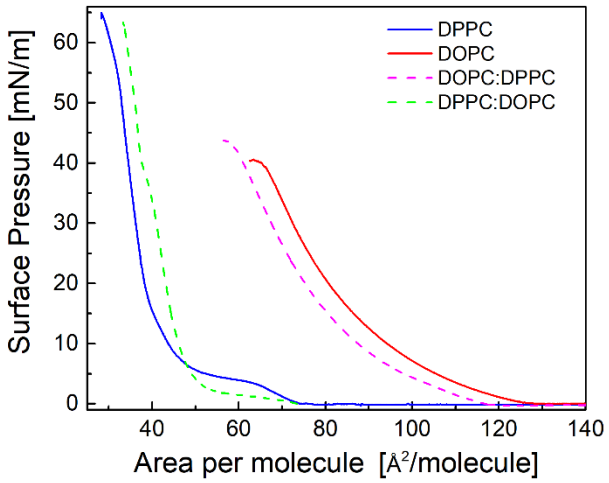

Figure 6.2 Surface pressure-area isotherms of one-and two-component phosphatidylcholine monolayers at the air-water interface. The DPPC, blue; DOPC, red; DOPC: DPPC (9:1), magenta; DPPC: DOPC (9:1), green. Adapted from the publication, *Anal. and Bioanal.Chem.* 2019, 411, 4861–4871, doi: 10.1007/s00216-019-01690-9.

The isotherm measurements were the same as reported before [193, 234]. The isotherm of saturated DPPC monolayers showed different phases including the liquid-expanded (LE) phase up to a pressure of 9 mN/m, the liquid-expanded–liquid-condensed (LE–LC) phase between 9 mN/m and 12 mN/m, and the LC phase above 12 mN/m during the compression (see Figure 6.2). The mean molecular area of the LC phase ranges from 30 to 40 $Å^2$/molecule whereas the collapse point of the DPPC monolayer on the water surface was observed to be at 65 mN/m. At 8 mN/m, the DPPC monolayer is observed in the 2D liquid phase where the mean area of the monolayer is 55-60 $Å^2$/molecule. The DOPC exists in the LE phase in water throughout the compression (red curve in Figure 6.2).

The collapse pressure of DOPC was observed at 40 mN/m. Comparing the DPPC and the mixture of DPPC:DOPC (9:1) (green curve in Figure 6.2) a slight deviation in isotherm was observed. This variation is due to the contribution of unsaturated DOPC in saturated DPPC that changes the mean molecular area. It is observed that the collapse point of the DPPC:DOPC (9:1) mixture was about 63 mN/m, slightly lower than the DPPC monolayer. The addition of DOPC to the DPPC increased the mean molecular area of the monolayer formed on the water surface and lowered the collapse pressure. This suggests that the number of *gauche* defects in their alkyl chains increased as a result of the addition of DOPC to the DPPC molecule.

The collapse pressure of the DOPC:DPPC (9:1) mixture was observed at 44 mN/m, slightly higher than the DOPC monolayer formed on the water surface. Besides, the DOPC:DPPC (9:1) mixture showed a minor decrease in the mean molecular area as compared to the DOPC

monolayer (magenta curve in Figure 6.2). This is because a small contribution of the DPPC in DOPC decreased the intermolecular distance. Thus, reduced the mean molecular area of the monolayer formed on the surface of the water. That is, the number of *gauche* defects in the chains of the PC decreased with the addition of DPPC.

6.1.3 BB-VSFG measurements data pre-processing

The BB-VSFG experimental setup was explained in detail in the Materials and Methods (see section 4.2, page 40). Briefly, the BB-VSFG spectra of Au (111) surface and polystyrene were obtained for the calibration of sample spectra. For this purpose, spectra were collected by overlapping the MIR and VIS beams spatially and temporally on Au (111), sequentially; the polystyrene spectra were obtained by inserting a 50 µm thin film on the MIR path while obtaining the BB-VSFG spectra on an Au (111) surface. Later, the HRR-BB-VSFG spectra of different PC monolayers were obtained by focusing the MIR and VIS beams on the sample. The vibrational spectra were obtained between 2800 cm^{-1} and 3600 cm^{-1}. The 100 kHz laser repetition rate and the integration time of 10 s were selected for all the BB-VSFG measurements. Additionally, the prepared monolayers were studied at the air-CaF_2 interface. Then, the data pre-processing was done after obtaining the raw BB-VSFG spectra of Au (111) surface, polystyrene thin film, and phospholipids monolayers. The pre-processing is performed as follows. First, the wavenumber axis was calculated from the wavelength axis. Then, the wavenumber axis was calibrated using the polystyrene absorption bands based on the NIST database. Next, all spikes were removed from the spectra. Additionally, the averaged background spectra were subtracted from the raw spectra. These background spectra were collected by keeping the VIS beam switched on. As a further step, the sample spectra were normalized by using gold spectra as a standard. This procedure is mandatory to obtain a reliable intensity ratio in the entire spectral range. All this pre-processing was performed using home-written MATLAB scripts. The Lorentzian line profiles were fitted on BB-VSFG spectra by using IGOR Pro software. Finally, the fitted parameters were assigned to vibrational modes.

6.2 HRR-BB-VSFG spectra of one-component phosphatidylcholine at different surface pressures

The biological functionality of monolayers depends on their surface pressures. Different surface pressures were applied in this work to mimic the structural organization and orientation of lung surfactants during the inhale-exhale process. The surface pressure values were selected for the

measurements based on the surface pressure versus area per molecule isotherms (see Figure 6.2). The minimum and maximum surface pressure values were selected to fall into the categories of LE, LE–LC, and LC phases of the DPPC monolayer. The BB-VSFG spectra of LB monolayers prepared at different surface pressures of 30 mN/m, 18 mN/m, and 8 mN/m were measured in the spectral range between 2800 cm^{-1} and 3600 cm^{-1}, however, Figure 6.3 shows the spectral range between 2800 cm^{-1} and 3000 cm^{-1}.

The different colored dots denote the experimentally obtained BB-VSFG spectra at the surface pressures of 30 mN/m, 18 mN/m, and 8 mN/m. The black traces demonstrate the sum of eleven Lorentzian line profiles fitted on the experimentally measured BB-VSFG spectra according to equation 3.14 (see section 3.3.3). The fitting of these vibrational spectra was not straightforward. The curves were not converging without fitting all the parameters presented in Table 6.2. The fitting was followed by the assignments of vibrational modes and summarized in Table 6.2.

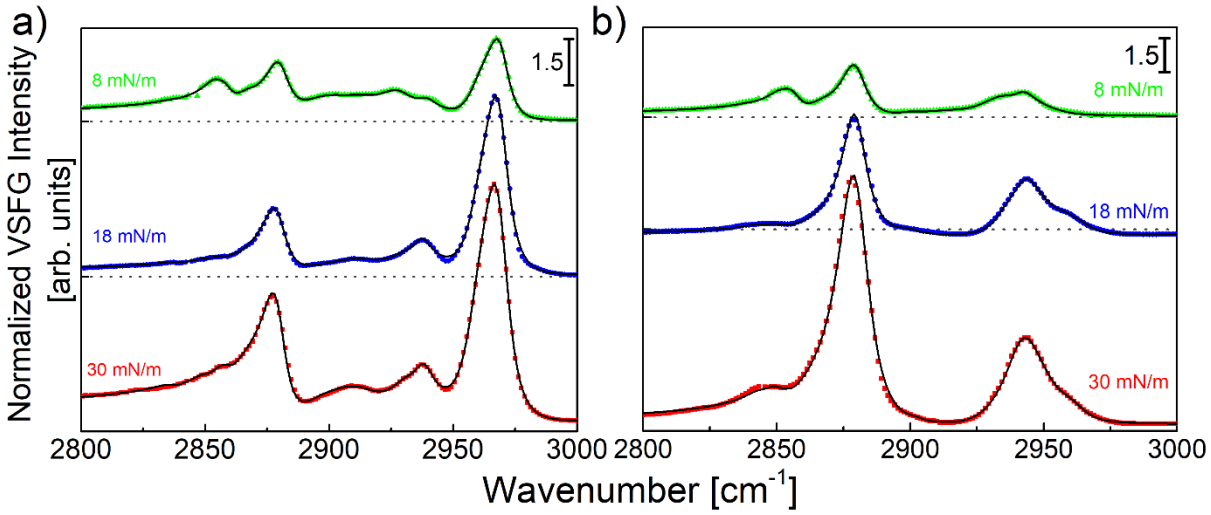

Figure 6.3 The BB-VSFG spectra of DPPC monolayer prepared on CaF_2 window by applying surface pressures of 30 mN/m, red; 18 mN/m, blue; 8 mN/m, green; collected using acquisition time of 10 s in a) ppp b) ssp polarization combinations. Adapted from the publication, *Anal. and Bioanal.Chem.* 2019, 411, 4861–4871, doi: 10.1007/s00216-019-01690-9.

6.2.1 C-H stretching region: 2800 cm^{-1} to 3000 cm^{-1}

The vibrational bands observed in this spectral range were the symmetric stretching, the asymmetric stretching, and the Fermi resonance features of the methyl and methylene groups. These vibrational bands were in good agreement with the DPPC spectra obtained using conventional BB-VSFG spectrometers [5, 198, 221-223]. Additional peaks were also observed in our spectra where these features are not surprising since extra bands were also observed by

several groups with the help of the high-resolution BB-VSFG spectrometer operated at 1 kHz [163, 235-237]. Nevertheless, a consistent assignment of the additional spectral bands to the vibrational modes has been elusive in the literature so far. The parameters obtained by fitting Lorentzian line profiles also revealed that there are many spectral features yet to be assigned to vibrational modes.

Table 6.2 Fitting parameters of DPPC monolayers at different surface pressures in ppp and ssp polarization combinations are given below. The resonance wavenumber and damping factor values in each row correspond to the average of the corresponding values obtained at all three surfaces. Adapted from the publication, *Anal. and Bioanal.Chem.* 2019, 411, 4861–4871.

		A_ν (30 mN/m)		A_ν (18 mN/m)		A_ν (8 mN/m)	
ω_ν [cm^{-1}]	Γ_ν [cm^{-1}]	ppp	ssp	ppp	ssp	ppp	ssp
2839.9±2.98	4.38±0.07	0.23±0.05	0.46±0.09	0.18±0.06	0.46±0.10	0.09±0.02	0.11±0.03
2850.7±2.22	3.77±0.50	0.23±0.05	0.45±0.11	0.16±0.06	0.26±0.12	0.72±0.03	0.32±0.03
2855.9±3.10	4.45±0.52	0.55±0.04	0.86±0.12	0.25±0.05	0.52±0.12	1.31±0.03	3.05±0.03
2867.6±1.80	6.46±0.30	0.66±0.07	0.18±0.08	0.02±0.07	0.30±0.09	1.07±0.03	1.10±0.04
2879.5±0.84	6.14±0.54	9.08±0.05	23.86±0.04	6.48±0.05	13.33±0.04	4.74±0.02	8.28±0.02
2899.4±1.19	9.65±4.08	3.37±0.20	0.76±0.18	1.44±0.21	1.35±0.12	4.71±0.07	0.89±0.07
2912.7±1.34	12.22±3.85	10.84±0.21	0.48±0.25	5.69±0.22	0.07±0.26	5.51±0.08	4.63±0.13
2931.9±2.55	8.60±2.51	9.69±0.16	0.23±0.16	5.92±0.16	2.47±0.19	5.76±0.05	8.87±0.08
2939.5±2.04	5.96±2.05	2.81±0.09	20.06±0.15	2.14±0.08	9.93±0.20	1.64±0.03	1.59±0.05
2957.4±1.52	8.19±0.89	-23.64±0.05	3.18±0.37	-18.12±0.04	1.06±0.27	-11.30±0.02	-1.50±0.19
2969.2±0.23	7.99±2.58	22.98±0.03	-9.99±0.57	16.54±0.02	-5.65±0.16	9.17±0.01	-0.29±0.11

I. CH_2 stretching modes and their Fermi resonances

In the lower wavenumber range, four bands at 2840 cm^{-1}, 2851 cm^{-1}, 2856 cm$^{-1,}$ and 2868 cm^{-1}, were observed in our spectra which were assigned to CH_2 symmetric stretching modes of the hydrocarbon alkyl chains. The fitting results were unsatisfactory without including all four bands in our modeling. The different subsets of these vibrational modes were also observed and reported [225, 238-240].

The band at 2851 cm^{-1} was assigned to the C-H symmetric stretching mode methylene groups. The band at 2851 cm^{-1} was previously observed in VSFG spectra [5, 198, 227, 241-243]. In our experiments, the amplitude of the methylene modes increases with a decrease in surface pressure, suggesting that they originate from *gauche* defects in the hydrophobic alkyl chains.

The symmetric C-H stretching of methylene has been used as a qualitative indicator to understand the conformational order in hydrocarbon chains of the phospholipids [152, 242, 244]. Even if the number of $CH_{2\text{-}S}$ vibrational modes is less, these vibrational modes could also be resolved using the HRR-BB-VSFG technique [163, 235]. There are three types of methylene groups in phospholipids. These include the methylene group attached to i) the choline head group, ii) the glycerol moieties, and iii) the hydrocarbon chains. Thus, many vibrational frequencies of these methylene groups are expected in this spectral range. We assign the band at 2868 cm^{-1} to C-H symmetric stretching of the methyl group of the choline head group. Recent studies [245], show that the vibrational mode at 2868 cm^{-1} comes from the head group of the DPPC molecules.

A broad feature appeared between 2899 cm^{-1} and 2932 cm^{-1} in both ppp and ssp polarization combinations (see Figure 6.3). Three vibrational resonances were fitted between this feature. These bands are more visible in the ppp polarization combination (see Figure 6.3a). In our spectra, these broadband features were distinguishable [246], where these vibrational bands were not resolved by typical-BB-VSFG spectrometers. The mode at 2899 cm^{-1} was assigned to the Fermi resonance of methylene groups, where this band is due to the splitting of methylene symmetric stretching by the overtone of C-H deformation mode at 1450 cm^{-1}. In this work, the component that has a larger amplitude is designated as the fundamental, and the complementary component is represented as the subscript FR.

Among these three vibrational resonances, another peak at 2913 cm^{-1} and 2932 cm^{-1} were observed and assigned to the methylene FR and asymmetric methylene stretching mode, respectively [235]. Li et al. [235] assigned the resonance at 2899 cm^{-1} to a stretching mode of the $R_3C–H$ group, and the peak at 2932 cm^{-1} to $CH_{2\text{-}AS}$ or $CH_{3\text{-}FR}$. The amplitude of the band at 2932 cm^{-1} was observed to increase with a decrease in surface pressure and was visible in both ppp and ssp polarization combinations (see Figure 6.3). This band observed at lower surface pressure suggests that a higher number of gauche defects and contradicts the assignment in ref. [235]. These results indicate that the spectrometer used in the present study to obtain the VSFG spectra of the DPPC monolayer has high sensitivity and high spectral resolution.

II. CH_3 stretching modes and their Fermi resonances

The dominant peak at 2880 cm^{-1} was assigned to the methyl symmetric C–H stretching, CH_3 of the terminal methyl group. This mode was visible both in ppp and ssp polarization

combinations (see Figure 6.3a). The vibrational mode at 2880 cm^{-1} was observed and reported earlier [152, 198, 227].

The shoulder band at 2940 cm^{-1} was assigned to FR of the symmetric methyl stretching and the overtone of methyl bending modes. In the ssp polarization combination, this mode is one of the most prominent modes, and its signal strength increases monotonously with the applied surface pressure (see Figure 6.3b). Our assignment is consistent with the literature [5, 157, 198, 222, 227]. This mode at 2940 cm^{-1} was often misassigned in the VSFG spectroscopy but reassigned by Wang et al. using polarization-dependent VSFG spectroscopy [222].

The bands at 2969 cm^{-1} and 2957 cm^{-1} were assigned to the methyl asymmetric C–H stretching, $CH_{3\text{-}AS}$ or the glycerol moieties at the interfacial region. The band at 2957 cm^{-1} appeared as a small shoulder which was included for a consistent fitting of Lorentzian line profiles. The vibrational modes at 2969 cm^{-1} were only visible in the ppp polarization. In ssp polarization, the frequency of the asymmetric stretching, $CH_{3\text{-}AS}$ was blue-shifted to 2964 cm^{-1} compared to ppp polarization. The band at 2967 cm^{-1} was visible in the sps polarization combination. The mode at 2957 cm^{-1} was observed to have a negative phase in ppp polarization and showed a positive phase at ssp and sps polarizations. The band at 2969 cm^{-1}/2964 cm^{-1} was assigned to the in-plane component of an asymmetric C-H stretching of the methyl groups. The peak at 2957 cm^{-1} was attributed to the out-of-plane component of methyl stretching $CH_{3\text{-}AS}$ in Chapter 5. The band at 2957 cm^{-1} was assigned to the methylene symmetric stretching of the glycerol moieties of the interfacial region probed by different deuterated and non-deuterated DPPC monolayers [226]. The shoulder at 2957 cm^{-1} was not obtained from a monolayer of cholesterol by Wang et al. [163] where it was detected on octadecylphosphonic acid and sphingomyelin monolayers only in ssp polarization [235, 239].

6.2.2 BB-VSFG spectra of low surface coverage saturated and unsaturated phosphatidylcholine

To study the alkyl chain-chain interactions, both saturated and unsaturated phospholipids were selected for the comparison. The saturated DPPC and unsaturated DOPC monolayers were prepared by applying low surface pressures at the LE phase for the VSFG measurements. Figure 6.4 shows the BB-VSFG spectra of DPPC and DOPC monolayers prepared at low surface pressures (8 mN/m and 5 mN/m). The spectral features of both the PCs were compared at ppp and ssp polarization combinations and represented below as red and blue curves. The

experimental spectra were fitted with the sum of eleven Lorentzian line profiles and the corresponding fitted parameters are listed in Table 6.3.

The BB-VSFG spectra of DPPC and DOPC at low surface pressure showed a high SNR and were reported for the first time to our knowledge, which was previously challenging to obtain using typical-VSFG spectrometers (see Figure 6.3). The VSFG spectra of both DPPC (16:0) and DOPC (18:1) molecules differ as they have different conformations of the alkyl chains, i.e., all-trans and Δ9-cis for DPPC and DOPC, respectively. In both the ppp and ssp polarization combination of the DOPC monolayer, the intensity of the band at 2899 cm^{-1} was observed to be the most dominant band and the band at 2969 cm^{-1} almost diminishes from the BB-VSFG spectra (see Figure 6.4).

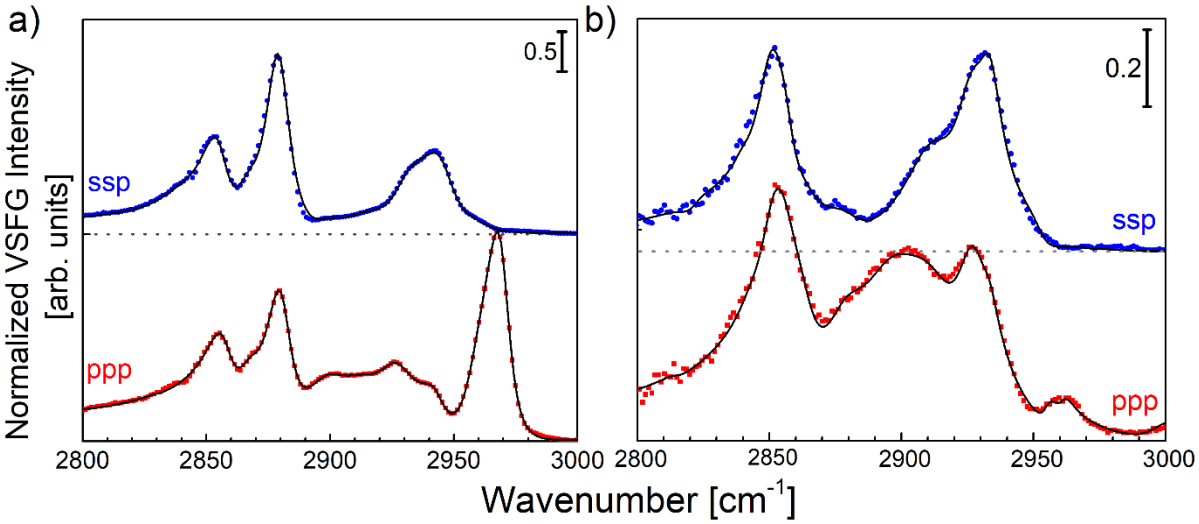

Figure 6.4 Normalized BB-VSFG spectra of a) DPPC monolayer at 8 mN/m and b) DOPC monolayer at 5 mN/m. Experimental parameter: 10 s acquisition time. Adapted from the publication, *Anal. and Bioanal.Chem.* 2019, 411, 4861–4871, doi: 10.1007/s00216-019-01690-9.

The DPPC molecules in the LE phase showed higher amplitudes of the C-H stretching modes of the methylene group than in the LC phase (see Figure 6.3, green curves; Figure 6.4a). This indicates that the number of *gauche* defects in the monolayer at the LE phase was higher than the monolayers in the LC phase. Specifically, the vibrational modes at 2899 cm^{-1} ($CH_{2\text{-}FR}$), 2911 cm^{-1} ($CH_{2\text{-}AS}$), and 2927 cm^{-1} ($CH_{2\text{-}FR}$) are more intense in DOPC than in DPPC (see Figure 6.4b versus a). Besides, a vibrational band at 2868 cm^{-1} was observed in DPPC where the mode is observed at 2863 cm^{-1} in DOPC. This vibrational mode was assigned to the $CH_{2\text{-}S}$ stretching mode of the alkyl chains. The observation is consistent in all the ppp, ssp, and sps polarization combinations (see Table 6.3). Nonetheless, the intensity of the terminal methyl group ($CH_{3\text{-}S}$) of the alkyl chain remains high. As the intensity ratio of the methylene and methyl

modes depends on the number of gauche defects in the alkyl chains [142, 189, 225, 232], the intensity ratio of the methylene and methyl symmetric stretching modes, at 2851 cm^{-1} and 2880 cm^{-1} were used to quantify the molecular conformational order and discussed the following section.

Table 6.3 The sum of eleven Lorentzian fitted VSFG vibrational mode assignments and corresponding wavenumber of phosphatidylcholine (DPPC and DOPC) in the C-H stretching region between 2800 cm^{-1} and 3000 cm^{-1}. ω_v, $\Gamma_{v,}$ and A_v represent the central frequency, line width, and amplitude of the vth vibrational mode, respectively. Adapted from the publication, *Anal. and Bioanal.Chem.* 2019, 411, 4861–4871.

DPPC (8 mN/m)				DOPC (5 mN/m)			
ω_v [cm^{-1}]	Γ_v [cm^{-1}]	A_v ppp	A_v ssp	ω_v [cm^{-1}]	Γ_v [cm^{-1}]	A_v ppp	A_v ssp
				2815.0±0.06	4.24±0.20	0.07±0.09	0.05±0.04
				2819.4±1.95	4.18±0.18	0.01±0.08	-0.11±0.04
2839.9±2.98	4.38±0.07	0.09±0.02	0.11±0.03	2842.87±1.54	3.65±0.02	0.05±0.02	0.08±0.03
2850.7±2.22	3.77±0.50	0.72±0.03	0.32±0.03	2851.99±0.57	5.09±1.07	0.37±0.04	1.26±0.05
2855.9±3.10	4.45±0.52	1.31±0.03	3.05±0.03	2856.47±0.65	5.56±0.15	0.97±0.06	1.30±0.06
2867.6±1.80	6.46±0.30	1.07±0.03	1.10±0.04	2863.33±0.93	9.62±1.39	3.01±0.06	1.97±0.09
2879.5±0.84	6.14±0.54	4.74±0.02	8.28±0.02	2880.39±3.77	9.81±1.81	1.91±0.06	1.38±0.08
2899.4±1.19	9.65±4.08	4.71±0.07	0.89±0.07	2898.81±3.52	14.52±1.85	7.78±0.12	0.28±0.10
2912.7±1.34	12.22±3.85	5.51±0.08	4.63±0.13	2911.19±1.20	13.19±2.85	5.54±0.10	4.28±0.08
2931.9±2.55	8.60±2.51	5.76±0.05	8.87±0.08	2926.79±0.73	8.94±1.45	3.00±0.05	3.34±0.06
2939.5±2.04	5.96±2.05	1.64±0.03	1.59±0.05	2934.80±1.63	6.39±2.54	0.27±0.03	1.35±0.04
2957.4±1.52	8.19±0.89	-11.30±0.02	-1.50±0.19	2954.82±2.31	5.83±1.35	0.38±0.04	-0.68±0.10
2969.2±0.23	7.99±2.58	9.17±0.01	-0.29±0.11	2962.20±1.36	6.21±2.29	0.31±0.05	0.05 ± 0.1

I. Order of one-component phosphatidylcholine monolayers at air-CaF_2

To completely examine the effect of concentration and surface pressure on molecular order, the intensity ratio of the methylene symmetric stretching to the methyl symmetric stretching is plotted in Figure 6.5. The intensity ratios, I ($CH_{2\text{-}S}$)/I ($CH_{3\text{-}S}$) of DPPC and DOPC monolayers are shown at different surface pressures such as 30 mN/m, 18 mN/m 8 mN/m, and 5 mN/m. For this purpose, the intensity values used were the amplitudes of the methyl and methylene symmetric C-H stretching modes determined from the fitting. Specifically, vibrational modes at 2850 cm^{-1} and 2880 cm^{-1} were selected for the order parameter analysis.

The intensity ratios of DPPC monolayer prepared by applying 30 mN/m and 18 mN/m were calculated nearly zero whereas the DOPC monolayers prepared by applying 5 mN/m showed above one. This drastic change is due to the disruption of the monolayer at the interface for several reasons such as electrostatic interaction of the head group, ion-pair formation, and local micellar type structure. In VSFG, the intensity depends on the symmetry, orientation, and conformation of the molecules. A well-ordered alkyl chain shows resonances due to the terminal methyl group. The resonant signal from the methylene groups vanishes in systems with a high degree of order within the alkyl chains. The methylene resonances in the spectra indicate the presence of gauche defects, thus less ordered alkyl chains. The intensity ratios of 2850 cm^{-1} to 2885 cm^{-1}, are more sensitive to chain conformation [247], than those of the 1100 cm^{-1} C-C stretching [248] region to determine the relative all-trans to gauche conformation. The relative intensities of the 2850 cm^{-1} and 2885 cm^{-1} were proved to be sensitive to small structural changes in systems [247].

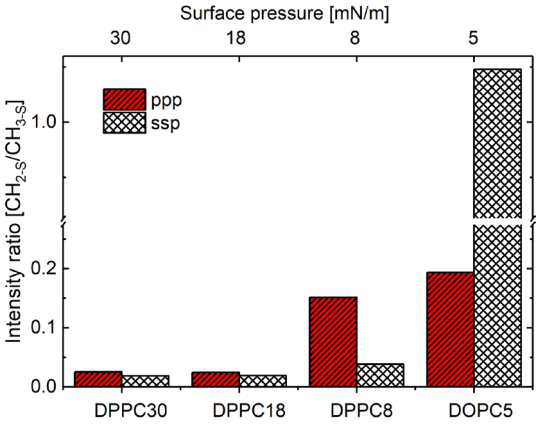

Figure 6.5 The intensity ratios of DPPC and DOPC molecules at different surface pressures of 30 mN/m, 18 mN/m, 8 mN/m, and 5 mN/m. The number in the name of each lipid represents the surface pressure applied during the preparation of monolayers. This figure is adapted from the publication, *Anal. and Bioanal.Chem.* 2019, 411, 4861–4871, doi: 10.1007/s00216-019-01690-9.

In the case of DOPC, the high value of intensity ratio I ($CH_{2\text{-}S}$) / I ($CH_{3\text{-}S}$) indicates a large conformational disorder and/or lower packing density in the monolayers and the presence of DOPC in DPPC:DOPC disturbed the all-*trans* conformation of the alkyl chains. This method was used by Richmond et al. to study the order of phospholipids at the vapor/water interface in VSFG [224]. Membrane order quantification is often studied using this intensity ratio approach in both IR and Raman spectroscopy. This method was first proposed by Snyder et al. to probe hydrocarbon chain conformation in alkanes and later applied to monitor the distribution of gauche bonds in a variety of solids [228, 249-251]. Snyder et al. showed that the ratios band

intensities can be used to quantify the trans-*gauche* isomerization in the polyethylene chains [252].

In particular, the relative number of *gauche* defects in the DOPC monolayer is drastically higher than the DPPC monolayer (see Figure 6.5). From Figure 6.3 and Table 6.2, a correlation between the vibrational modes and the surface pressure can be obtained. It suggests that the amplitude of the vibrational modes depends on the number of molecules (surface pressure), orientation, and packing of the monolayers. The amplitudes of asymmetric methyl (CH_3) stretching modes at 2969 cm^{-1} increased as the surface pressure increases from 8 mN/m to 30 mN/m. In more detail, the overall intensity of the vibrational modes in the BB-VSFG spectra was observed as highest at 30 mN/m among 18 mN/m and 8 mN/m. At the LC phase of the DPPC monolayer, the calculated mean molecular area was about 30–40 $Å^2$/molecule. Besides, the DPPC monolayer prepared at 8 mN/m surface pressure where they exist in the LE phase (see Figure 6.3, green curve) behaved as a 2D liquid with a mean area of 55–60 $Å^2$/molecule. At 8 mN/m, LE phase, the larger amplitudes of the CH_2 groups in BB-VSFG spectra when compared to the LC phase (compare Figure 6.3, red and blue with green) suggest that the molecules are loosely packed with *gauche* defects in the alkyl tails of the molecules. When decreasing the surface pressure, the amplitude of the CH_3 vibrational mode becomes less intense (Figure 6.3), indicating that the orientational ordering of the terminal methyl group in the LE phase (8 mN/m) is different from that in the LC phase (beyond 10 mN/m).

II. O-H stretching region: 3000 cm^{-1}-3600 cm^{-1}

The BB-VSFG spectra of DPPC monolayer between 2800 cm^{-1} and 3550 cm^{-1}, were observed in both the C–H and the O–H stretching vibrational regions. The DPPC monolayers were prepared at three surface pressures as 8 mN/m, 18 mN/m, and 30 mN/m. Figure 6.6shows the BB-VSFG spectra of the O–H stretching region from 3000 cm^{-1} to 3550 cm^{-1}. The O−H modes suggest the presence of a water layer between the monolayers and the CaF_2 substrates. The thickness of the water layer is approximately 0.5 nm – 1.5 nm. The structural investigation of this interfacial water layer is experimentally challenging [5, 52]. The structure of water molecules at the lipid interfaces with distinct hydrogen-bonding sites and their net orientation can be experimentally observed by employing VSFG spectroscopy.

Two prominent broadband features centered at ~ 3200 cm^{-1} and 3420 cm^{-1} appeared in the O−H stretching region (see Figure 6.6). This doublet at 3200 cm^{-1} and 3400 cm^{-1} is due to intra- and intermolecular vibrational couplings [10]. The band at 3200 cm^{-1} and 3400 cm^{-1}

were assigned to the water molecules near the phosphate groups and broken hydrogen bonding adjacent to the quaternary ammonium. This band shifted from ~ 3150 to 3200 cm^{-1} with increasing surface pressure (see Figure 6.6). The bands were attributed to the water molecules with moiety (choline) of the headgroup. Another prominent feature in the O-H stretching region is observed in between 3500 and 3800 cm^{-1} often assigned to the water molecules near carbonyl moiety. The spectra shown below do not have these features, as our MIR beam is only 800 cm^{-1} broad at the time of acquisition. Our assignments agree with the assignments in literature [229, 253, 254].

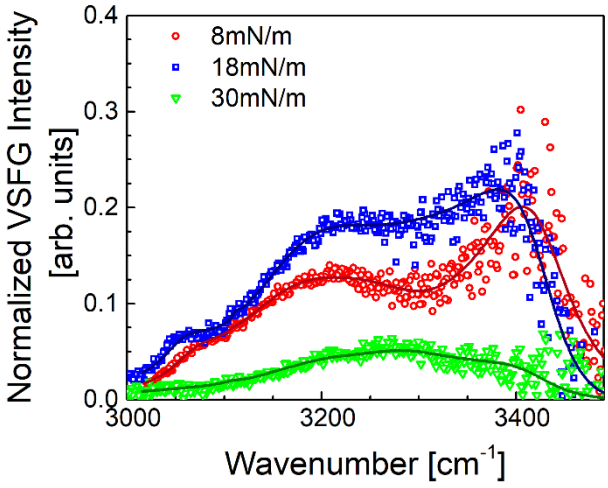

Figure 6.6 The BB-VSFG spectra of DPPC monolayer prepared at a surface pressure of 8 mN/m, 18 mN/m, and 30 mN/m, on the CaF_2 window. The spectral range between 3000 cm^{-1} and 3550 cm^{-1} shows the O−H stretching vibrational modes from the water molecules.

Table 6.4 The parameters of Lorentzian line profiles of 30 mN/m, 18 mN/m, and 8 mN/m in the O-H stretching region. ω_v, Γ_v, and A_v represent the central frequency, line width, and amplitude of the vth vibrational mode, respectively.

30 mN/m		**18 mN/m**		**8 mN/m**	
ω_v [cm^{-1}]	A_v [cm^{-1}]	ω_v [cm^{-1}]	A_v [cm^{-1}]	ω_v [cm^{-1}]	A_v [cm^{-1}]
3058	0.2±0.55	3056	2.4±0.4	3070	2.05±0.3
3112	0.05±0.01	3111	0.04±0.12	3109	0.03±0.1
3205	17.2±0.10	3165	24.4±0.7	3146	26.8±0.6
3277	5.70±0.10	3280	0.94±0.8	3281	-4.1±0.6
3420	-10.44±0.44	3422	-24.3±0.5	3422	-27.2 ±0.2

The strength of the two vibrational features at ~ 3200 cm^{-1} and 3400 cm^{-1} varies with the surface pressure of the DPPC molecules at the water surface [9, 10, 224, 255-257]. The spectra

showed higher peaks at 18 mN/m compared to those at 30 mN/m and 8 mN/m. The high spectral peaks, at a surface pressure of 18 mN/m, suggest that the water molecules were in a well-ordered state. In this surface pressure, the DPPC monolayer was in the LC phase where they are in all-*trans* or near t*rans* conformation. We obtained similar broadband O–H stretching modes when decreasing the surface pressure, however, the strength of the O–H modes diminishes. This change may be due to the less-ordered water structure between the head groups and/or between head groups and the substrate. At the surface pressure of 30 mN/m, the BB-VSFG spectra showed only one broadband feature. In this case, the peak at 3200 cm^{-1} disappeared and merged into one peak with a frequency in between the 3200 cm^{-1} and 3400 cm^{-1}, closer to 3400 cm^{-1}. Backus et al. reported this merging of O-H mode upon isotopic dilution [258] due to the removal of the intra- and intermolecular vibrational couplings. This shift in 3200 cm^{-1} indicates that the compression of the monolayer squeezes out the water molecules creating a low lateral distance between the DPPC. The result showed that the number of water molecules decreased as the surface pressure was increased. This phenomenon was also observed previously with VSFG at the air-water interface [9, 253]. While observing these spectral features in the O–H stretching region, we can study the two-dimensional fluidity and hydration of the monolayer. To fully understand the orientational changes of this interfacial hydration layer, further systematic analysis is required. In addition to the strong water peaks, two peaks at ~ 3065 cm^{-1} and ~ 3110 cm^{-1} were also needed in the fit in all cases and were attributed to the methyl asymmetric stretching of the choline headgroup [32]. The origin of the spectral feature at 3110 cm^{-1}has been debated. The band at ~ 3065 cm^{-1} that appeared in this region was attributed to the asymmetric stretching of the choline head group, N-$(CH_3)_3$. Conboy et al. assigned this choline headgroup for the first time in VSFG spectroscopy [198], and it is also often assigned to stretching of NH_3^+ mode. These resonances were previously reported in VSFG, IR, and Raman studies of phospholipids [198, 241, 259]. The presence of the methyl signal from the choline head group above a surface pressure of 18 mN/m also suggests that the choline head groups were well-ordered with enough space between the molecules for water molecules.

The orientation of water is determined from the sign of the second-order nonlinear susceptibility, $\chi^{(2)}$. Our homodyne BB-VSFG technique cannot obtain the sign of $\chi^{(2)}$ where it measures the absolute square of $\chi^{(2)}$ ($|\chi^{(2)}|^2$). Complex $\chi^{(2)}$ can be directly measured by phase-sensitive VSFG, [9, 260, 261] multiplex heterodyne detected VSFG (HD-VSFG), [10, 217, 253, 256, 262] and very recently developed single-channel HD-VSFG [263] spectroscopies. The imaginary part of $\chi^{(2)}$ (Im $\chi^{(2)}$) is far more informative than $|\chi^{(2)}|^2$ for studying the structure and

the orientation of water molecules at the interface. The positive sign of the Im $\chi^{(2)}$ sign represents the net H-up orientation of water, and the negative sign demonstrates the net H-down orientation of water. Sovago et al. first reported the orientation of the water molecules zwitterionic and negatively charge lipids [257]. They concluded that the water molecules in the lipid interfaces always point their hydrogen atoms into the bulk water, irrespective of the electric charge of the lipid head group based on the maximum entropy phase retrieval analysis (MEM) of homodyne VSFG spectra [257]. Later, Tahara's group [256] and Allen's group [9] reported that the orientation of water molecules at the lipid interfaces is influenced by the net charge of the lipid head group. Mondal et al. investigated the phosphatidylcholine (POPC) monolayer at the water interface by HD-VSFG spectroscopy [253]. They found three distinct features, a doublet feature was observed at 3200 cm^{-1} and 3400 cm^{-1} which were attributed to two types of hydrogen-bonded water existing at the interface. They concluded the water molecules near the negatively charged phosphate group which has net H-up orientation, and the water near the positively charged choline group has net H-down orientation. Another positive Im $\chi^{(2)}$ band around 3600 cm^{-1} and attributed to the presence of weakly interacting water molecules with net H-up orientation in the hydrophobic region of the lipid monolayer interface. Ishibashi et al. investigated the orientation of water molecules at a non-ionic surfactant/water interface [264]. They claimed that water molecules at the non-ionic interface are oriented with their hydrogen atoms towards the bulk. Nojima et al. reported weakly hydrogen-bonded water inside anionic and cationic phospholipid monolayer at the water interface [10]. They reported the water molecules above the head group for the first time. Recently, Cremer et al. reported that the water structure at positively charged species as well as negatively charged species. They claimed that the positively charged species decreased the water structure, whereas negatively charged species enhanced it [229].

6.2.3 HRR-BB-VSFG spectra of alkyl chains of two-component phosphatidylcholine at different concentration

To mimic realistic lung surfactants, monolayers of DOPC:DPPC (9:1, v:v) and DPPC:DOPC (9:1, v:v) were prepared at a surface pressure of 30 mN/m and 5 mN/m. The VSFG spectra were collected as fast as possible after preparing the monolayers. In the case of DOPC:DPPC (9:1, v:v), the surface pressure of 5 mN/m was applied to create monolayers. The monolayer of DOPC:DPPC (9:1, v:v) was only prepared by applying 5 mN/m for the measurements as it exists in the LE phase even at higher surface pressures. The surface pressure versus area per molecule isotherms is shown in Figure 6.2. The BB-VSFG spectra measured in different

polarization combinations, namely ppp, ssp, and sps are shown in Figure 6.7. The fitted parameters are shown in Table 6.6. Different polarization combinations of BB-VSFG spectra were measured as the spectra yield information about different elements/element combinations of the hyperpolarizability tensor of a particular molecular group in a well-packed molecular layer [150, 157].

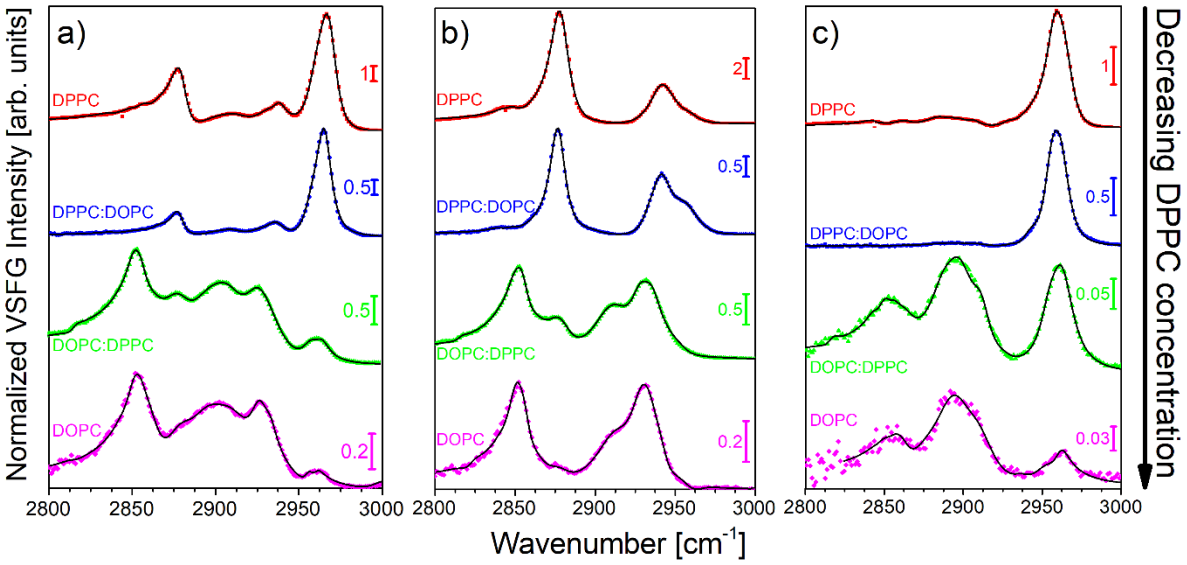

Figure 6.7 Normalized BB-VSFG spectra of one-and two-component lipid monolayers of DOPC, magenta; DOPC:DPPC, green; DPPC:DOPC, blue; and DPPC, red at a) ppp b) ssp c) sps polarization combinations. The symbols represent the measured data and the black lines show the fitted Lorentzian curves, respectively. Adapted from the publication, *Anal. and Bioanal. Chem.* 2019, 411, 4861–4871, doi: 10.1007/s00216-019-01690-9.

The red, blue, green, magenta represent the DPPC, DPPC:DOPC, DOPC:DPPC, and DOPC BB-VSFG spectra, respectively. The spectra measured in ssp (see Figure 6.7 b) and sps (see Figure 6.7 c) polarization combinations are related to one tensor element, however, the ppp polarization combination constitutes different tensor elements, section 3.3.3 equation 3.14, page 29. The one-component DPPC monolayer prepared by applying 30 mN/m surface pressure showed the most intense spectra in all three polarization combinations. Comparing DPPC to the DPPC:DOPC (9:1, v:v) spectra, the slight addition of unsaturated DOPC to the saturated DPPC drastically reduced the spectral intensity of the BB-VSFG spectra.

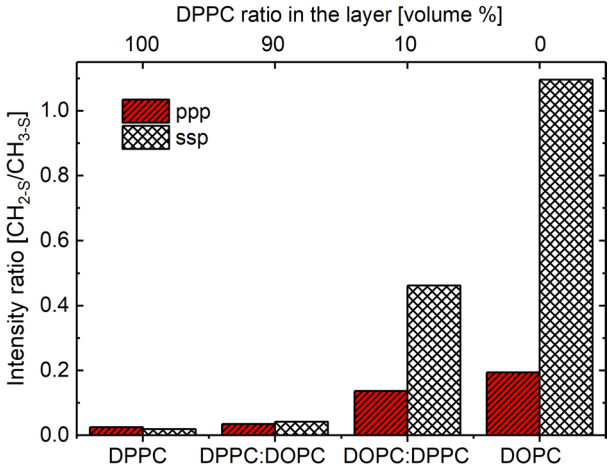

Figure 6.8 The intensity ratio, I ($CH_{2\text{-}S}$)/ I ($CH_{3\text{-}S}$) of one and two-component monolayers of DOPC and DPPC prepared at 30 mN/m and 5 mN/m. A volume ratio of 9:1 is used in the two-component DPPC:DOPC and DOPC: DPPC. Adapted from the publication, Anal. and Bioanal. Chem. 2019, 411, 4861–4871, doi: 10.1007/s00216-019-01690-9.

The comparison of the intensity ratios of DPPC and DPPC:DOPC (9:1) monolayers prepared at 30 mN/m surface pressure infer the conformational order of the two-component layers. It suggests that the spectral features of DPPC:DOPC (9:1, v:v) monolayer are identical to that of the one-component DPPC layer deposited under a surface pressure of 10–15 mN/m. Significantly, these observations suggest that the presence of unsaturated DOPCs can act as fluidizing minor components in the membrane and reduce the actual surface pressure. Previous studies reported that the addition of DOPC to the monolayer might increase the permeability of the membrane to molecules indispensable for lung surfactants and respiration [265, 266]. Comparing the methylene $CH_{2\text{-}S}$ to methyl $CH_{3\text{-}S}$ bands ratio of DOPC and DOPC: DPPC (9:1, v:v), suggests that the addition of a small amount of saturated DPPC onto unsaturated DOPC molecules highly improved the conformational order of the monolayer as visualized in Figure 6.8. Specifically, the addition of 10% of the volume of saturated lipids decreased the number of *gauche* defects to approximately half of its original value (see DOPC versus DOPC: DPPC in Figure 6.8). The result obtained here showed that it is possible to discriminate against the VSFG signals of heterogeneous mixtures at the interface even in low surface coverages. It should be noted that these results were possible only because of the improved sensitivity of the BB-VSFG spectrometers.

6.3 The applicability of the HRR-BB-VSFG spectrometer to studies of phospholipids at interfaces

6.3.1 Minimal integration time for spectral acquisition

To study the shortest integration time possible for collecting a BB-VSFG spectrum, the experiments were performed on a DPPC monolayer prepared on a CaF_2 window applying a 30 mN/m surface pressure. The normalized BB-VSFG spectra were collected with a single-acquisition time of 500 ms in both ppp and ssp polarization combinations are shown in Figure 6.9.

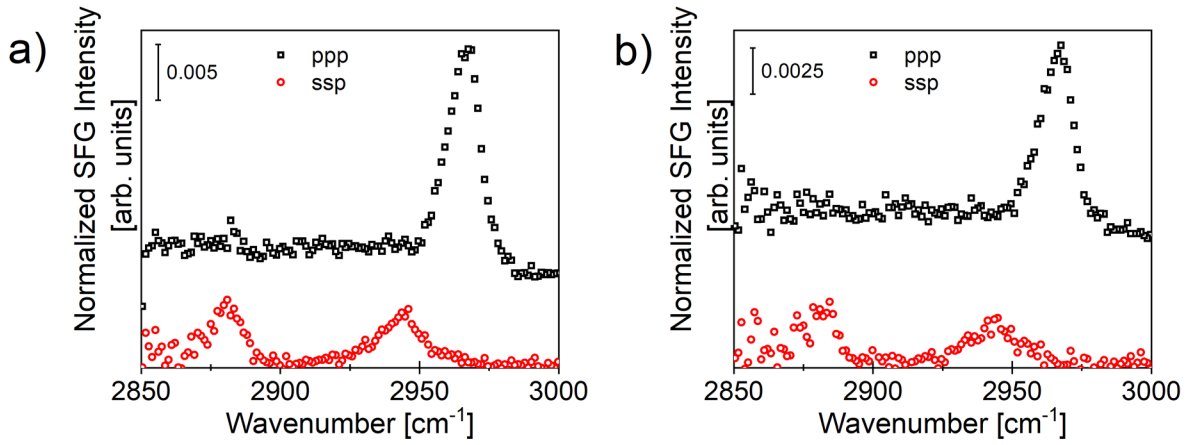

Figure 6.9 The BB-VSFG spectra of DPPC monolayer obtained at a) 1 s and b) 500 ms integration time in ppp, black and ssp, red polarization combinations.

The SNR values of BB-VSFG spectra obtained at integration times of 1 s and 500 ms are 54 and 30, respectively. These results show that by employing our spectrometer, it is possible to track second-scale changes in the C–H stretching region. The spectrum collected at an acquisition time less than 1 s has the potential to follow fast, < 10 min, catalytically mediated reactions or biomolecular interactions in real-time at heterogeneous surfaces with interfacial structural and orientational information.

The VSFG spectra of unsaturated PC monolayers on a solid substrate change over time that indicating the degradation of alkyl tails in ambient laboratory conditions [218]. Often these changes were observed in the VSFG spectra as spectral distortions within 20 min [218, 234]. In our case, the 100 kHz BB-VSFG spectrometer provided an opportunity to acquire rapid (< 5 min) data that ensured the minimum lipid decomposition. These experiments can also state that the HRR-BB-VSFG spectrometer employed for the measurements is an excellent label-

free tool that can probe interfacial molecules even at low surface coverage with high sensitivity. The spectral features of the PC monolayers remain unchanged even after the data collection of two or three different polarization combinations [221] as shown in Chapter 5.

Table 6.5 The summary of BB-VSFG assignments of DPPC monolayer in the C-H, N-H, and O-H stretching region.

DPPC ω_ν **[cm^{-1}]**	**Assignments**	**References**
2840	CH_2 sym. str. of hydrocarbon chains or choline or glycerol moiety	[235]
2851	CH_2 sym. str. of hydrocarbon chain	[5, 198, 227, 235, 262]
2856	CH_2 sym. str. of choline or glycerol group	[198, 235]
2868	CH_3 sym. str. of choline head group	[245]
2880	CH_3 sym. str. of end group	[5, 198, 227]
2899	R_3C-H / CH_2 Fermi resonance	[5, 198, 227, 235]
2913	CH_2 Fermi resonance (C-H str. + H-C-H bend)	[5, 198, 227, 262]
2932	CH_2 asym. str.	[228]
2940	CH_3 Fermi resonance (C-H str. + H-C-H bend)	[5, 198, 227, 228]
2957	CH_3 sym. str. of choline group	[226, 262]
2969	CH_3 asym. str. of end group (in-plane component)	[5, 198, 227]
3065	CH_3 asym. stretching of choline group	[5, 198]
3200	O-H str. of water near phosphate and choline group	[229, 253, 254]
3400	O-H str. of water near phosphate and choline group	[229, 253, 254]

sym.: symmetric, asym.: asymmetric, str.: stretching

Table 6.6 The fitted parameters of one-component, DPPC, and DOPC, two-component, 9:1 (v:v) of DPPC:DOPC and DOPC:DPPC monolayers in ppp, ssp, and sps polarization combinations. DPPC and DPPC:DOPC monolayers were prepared at 30 mN/m, while DOPC and DOPC:DPPC 9:1, monolayers at 5 mN/m surface pressures. ω_v, Γ_v, and A_v represent the central frequency, line width, and amplitude of the vth vibrational mode, respectively. Adapted from the publication, 2019, 411, 4861–4871.

	ω_v [cm^{-1}]	Γ_v [cm^{-1}]	A_v (DPPC)	A_v (DPPC: DOPC)	ω_v [cm^{-1}]	Γ_v [cm^{-1}]	A_v (DOPC)	A_v DOPC: DPPC
					2815.00±0.06	4.24±0.20	0.07±0.09	-0.25±0.06
					2819.40±1.95	4.18±0.18	0.01±0.08	0.02±0.07
	2839.9±2.98	4.38±0.07	0.23±0.05	0.20±0.09	2842.87±1.54	3.65±0.02	0.05±0.02	0.04±0.04
	2850.7±2.22	3.77±0.50	0.23±0.05	0.12±0.10	2851.99±0.57	5.09±1.07	0.37±0.04	0.63±0.07
	2855.9±3.10	4.45±0.52	0.55±0.04	0.16±0.08	2856.47±0.65	5.56±0.15	0.97±0.06	1.98±0.10
	2867.6±1.80	6.46±0.30	0.66±0.07	0.76±0.09	2863.33±0.93	9.62±1.39	3.01±0.06	3.24±0.13
p								
p	2879.5±0.84	6.14±0.54	9.08±0.05	3.46±0.05	2880.39±3.77	9.81±1.81	1.91±0.06	4.60±0.11
p	2899.4±1.19	9.65±4.08	3.37±0.20	0.42±0.15	2898.81±3.52	14.52±1.85	7.78±0.12	4.34±0.17
	2912.7±1.34	12.22±3.85	10.84±0.21	3.06±0.18	2911.19±1.20	13.19±2.85	5.54±0.10	7.09±0.17
	2931.9±2.55	8.60±2.51	9.69±0.16	2.10±0.18	2926.79±0.73	8.94±1.45	3.00±0.05	7.54±0.19
	2939.5±2.04	5.96±2.05	2.81±0.09	3.05±0.14	2934.80±1.63	6.39±2.54	0.27±0.03	1.96±0.19
	2957.4±1.52	8.19±0.89	-23.64±0.05	-10.41±0.06	2954.82±2.31	5.83±1.35	0.38±0.04	1.62±0.11
	2969.2±0.23	6.01±0.56	22.98±0.03	12.00±0.02	2962.20±1.36	6.21±2.29	0.31±0.05	1.26±0.11
					2815.00±0.06	4.24±0.20	0.05±0.04	-0.24±0.08
					2819.40±1.95	4.18±0.18	-0.11±0.04	0.08±0.07
	2839.9±2.98	4.38±0.07	0.46±0.09	0.32±0.10	2842.87±1.54	3.65±0.02	0.08±0.03	0.06±0.03
	2850.7±2.22	3.77±0.50	0.45±0.11	0.39±0.10	2851.99±0.57	5.09±1.07	1.26±0.05	2.17±0.08
	2855.9±3.10	4.45±0.52	0.86±0.12	0.01±0.07	2856.47±0.65	5.56±0.15	1.30±0.06	2.05±0.07
	2867.6±1.80	6.46±0.30	0.18±0.08	0.12±0.07	2863.33±0.93	9.62±1.39	1.97±0.09	3.18±0.09
s								
s	2879.5±0.84	6.14±0.54	23.86±0.04	9.38±0.04	2880.39±3.77	9.81±1.81	1.38±0.08	4.70±0.07
p	2899.4±1.19	9.65±4.08	0.76±0.18	1.61±0.17	2898.81±3.52	14.52±1.85	0.28±0.1	1.87±0.21
	2912.7±1.34	12.22±3.85	0.48±0.25	0.04±0.20	2911.19±1.20	13.19±2.85	4.28±0.08	7.95±0.22
	2931.9±2.55	8.60±2.51	0.23±0.16	1.70±0.19	2926.79±0.73	8.94±1.45	3.34±0.06	5.08±0.08
	2939.5±2.04	5.96±2.05	20.06±0.15	7.90±0.20	2934.80±1.63	6.39±2.54	1.35±0.04	2.14±0.08
	2957.4±1.52	8.19±0.89	3.18±0.37	2.19±0.22	2954.82±2.31	5.83±1.35	-0.68±0.1	-0.78±0.15
	2962.3±2.14	7.99±2.58	-9.99±0.57	-7.55±0.22	2962.20±1.36	6.21±2.29	0.05 ± 0.1	-0.19±0.16
					2815.00±0.06	4.24±0.20		-0.08±0.02
					2819.40±1.95	4.18±0.18		0.05±0.02
	2839.9±2.98	4.38±0.07	0.65±0.05	0.21±0.25	2842.87±1.54	3.65±0.02	0.03±0.04	0.07±0.01
	2850.7±2.22	3.77±0.50	0.18±0.05	0.03±0.44	2851.99±0.57	5.09±1.07	0.11±0.05	0.19±0.02
	2855.9±3.10	4.45±0.52	0.00±0.05	0.00±0.50	2856.47±0.65	5.56±0.15	0.02±0.09	0.23±0.03
s	2867.6±1.80	6.46±0.30	1.09±0.06	0.08±0.33	2863.33±0.93	9.62±1.39	0.74±0.08	1.02±0.04
p								
s	2879.5±0.84	6.14±0.54	1.73±0.07	0.25±0.34	2880.39±3.77	9.81±1.81	0.12±0.06	0.30±0.06
	2899.4±1.19	9.65±4.08	3.53±0.09	3.00±0.52	2898.81±3.52	14.52±1.85	3.8±0.12	3.92±0.06
	2912.7±1.34	12.22±3.85	0.81±0.05	0.25±0.22	2911.19±1.20	13.19±2.85	2.91±0.13	1.00±0.03
	2931.9±2.55	8.60±2.51	0.50±0.04	0.37±0.15	2926.79±0.73	8.94±1.45	0.16±0.12	0.20±0.04
	2939.5±2.04	5.96±2.05	9.75±0.09	2.22±0.16	2934.80±1.63	6.39±2.54	0.50±0.10	0.03±0.03
	2957.4±1.52	8.19±0.89	-20.46±0.03	-10.78±0.04	2954.82±2.31	5.83±1.35	0.76±0.06	0.70±0.03
	2965.1±2.33	7.78±0.34	13.87±0.02	10.91±0.05	2962.20±1.36	6.21±2.29	0.76±0.06	2.70±0.03

6.4 Conclusion

In this chapter, the HRR-BB-VSFG spectra of one- and two-component solid-supported lipid monolayers of saturated DPPC and unsaturated DOPC were studied at different surface pressures and mixing ratios. The spectra were collected at the C-H and O-H stretching region as the alkyl chain of the phospholipids plays an important role in maintaining the structure, stability, and fluidity of the lung surfactants.

The vibrational spectra were carefully studied to elucidate the interfacial structural information of alkyl chains of the phospholipid monolayers at the air-CaF_2 interface. The fitting of the spectral features was challenging and tedious. In this work, the BB-VSFG spectra of alkyl chains were fitted using a sum of eleven Lorentzian line profiles. In general, only five to six vibrational resonances are resolved using conventional spectrometers [6, 7, 198, 224]. Subsequently, the spectral peaks were assigned to vibrational resonances. The results of a systematic study of phospholipids at different surface pressure revealed that the vibrational bands near 2850 cm^{-1} are better resolved, and enabled in quantifying the defects in the alkyl chain of the phospholipids, compared to the standard VSFG spectra. Additionally, the overtones and combinations of vibrational modes at 2899 cm^{-1}, 2913 cm^{-1}, and 2932 cm^{-1} in the present work were better resolved than the typical VSFG spectrometer. The band at 2868 cm^{-1}, was assigned to the symmetric stretching of the methyl group from the head group. The new vibrational bands of the PC monolayers in the C-H stretching region are observed to have an unprecedented SNR value of ~ 2000, which can prove tremendously beneficial in the investigation of heterogeneous interfaces. We were able to maintain natural lipid structure without introducing measurement artifacts due to labeling and sample deterioration during spectral acquisition. The result shows remarkable SNR at low surface coverages. These results of high SNR from the low surface coverage samples were reported first time in BB-VSFG spectroscopy, as the sensitivity of the BB-VSFG spectrometer limits the characterization of the low surface coverage PC monolayers. The spectra of the O-H stretching region were studied to obtain the structure of the water molecules entrapped within the monolayers and between the substrate and phospholipid head groups.

In conclusion, the vibrational features acquired in multiple polarization combinations provided qualitative and quantitative interfacial structural information of both one- and two-component phospholipid monolayers. The spectral features obtained here showed newly observed vibrational bands in the C-H stretching region which can offer valuable information on the packing of the lipid hydrocarbon chains and diffusion properties of lipid bio-membranes. The

shorter timescale for obtaining VSFG spectra promises to study structural and orientational information of catalytically mediated reactions or biomolecular interactions at heterogeneous interfaces. The fast measurements promise the characterizing heterogeneous interfaces over macroscopic biological timescales. The structure of PC discussed in this chapter may help the development of new synthetic surfactants and enable to study of changes in lipid structure during interactions.

7. Interfacial structure of head groups of phosphatidylcholines

The head groups including the glycerol moieties of phospholipids have crucial importance in the hydration of lipids, interaction with solvents and solutes, variations in physiological pH, and the inter- and intra- molecular interactions. The hydration of the phospholipids leads to the formation of several lyotropic mesomorphic structures that include monolayers, bilayers, micelles, and vesicles in the aqueous environment. The formation of these polymorphic structures depends on several factors such as chemical structure [267], stereoisomerism [268, 269], lipid polarity, the ionic (or zwitterionic) character, or the size of the lipid head groups. Different phospholipids differ in the inter- and intra-chain interactions [270]. The interaction of lipids depends on the physical and chemical properties of the interaction partner. Amphiphilic molecules interact with both the head groups and fatty acid chains. The polar molecules directly interact with the head groups, and the non-polar molecules mostly show an affinity for the alkyl chains. Additionally, phospholipids interact with different anions and cations depending on the surface charge density of the head groups [8, 271-274].

The vibrational information of the phosphate and ester moiety of lipids reveal information about interactions, for example, hydration, ion-dipole interactions between phospholipids and interfacial water, Columbic forces between the headgroup, and ions, and/or other biomolecules. The fingerprint region of the vibrational spectra is rich in vibrational modes therefore many vibrational modes are observed to overlap one another. Investigating phospholipids using a high-resolution, highly sensitive spectrometer such as HRR-BB-VSFG in the fingerprint region provides further information on their interfacial structures. In this section, the head groups of partially deuterated (DPPC-d62) and non-deuterated saturated (DPPC), and unsaturated

(DOPC) phosphatidylcholines were probed using the HRR-BB-VSFG spectrometer. The monolayers of different phosphatidylcholines were prepared using Langmuir-Blodgett (LB) depositions and the BB- VSFG spectra were obtained in the fingerprint region. The BB-VSFG spectra of DPPC-d62, DPPC, and DOPC were studied and compared to observe the changes in the interfacial structure of the head group including the glycerol moieties with different fatty acid chains.

7.1.1 Sample preparation

Partially deuterated and non-deuterated phospholipid monolayers were prepared for investigating the interfacial structure in detail. Phospholipids used for the VSFG measurements were 1,2-dipalmitoyl-sn-glycero-3-phosphocholine (16:0 PC, DPPC), 1,2-dioleoyl-sn-glycero-3-phosphocholine (18:1 Δ9-*cis* PC, DOPC) and 1,2-dipalmitoyl-d62-sn-glycero-3-phosphocholine (16:0, DPPC-d62). These three PCs have different physicochemical properties due to their chemical structure. The chemical structures of DPPC, DOPC, and DPPC-d62 are illustrated in Figure 7.1. The head groups of each molecule are identical, but the alkyl chains differ. In the case of non-deuterated DPPC, the chains are fully hydrogenated and the majority of the methylene groups lie in a locally centrosymmetric environment, specifically, all-trans conformation. The DOPC molecules have a C=C bond in each of their chains, whereas partially deuterated DPPC-d62 have fully deuterated chains in all-trans conformation. Comparing the structure of DPPC (16:0) to DOPC(18:1), they have the identical choline head group, and their alkyl chains differ in length and the conformation, i.e., all-trans and Δ9-cis for DPPC and DOPC, respectively.

The monolayers of DPPC, DOPC, and DPPC-d62 were prepared by Langmuir-Blodgett (LB) deposition technique. Kibron MicroTrough XS apparatus controlled by Filmware X 4.0 software (Kibron, Helsinki, Finland) [64, 65, 233] was used for the deposition. The procedures were as follows. First, the LB trough and the two barriers were cleaned thoroughly with ethanol and water. The barriers were placed in the initial position and the LB trough was filled with water after the cleaning. Then, the calibration of surface pressure was performed in air and water using a dyne probe. After calibration, the previously cleaned CaF_2 window was clamped to the dip coater and gently immersed into the water (see 4.2.2). The CaF_2 plates used for the deposition were freshly cleaned to avoid any contamination on the surface. The plates were initially sonicated for 20 min in ethanol and water. After initial cleaning with organic solvents, the plates were annealed at 500°C for 2 hours. The plates were lifted and placed to clean both

sides of the CaF_2 window in a quartz chamber during the annealing process. A nitrogen flux was applied for 2 min in three steps to eliminate impurities from the surface of the plates. The steps were as follows: i) during the start of the annealing, ii) after 1 hour, and iii) after 2 hours until the plate temperature reduced to low enough values to be removed from the quartz chamber. The CaF_2 windows were dipped in water to avoid contaminations until the LB deposition.

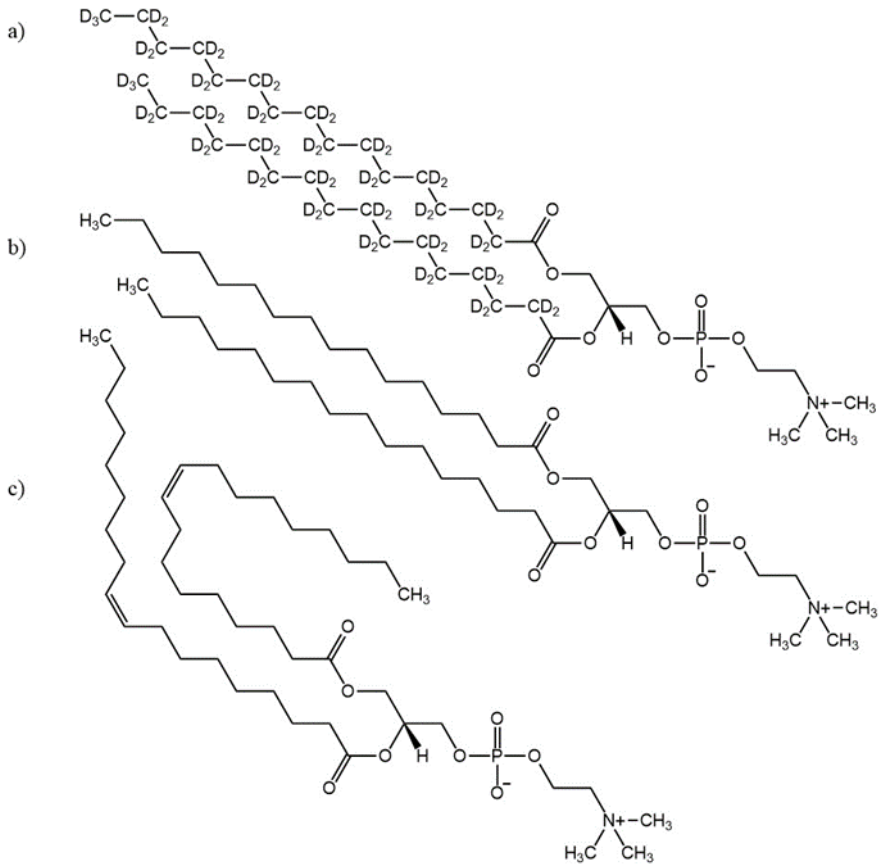

Figure 7.1 The chemical structure of a) partially deuterated and saturated 1,2-dipalmitoyl-d62-sn-glycero-3-phosphocholine (DPPC-d62), b) non-deuterated and saturated 1,2-dipalmitoyl-sn-glycero-3-phosphocholine (DPPC, 16:0), and c) non-deuterated and unsaturated 1,2-dioleoyl-sn-glycero-3-phosphocholine (18:1 Δ9-*cis* PC, DOPC).

A volume of 20 µl of the stock solution was spread on the water surface using a Hamilton syringe. The preparation of the stock solution was elaborated in Material and Methods. The 1 mg/ml stock solutions of these PCs were prepared in chloroform: methanol (9:1, v: v) mixture. The PC solutions were handled with care to prevent contamination, degradation, and to maintain a stable concentration. The PC stock solutions were kept in the freezer (i.e., -20°C), as they are sensitive to the ambient conditions. The stock solutions were stored in glass containers with Teflon sealing as the chloroform can dissolve the plastic vials.

The monolayer formed at the air-water interface was kept for 15 min to evaporate the organic solvents. The barriers were moved to apply surface pressure of 30 mN/m on the monolayers. A constant barrier moving speed of 5 mm/min was applied during the compression processes. When the surface pressure reached 30 mN/m, the monolayer of PCs at the air-CaF_2 interface was transferred to the CaF_2 window by vertically lifting it at a raising speed of 1 mm/min. The monolayer formed on the surface of the water was transferred to the CaF_2 window due to the amphipathic nature of the phospholipids. The transferred monolayers were measured using the BB-VSFG spectrometer within < 2 min.

7.1.2 Surface pressure-area isotherm of partially deuterated and non-deuterated phosphatidylcholine

For the VSFG measurements, monolayers were prepared by applying the surface pressures of 30 mN/m. The surface pressure-area per molecule isotherms for each sample were collected during the sample preparation. The isotherms of deuterated DPPC-d62 and non-deuterated DPPC and DOPC, monolayers are shown in Figure 7.2. These isotherms were measured at 24°C on a pure water sub-phase.

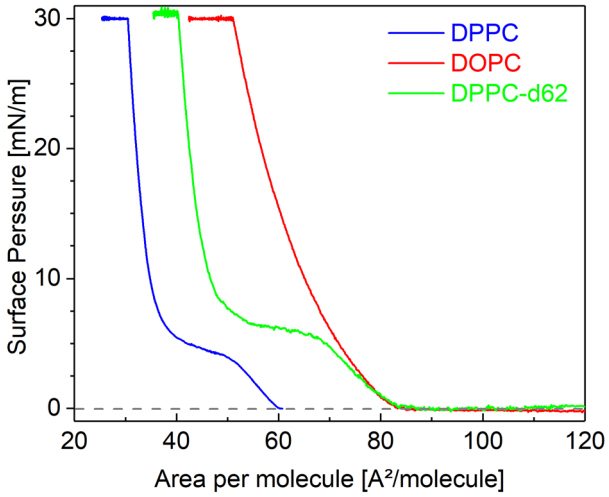

Figure 7.2 The surface pressure-area isotherms of partially deuterated and non-deuterated phosphatidylcholine monolayers at the air-water interface. The blue, green, and red curves illustrate DPPC, DPPC-d62, and DOPC.

The isotherms were similar as reported before [193, 234]. As discussed in Chapter 6, the non-deuterated DPPC monolayer experiences all the 2-dimensional liquid phases such as gas-liquid expanded (G-LE), liquid-expanded (LE), liquid-expanded-liquid-crystalline (LE-LC), liquid crystalline (LC) where all these phases are visible in Figure 7.2. The rising of surface pressure was observed at ~60 $Å^2$/molecule in the case of DPPC. The mean molecular area of the LC

phase ranges from 30 to 37 Å^2/molecule whereas the collapse point of the DPPC monolayer on the water surface was observed to be at 65 mN/m (see Figure 6.2). The rising area of the DOPC and the DPPC-d62 were observed around 87 - 88 Å^2/molecule. The collapse point of the DPPC-d62 mixture was reported at about 63 mN/m, slightly lower than the pure DPPC monolayer [275]. The DOPC exists in the LE phase in water throughout the compression. The collapse pressure of DOPC was observed at 40 mN/m (see Figure 6.2). Comparing the DPPC and the DOPC (blue and red curves in Figure 7.2), a vast deviation in isotherm was observed. This difference is due to the increase in the number of gauche conformers in the alkyl chains of the DOPC, which increases the mean molecular area between the molecules.

7.1.3 BB-VSFG measurements data pre-processing

Initially, the BB-VSFG spectra of polystyrene and Au (111) were obtained by spatially and temporally overlapping the MIR and VIS beams for calibration of the sample spectra. The MIR and VIS beams were focused on the phospholipid monolayers to obtain the BB-VSFG spectra after collecting the Au (111) spectra and polystyrene spectra. The vibrational spectra of the phospholipid's head groups were obtained between 1000 cm^{-1} and 1370 cm^{-1} where the central frequency of the MIR beam was at 1240 cm^{-1}. After obtaining the raw BB-VSFG spectra of phospholipids, the pre-processing was performed as follows. First, the wavenumber axis was calculated from the wavelength axis. Then, the spectra were calibrated with two absorption bands at 1154 cm^{-1} and 1181 cm^{-1} of polystyrene on the NIST database. These absorption bands of polystyrene were obtained by inserting a 50 μm thick film in the path of the MIR beam while obtaining the BB-VSFG spectra of Au (111) surface. This was followed by removing all spikes from the spectra. Finally, the background spectra were averaged and subtracted from the raw BB-VSFG spectra. These background spectra were obtained by keeping the VIS beam switched ON. Finally, the Au (111) spectrum was used to normalize the spectra. The normalization of each spectrum with Au (111) spectrum is a mandatory procedure to have a reliable intensity ratio in the entire spectral range. The spectral features were assigned to vibrational modes. These spectral assignments presented here are preliminary. All procedures above were carried out by using home-written MATLAB scripts. More details about the BB-VSFG experimental setup and data pre-processing are explained in detail in Materials and Methods (section 4.2).

7.2 HRR-BB-VSFG spectra of deuterated and non-deuterated phosphatidylcholines

To compare the interfacial structure of headgroups of phospholipids, the BB-VSFG spectra of non-deuterated (DPPC) and partially deuterated (DPPC-d62) were obtained. The normalized BB-VSFG spectra obtained by ppp and ssp polarization combinations in the spectral range between 1000 cm^{-1} and 1370 cm^{-1} with an acquisition time of 30 s are shown in Figure 7.3.

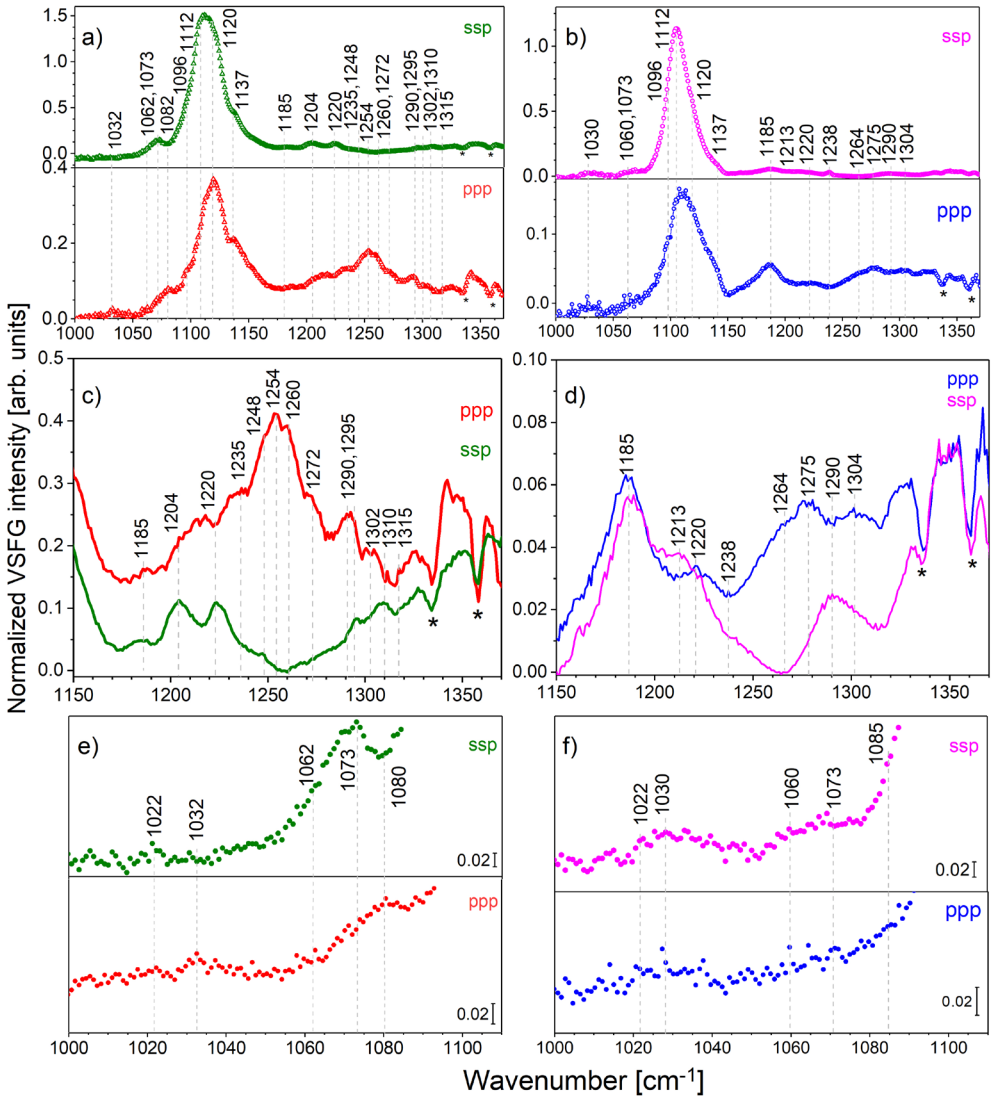

Figure 7.3 Normalized BB-VSFG spectra of non-deuterated DPPC (a and c), and partially deuterated DPPC-d62 (b and d) monolayers obtained by ppp and ssp polarization combinations on the surface of the CaF_2 window with 30 s integration time. The c) and d) are the inserts of the BB-VSFG spectra non-deuterated DPPC and partially deuterated DPPC-d62 between 1150 cm^{-1} and 1370 cm^{-1}. The asterisk symbols represent the rotational absorption of water vapor in ambient conditions. The e) and f) are the insert of the BB-VSFG spectra of non-deuterated DPPC and partially deuterated DPPC-d62 between 1000 cm^{-1} and 1090 cm^{-1}.

In Figure 7.3, the red and green lines represent the DPPC monolayers where the blue and magenta denote the DPPC-d62 monolayers obtained at the ppp and ssp polarization combinations, respectively. The inserts of the BB-VSFG spectra were shown in Figure 7.3 c-f. The spectra in the fingerprint region are generally rich with vibrational modes. The vibrational modes observed in this spectral range are symmetric and asymmetric PO_2^-, CH_2 wagging, C-C, and CO-O-C stretching modes. The preliminary spectral assignments of vibrational resonances of DPPC and DPPC-d62 monolayers measured at the air-CaF_2 interface in the spectral range of 1000 cm^{-1}-1370 cm^{-1} are summarized in Table 7.1.

7.2.1 Non-deuterated and partially deuterated phosphatidylcholines

PO_2^- symmetric mode

In our BB-VSFG spectra of the DPPC monolayer, we observed a prominent feature centered at 1110 cm^{-1}, where several vibrational bands overlap. A band that appeared as a shoulder of this feature at 1096 cm^{-1} was assigned to the PO_2^- symmetric stretching mode [8, 276]. Our observation was in accordance with previous results [5, 7, 102, 103] where this region from 1000 cm^{-1} to 1370 cm^{-1} was extensively studied using IR and Raman spectroscopy [102, 106, 277, 278]. The vibrational frequencies of the phosphate group were estimated by Shimanouchi et al. in 1964 [279, 280]. Lippert et al. reported the transition band at 1100 cm^{-1} where this spectral feature was assigned to the skeletal modes of phospholipids which come from both the hydrocarbon rotamers and the phosphate group [281]. Later, Brown et al. assigned this feature around 1100 cm^{-1} to PO_2^- symmetric stretching [118]. Spiker and Levin observed a distinct band that appears at 1081 cm^{-1} which is assigned to the PO_2^- symmetric stretching mode of phosphate head group in lysolecithin [119]. They emphasize that the 1100 cm^{-1} region of the phospholipid is a superposition of the C-C modes of the all-trans hydrocarbon in gel or crystalline states, C-C modes of the gauche hydrocarbon chains, and the symmetric PO_2^- stretching mode [119]. They concluded that the phosphate mode of DPPC is buried within the 1100 cm^{-1} by calculating the band areas and comparing the intensity ratios of lysolecithin and dipalmitoylphosphatidylcholine [119].

PO_2^- asymmetric and P=O stretching modes

A broad vibrational band appears around 1254 cm^{-1}, which showed a positive and negative sign in ppp and ssp polarization combinations of non-deuterated DPPC spectra and blue-shifted to 1264 cm^{-1} in the case of partially deuterated DPPC-d62 spectra, respectively. We assigned this vibrational mode to PO_2^- asymmetric stretching [276, 280]. The reason for this blue shift of

asymmetric PO_2^- stretching to 1264 cm^{-1} can be due to the effect of dehydration of the DPPC-d62 monolayer, or the absence of CH_2 wagging propagation in the deuterated chains. Additionally, any changes in the orientation of the transition moment of the PO_2 bonds may also cause this blue shift, which has been proposed to lay in the plane of the monolayer or bilayer, compared to the DPPC molecule [282]. The VSFG band at 1254 cm^{-1} was first observed and assigned by Liljeblad et al. in VSFG spectroscopy [5]. The behavior of the phosphate vibrations changes drastically upon hydration and is reported as the most hydrated moieties of phospholipid molecules [283]. They solvate in water forming strong hydrogen bonds [283-286]. Wallach et al. [287] observed that the asymmetric PO_2^- shifts about 32 cm^{-1} when hydrating dry films of non-deuterated DPPC and 1,2-dipalmitoyl-sn-glycero-3-phosphoethanolamine (DPPE). The asymmetric PO_2^- stretching modes show a blue shift upon dehydration [288, 289]. This mode was observed to shift from 1250 cm^{-1} to 1230 cm^{-1} with increasing hydration levels. Elsaesser and Hynes studied the structural dynamics of asymmetric PO_2^- stretching mode of DNA and/ or phospholipids in an aqueous environment [288, 290]. In fully hydrating the phosphate head group, the O-P-O^- bond angle changes by approximately 3° [284]. The phosphate groups are primary hydration sites up to six water molecules building a local water shell around the PO_2^- units [290]. Thus, phosphate groups can be used as reporter modes of hydration. A vibrational band appeared at 1248 cm^{-1} in DPPC and at 1238 cm^{-1} in DPPC-d62, which was assigned to the P=O stretching band [108]. This vibrational mode was observed in both polarization combinations. The P=O stretching mode shows peak splitting due to the presence of rotational isomers in the solution, [291, 292]. We observed this band at the same position as reported for monohydrate DPPC studied by Wallach et al. [287]. This band was not observed in the partially deuterated DPPC-d62. The absence of this band might be due to the change in the orientation of the phosphate group.

C-C stretching modes

Other features appeared at 1060 cm^{-1}, and 1120 cm^{-1}, in the BB-VSFG spectra of DPPC monolayers. These bands were assigned to skeletal optical modes of the phospholipid alkyl chains, namely, C-C stretching of all-*trans* conformation where we assigned the band at 1082 cm^{-1} to the C-C stretching associated with different kinds of the *gauche* structure due to the bond rotation of the terminal methyl group. The band at 1112 cm^{-1} was assigned to the C-C stretching coupled with the end group. These skeletal optical vibrational modes in n-paraffin chains were theoretically modeled by Snyder et al. [293, 294]. These bands were also observed and assigned in Raman spectroscopy [119]. Gaber et al. studied these vibrational modes and

used them to quantify the conformational order of alkyl chains in phospholipids at different temperatures [248]. Liljeblad et al. assigned 1030 cm^{-1} to the C-C vibrational mode. Based on the information obtained from the literature, the C-C stretching appears at higher frequencies. More information about the C-C stretching in our spectra can be only discussed after fitting Lorentzian line profiles and considering the area under the spectral feature around 1100 cm^{-1}.

CH_2 wagging and twisting modes

New bands were observed further at 1185 cm^{-1}, 1204 cm^{-1}, 1220 cm^{-1}, 1235 cm^{-1}, 1266 cm^{-1}, 1272 cm^{-1}, 1290 cm^{-1}, 1295 cm^{-1}, 1302 cm^{-1}, and 1310 cm^{-1}. We assign the bands at 1170 cm^{-1}, 1235 cm^{-1}, 1266 cm^{-1}, 1295 $cm^{-1,}$ and 1310 cm^{-1} to the methylene (CH_2) wagging propagation along the alkyl chains [108, 277, 295, 296]. These vibrational modes were observed in DPPC and they were absent in DPPC-d62, suggesting that these modes arise from the C-H wagging progression of the alkyl chains. The bands at 1185 cm^{-1}, 1204 cm^{-1}, 1220 cm^{-1}, 1290 cm^{-1}, and 1304 cm^{-1} were observed in both DPPC and DPPC-d62 suggesting that these vibrational modes are occurring as a result of the wagging motion of the CH_2 groups present in the choline head region.

Our results show that the methylene wagging from the head groups of deuterated DPPC-d62 can be discriminated by using HRR-BB-VSFG spectrometers. These observations were possible because of the applied high laser repetition rate and the resulting high signal-to-noise ratio of the BB-VSFG spectrometer [3, 4]. This CH_2 wagging progression was observed in long-chain fatty acids [297] and predicted in n-paraffin [293, 294] and later, observed in phospholipids by Chapman et al. [101]. The deuteration of alkyl chains of the phospholipids leads to a simplification of the BB-VSFG spectra in the fingerprint region as the methylene wagging progressions and rocking-twisting bands disappear from their normal position in the 1200-1370 cm^{-1} region. A drastic change in the spectral range between 1150 cm^{-1} and 1370 cm^{-1} was observed in the case of DPPC-d62 compared to DPPC. It should be noted that the relative intensity of the bands was observed to be much less in DPPC-d62 compared to DPPC.

R-O-P-O-R, C-O-P, and CO-O-C modes

A broad band feature centered around 1072 cm^{-1}, has many vibrational frequencies, and it is challenging to assign exact vibrational modes to each of them. From the preliminary perspective, the bands centered at 1030 cm^{-1} and 1060 cm^{-1}, we assigned to C-O-P out-of-phase and C-O-P in-phase symmetric stretching vibrations of the polar head groups in the

phosphate, respectively [229]. In our spectra, the vibrational mode around 1030 cm^{-1} was observed in the BB-VSFG spectra of DPPC, which is less intense in the DPPC-d62 monolayer. This might be due to the change in orientation of the head groups or the hydration level of partially deuterated DPPC-d62 compared to the non-deuterated DPPC.

We assigned these vibrational bands by comparing our spectral features with triethyl phosphate [108]. The band at 1070 cm^{-1} was assigned to the C-O symmetric stretching of the CO-O-C ester group [229]. The feature at 1080 cm^{-1} was assigned to the R-O-P-O-R [229]. In the VSFG community, contradictions among research groups in assigning these vibrational modes were noted [5, 8]. Liljeblad et al. assigned 1072 cm^{-1} to the C-O symmetric stretching of the glycerol CO-O-C ester group, where Allen et al. assigned the same vibrational mode to R-O-P-O-R. Arrondo et al. observed the band at 1060 cm^{-1} and assigned to R-O-P-O-R [298]. Casal et al. observed the band at 1050 cm^{-1} and assigned it to a C-O-P vibrational mode [278]. The C-O stretching bands of the ester group have generally less characteristic frequencies. As these vibrational modes are coupled with the C-C stretching vibrations, the band assignments are generally difficult. Additionally, the longer and the shorter chains in the phospholipids give rise to vibrational modes of higher and shorter frequencies, respectively [245]. We assigned the band at 1137 cm^{-1} vibrational modes to asymmetric stretching of C-O single bond stretching of CO-O-C of the ester groups in the phospholipids [229, 276]. Theoretical modeling of dimyristoyl phosphatidylcholine predicted that the C-O stretching modes of both the chains are observed a few frequencies apart. We also assign the band at 1170 cm^{-1} to C-O stretching for this reason. Fringeli et al. conducted a detailed investigation on the ester linkage groups and assigned these vibrational bands in phospholipids and observed that these modes may shift in the range between 1160 cm^{-1} and 1190 cm^{-1} depending on the hydration [106]. The ester groups are hydrophilic groups after the phosphate moiety in phospholipids [299, 300]. In this region between 1000-1150 cm^{-1}, we also considered the contributions from the C-C skeletal optical modes and assigned them to appropriate wavenumbers.

Table 7.1 The BB-VSFG central wavenumbers and the assignments of DPPC and DPPC-d62 monolayer at the air-CaF_2 in the fingerprint region between 1000 cm^{-1} and 1370 cm^{-1}.

ν_{DPPC} [cm^{-1}]	$\nu_{DPPC\text{-}d62}$ [cm^{-1}]	Assignments	References
1032	1030	C-O-P out-of-phase str.	[108, 229]
1062	1060	C-O-P in-plane, C-C str. all-*trans* conformation	[293, 301]
1073	1072	C-O sym. str. of CO-O-C	[8, 102, 229, 243, 276, 298]
1080	1085	R-O-P-O-R sym. str., C-C str. *gauche* conformation	[204, 229, 245, 276, 301]
1096	1096	PO_2^- sym. str., parallel to the bisector of O-P-O angle	[7, 8, 120, 229, 302]
1112	1112	C-H deformations	[276, 293, 294]
1120	1120	C-C str. of all-*trans* conformation	[204, 301]
1137	1137	C-O asym. str. of CO-O-C	[229, 245]
1170		C-O str. of CO-O-C	[245, 288]
1185	1185	CH_2 wagging of alkyl chains + head groups	[295, 297]
1204	1213	CH_2 wagging of alkyl chains + head groups	[276, 295, 297]
1220	1220	CH_2 wagging of alkyl chains + head groups	[295, 297]
1235		CH_2 wagging alkyl chains	[295, 297]
1248	1238	P=O str., or CH_2 wagging alkyl chains	[108, 276, 295, 297]
1254	1264	PO_2^- asym. str., perpendicular to the bisector of O-P-O angle	[120, 276]
1266		CH_2 wagging of lipid alkyl chains	[295, 297]
1272	1275	CH_2 wagging of alkyl chains + head groups	[295, 297]
1290	1290	CH_2 wagging of alkyl chains + head groups	[295, 297]
1295		CH_2 twisting of alkyl chains	[302]
1302	1304	CH_2 wagging of both alkyl chains +head groups	[295, 297]
1310		CH_2 wagging of alkyl chains	[295, 297]

str.: stretching, sym. str.: symmetric stretching, asym. str.: asymmetric stretching.

7.2.2 Comparison of vibrational signatures of saturated and unsaturated phosphatidylcholine

To understand the effect of different chain groups on the head group moieties, the vibrational signatures of unsaturated DOPC (18:1), saturated DPPC (16:0), and partially deuterated DPPC-d62 were investigated and compared. Unsaturated phospholipids have at least one C=C double bond in their alkyl chains. The chemical structures were discussed in 7.1.1. The BB-VSFG spectra were measured using ppp and ssp polarization and shown in Figure 7.4 and the VSFG spectra of DOPC were directly compared with DPPC and DPPC-d62.

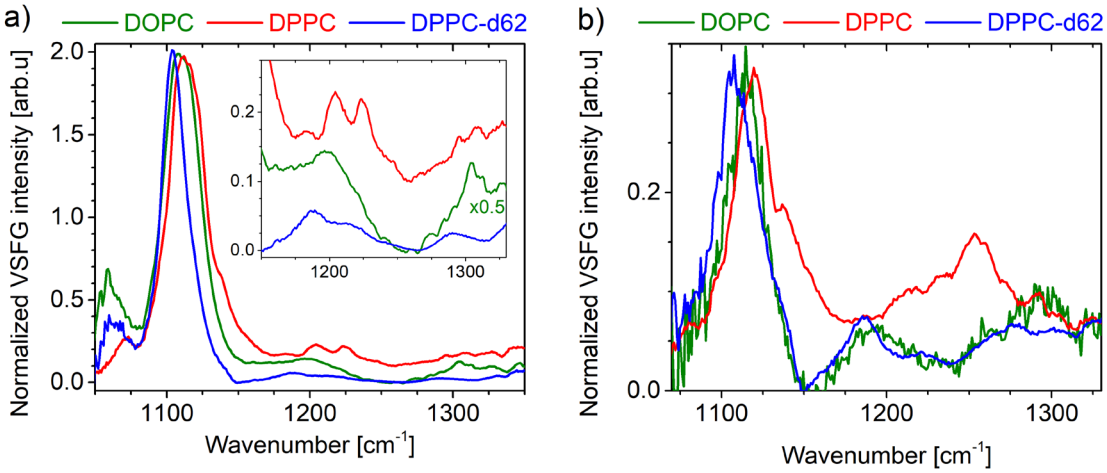

Figure 7.4 Normalized BB-VSFG spectra of DOPC (green), DPPC (red), and DPPC-d62 (blue). The left and right panels represent the BB-VSFG spectra obtained by using ssp and ppp polarization combinations, respectively. The insert is the magnification of the BB-VSFG spectra in the spectral range between 1150 and 1330 cm^{-1}.

The prominent feature around 1100 cm^{-1} in the BB-VSFG spectra of DPPC-62 (blue, see Figure 7.4), was blue shifted to the higher frequencies in the case of DOPC (green) and DPPC (red). The DOPC showed a minimal shift compared to DPPC. The red-shifted DPPC-d62 has a maximum in ssp at 1103 cm^{-1}, where DOPC and DPPC are blue-shifted by 5 cm^{-1} and 9 cm^{-1}, respectively. The central frequency in ppp differs from ssp: DPPC-d62: 1106 cm^{-1}, DOPC: 1114 cm^{-1}, and DPPC: 1120 cm^{-1}. This blue shift observed on the vibrational mode around 1100 cm^{-1} is similar to the effect of the surface pressure. That is, the area of molecules at a surface pressure of 30 mN/m vary and the different chains of phospholipids influences their membrane order (see in Figure 7.2), which will affect the orientation of the head groups. In our case, the DPPC, DOPC, and DPPC-d62 were prepared at 30 mN/m where the DPPC and DPPC-d62 exist in the LC phase and DOPC in the LE phase. This effect was also observed and reported by Allen et al. Studies show that the number of water molecules in the interfacial region varies

from ~9 per DPPC in the LC phase to ~4 per DPPC in the gel phase [57]. Their results showed that complete removal of water molecules from the head group is not likely. The blue shift of PCs suggests that there is either the orientation or hydration of the phosphate group of each phospholipid changed at the interface. Since the phospholipids were studied right after the deposition for each sample, the hydration state of the monolayers should be very similar to each other. Therefore, in our case, the head group orientations were probably different for the different lipids.

The PO_2^- symmetric stretching modes were observed and assigned by Allen et al. in VSFG spectroscopy [7]. Allen et al. studied the head group of deuterated and non-deuterated DPPC at different surface pressures ranging from 12 mN/m to 45 mN/m. They observed that the PO_2^- symmetric mode shifts from 1094 cm^{-1} to 1104 cm^{-1} as the surface pressure increases. They concluded that this blue shift is due to the dehydration of the phosphate group by compression of the monolayer. This phosphate frequency shift upon hydration was theoretically modeled on an analogous molecule of methylphosphocholine (MePC). The results revealed that hydration of the phosphate group induces the loss of electron density of the PO_2^- bonds due to strong hyperconjugation with the O-H antibonding orbital of water and weakens the PO_2^- bonds leads to weakening of the P-O bond resulting in a redshift [284]. This 10 cm^{-1} to 15 cm^{-1} shift of PO_2^- stretching mode due to hydration was also reported before in IR spectroscopy [102, 303]. To further understand the influence of hydration/dehydration on the phospholipids, an extension to the O-H stretching region is required by using BB-VSFG spectroscopy. Not only hydration but ions can also shift the PO_2^- symmetric mode. Allen et al. studied the region from 1090 cm^{-1} to 1100 cm^{-1} and reported that the phosphate symmetric mode shifts by 10 cm^{-1} to 15 cm^{-1} depending on the monovalent or divalent counterions such as K^+, Na^+, Ca^{2+}, Mg^{2+}. Their results show that the Ca^{2+} strongly affects the lipid headgroup conformations and induces a tighter packing of lipids, thus promoting the liquid condensed phase, where Na^+ has a minor influence [8, 229, 276, 278]. It does so by binding to both the phosphate and carbonyl oxygens via direct and water-mediated binding modes, the ratios of which depend on the monolayer packing. They also studied the interaction of cations with dipalmitoyl-phosphatidic acid (DPPA) at different physiological pH conditions [272]. They reported that the cations are found to expand and stabilize the DPPA monolayer in the increasing order of $Na^+ > K^+ > Mg^{2+} > Ca^{2+}$ at pH 5.6, where they observed this monolayer requires higher pHs than expected to deprotonate. This is because the negatively charged monolayers attract H^+ to the surface. Based on their result, the binding affinity of divalent cations to the DPPA monolayer follows the order $Ca^{2+} > Mg^{2+} > Na^+ > K^+$. Allen et al. also investigated the orientation of the phosphate group at

silica and water interfaces. They calculated the orientation or tilt angle, referred to as the angle between the vector connecting the phosphorus atom and the nitrogen atom (P-N vector), of the headgroup of DPPC monolayers on water and silica surfaces and reported that they are oriented 59°± 3° and 72°±5° from the surface normal, respectively [8]. Even though Liljeblad et al. studied the DPPC monolayer at the air-CaF_2 interface, the orientation of the phosphate headgroup on the CaF_2 interface was not reported before [5]. Based on our results, the tilt angle between the P-N vector at the CaF_2 window will be extracted by applying the orientational analysis used by Allen et al.

The spectral range between the 1150 cm^{-1} and 1300 cm^{-1} in DPPC-d62 and DOPC molecules are similar. The spectral features of unsaturated DOPC are entirely different in this range compared to the DPPC molecules. This drastic change can be due to the influence of the C=C double bond on the alkyl chains of the phospholipid. Comparing the BB-VSFG spectra of all the three phospholipids, such as DOPC, DPPC, and DPPC-d62, one can see that the width of the spectral feature centered at 1110 cm^{-1} is narrow in the case of DPPC-d62. This narrow linewidth of the spectral feature can be due to the absence of C-H deformation modes in DPPC-d62, where the chains contain only CD_2 groups. Recently, the VSFG spectra of DPPC were reported [276], an additional feature at 1112 cm^{-1} as a result of Lorentzian fitting, and assigned it to COH and CH deformations modes [276]. The fitting of Lorentzian line profiles on our BB-VSFG spectra allows us to further discuss this feature at the air-CaF_2 interface.

7.3 Conclusions

This chapter discussed the vibrational features of different phospholipids in the fingerprint region obtained by HRR-BB-VSFG spectroscopy. The spectra of the head group including the glycerol moieties of three different phosphatidylcholines were obtained and the spectral features were assigned to vibrational modes. We observed many vibrational modes, which have not been reported in conventional VSFG studies as they have weak Raman depolarization ratios, which require high measurement sensitivity with good spectral resolution (< 4 cm^{-1}). The use of a partially deuterated lipid enables us to eliminate the CH_2 wagging progression from the alkyl chains and discriminate the wagging from the phospholipid head groups. The detailed spectrum analysis allowed us to observe vibrational modes, which were previously lost beneath the stronger bands. The spectra obtained in our case are about 400 cm^{-1} broad while using a traditional broadband spectrometer based on Ti: Sapphire oscillator, the spectral bandwidth is generally only 150 cm^{-1} – 200 cm^{-1} [8, 229]. The background-free, label-free vibrational

spectra obtained here will shine a light on the structure-related properties and enable to study of the effect of hydration on phospholipids' head groups. The band assignments performed here can be useful to understand the vibrational energy redistribution in the phospholipids and help to follow the interaction of different head group moieties with other important molecules, and/or ions.

8. Summary and outlook

Phospholipids are one of the main components of the cellular membranes and biological barriers, they have widespread interest in physics, chemistry, biology, material science, nanotechnology, and biotechnology. This thesis focused on the applicability of a newly developed 100 kHz laser-driven BB-VSFG spectrometer. Specifically, it discusses the optimization of experimental conditions, and the stability of phospholipids as a function of important laser parameters at ambient conditions. Moreover, the influence of acquisition time, surface coverage, and a varied heterogeneity of the mixtures were investigated. As was shown in the discussion, the spectra revealed detailed information on the structure and conformational order of the alkyl chains of saturated, unsaturated phospholipids and their mixtures, the structure of interfacial water molecules at different surface pressures around the phospholipids, and the structure of the head groups including the glycerol moieties.

In Chapter 5, the applicability of the high repetition rate BB-VSFG spectrometer was studied for the case of phosphatidylcholine. The experimental conditions were optimized for the studies of planar-supported lipid bilayers that were prepared by the vesicle fusion approach. Different from the majority of VSFG studies reported before, the samples were prepared on a CaF_2 window. The spectral intensity of the BB-VSFG spectra of phospholipids at four different repetition rates and different illumination conditions suggests that the phospholipids were stable during the measurements. It indicated that there was no photo-induced damage on the phospholipids when applying laser repetition rates from 5 kHz to 100 kHz. Due to the higher resolution of the spectrometer, the BB-VSFG spectra obtained here showed several vibrational features that cannot be observed using other spectrometers of this type. The measurements conducted here validate that the high-repetition-rate BB-VSFG spectrometer is a promising approach to study more complex biomolecules in a non-destructive manner with high spectral

resolution and high sensitivity in the future. The heterogeneous Egg-PC bilayers discussed in Chapter 5 provided high-intensity BB-VSFG spectra where the high amplitudes of the spectra indicated that the upper and lower leaflets of the bilayers were not symmetric otherwise leading to destructive interference of the signals.

The high quality of the BB-VSFG spectra allowed further discussion of the structure of phospholipids in Chapters 6 and 7. The structural variations of saturated DPPC and unsaturated DOPC and their heterogeneous mixtures as well as the interfacial water molecules were discussed in Chapter 6 for different surface coverages. Specifically, the interfacial structure of phospholipid monolayers at low surface coverage is largely unexplored. For this purpose, monolayers of phospholipids were prepared by Langmuir-Blodgett deposition. The BB-VSFG of spectra of saturated and unsaturated phospholipids at low surface coverage obtained showed remarkable spectral features and was reported here for the first time. The results revealed that the structure of a few molecules at the interface can be studied by employing an HRR-BB-VSFG spectrometer.

A systematic investigation of mixtures of saturated, and unsaturated, respectively, and their heterogeneous mixtures was conducted, and the intensity ratios of their methyl and methylene symmetric modes were obtained. These values changed when adding unsaturated DOPC to the saturated DPPC. This suggested changes in the order/disorder of the lipids at the interface, and therefore could be correlated to the fluidity of the monolayers. Although this result is not surprising, the change of the spectral features was found here to respond to even to small variations in the concentrations. This was visible even from the raw BB-VSFG spectra. While fitting with Lorentzian line profiles usually lead to five to six vibrational resonances, in this thesis eleven spectral features could be assigned to appropriate vibrational modes, including overtones and combinations. The vibrational modes around 2800 cm^{-1} and the overtones and combinations, as well as the spectral features at 2889 cm^{-1}, 2913 cm^{-1}, and 2932 cm^{-1}, were distinguishable and assigned to the components of CH_2 stretching modes and their Fermi resonances. The BB-VSFG spectra revealed the structure varies as the surface pressure changed from 5 mN/m to 30 mN/m. The intensity ratio of vibrational modes was used to quantify the conformational disorder in the alkyl chains. The interfacial structure of a small amount of water between the headgroup and the substrate was investigated for different surface pressures. The result showed that the change in surface pressure from high to low modified the interfacial structure of water molecules. The spectra at 18 mN/m showed strong amplitudes of bounded

O-H stretching modes suggests that the water molecules are well ordered between the phosphate and choline headgroups.

Another interesting point is the comparably short integration time for collecting a single BB-VSFG spectrum with the spectrometer that was available for the study. As was discussed in section 6.3, the integration time of a single spectrum of the phospholipids can be reduced from 20 min to 500 ms. This short integration time enables the multifaceted application of VSFG in biochemistry. Especially in the case of unsaturated phospholipids such fast acquisition reduces the chance of oxidation in ambient conditions and enables studies of the dynamics in the range of milliseconds-hours.

As discussed in Chapter 7, a comparison of the BB-VSFG spectra of deuterated DPPC-d62 and non-deuterated DPPC, and DOPC phospholipid monolayers showed that the effects of the hydrocarbon chains on the head group moieties can be easily discriminated. The so-called fingerprint spectral region shown here to be very rich in vibrational features and the BB-VSFG spectra of PCs between 1200 cm^{-1} and 1370 cm^{-1} were reported. The spectra of different phospholipids showed a frequency shift of the vibrational mode around 1100 cm^{-1} similar to the effect that was obtained by applying different surface pressure/compression. Therefore, this obtained frequency shift can be originated from the differently oriented phosphate groups (different angle of incidence to the surface normal) for the different lipids. The preliminary assignments provided here in this thesis suggest that further work must be conducted in the future to fit the individual spectral features.

In summary, this thesis demonstrated that the HRR-BB-VSFG spectrometer, used here to characterize lipids, is a promising tool that can be employed in bio-analytical chemistry to study the structure of biomolecules at interfaces. This thesis contributes to both the methodological advancement in vibrational bio-spectroscopy in general and provides new findings on the interfacial structure of the phospholipids. A further extension of this work is possible in several directions. First, the effect of hydration and solvation dynamics on phospholipids is an active field of research with many open questions. This can be studied by observing the vibrational modes of hydrophilic groups of phospholipids and the water molecules [274]. The second is to study the interaction between phospholipids and other biomolecules and/or biomimetic membranes. Recently, many research was conducted to study the interaction of phospholipids with small molecules such as drug molecules [304], surfactants [305], phenylalanine [230], to large proteins [306-308], peptides [309, 310], and glycosaminoglycans [276]. VSFG has also tremendous potential to understand protein folding and unfolding at various conditions. Third,

VSFG spectroscopy currently gained popularity in studying the interaction of biomolecules in situ and in real-time with membrane proteins. This was feasible by using isotope labeling of molecules to monitor the structures of interfacial biological molecules [311, 312]. Finally, this technique can be employed to study the orientation of interfacial molecules [156], as VSFG is a surface-specific technique the orientation can be determined through the hyperpolarizability tensor elements of a given interfacial molecule, which we can obtain from the measurements and analysis. As was revealed by the complexity of the data revealed especially in the fingerprint region, the interpretation of the VSFG data needs a more accessible technique to draw conclusions. In the future, studies on the orientation of different biomolecules will help a wide range of applications such as antiviral, antifungal, bio-coatings, polymer surfaces to optimize the molecular properties at interfaces.

Bibliography

1. Veldhuizen, R., K. Nag, S. Orgeig, and F. Possmayer, *The role of lipids in pulmonary surfactant.* Biochimica et Biophysica Acta (BBA) - Molecular Basis of Disease, 1998. 1408(2): p. 90-108.
2. Zuo, Y.Y., R.A.W. Veldhuizen, A.W. Neumann, N.O. Petersen, and F. Possmayer, *Current perspectives in pulmonary surfactant — Inhibition, enhancement and evaluation.* Biochimica et Biophysica Acta (BBA) - Biomembranes, 2008. 1778(10): p. 1947-1977.
3. Heiner, Z., V. Petrov, and M. Mero, *Compact, high-repetition-rate source for broadband sum-frequency generation spectroscopy.* APL Photonics, 2017. 2(6): p. 066102.
4. Heiner, Z., L. Wang, V. Petrov, and M. Mero, *Broadband vibrational sum-frequency generation spectrometer at 100 kHz in the 950-1750 cm−1 spectral range utilizing a LiGaS2 optical parametric amplifier.* Optics Express, 2019. 27(11): p. 15289-15297.
5. Liljeblad, J.F.D., V. Bulone, M.W. Rutland, and C.M. Johnson, *Supported Phospholipid Monolayers. The Molecular Structure Investigated by Vibrational Sum Frequency Spectroscopy.* The Journal of Physical Chemistry C, 2011. 115(21): p. 10617-10629.
6. Liu, W., Z. Wang, L. Fu, R.M. Leblanc, and E.C.Y. Yan, *Lipid Compositions Modulate Fluidity and Stability of Bilayers: Characterization by Surface Pressure and Sum Frequency Generation Spectroscopy.* Langmuir, 2013. 29(48): p. 15022-15031.
7. Ma, G. and H.C. Allen, *DPPC Langmuir Monolayer at the Air−Water Interface: Probing the Tail and Head Groups by Vibrational Sum Frequency Generation Spectroscopy.* Langmuir, 2006. 22(12): p. 5341-5349.
8. Casillas-Ituarte, N.N., X. Chen, H. Castada, and H.C. Allen, *Na+ and Ca2+ Effect on the Hydration and Orientation of the Phosphate Group of DPPC at Air−Water and Air−Hydrated Silica Interfaces.* The Journal of Physical Chemistry B, 2010. 114(29): p. 9485-9495.
9. Chen, X., W. Hua, Z. Huang, and H.C. Allen, *Interfacial Water Structure Associated with Phospholipid Membranes Studied by Phase-Sensitive Vibrational Sum Frequency Generation Spectroscopy.* Journal of the American Chemical Society, 2010. 132(32): p. 11336-11342.
10. Nojima, Y., Y. Suzuki, and S. Yamaguchi, *Weakly Hydrogen-Bonded Water Inside Charged Lipid Monolayer Observed with Heterodyne-Detected Vibrational Sum Frequency Generation Spectroscopy.* The Journal of Physical Chemistry C, 2017. 121(4): p. 2173-2180.
11. Dreier, L.B., M. Bonn, and E.H.G. Backus, *Hydration and Orientation of Carbonyl Groups in Oppositely Charged Lipid Monolayers on Water.* The Journal of Physical Chemistry B, 2019. 123(5): p. 1085-1089.
12. Allhusen, J.S. and J.C. Conboy, *The Ins and Outs of Lipid Flip-Flop.* Accounts of Chemical Research, 2017. 50(1): p. 58-65.

13. Schreier, S., C.F. Polnaszek, and I.C.P. Smith, *Spin labels in membranes problems in practice.* Biochimica et Biophysica Acta (BBA) - Reviews on Biomembranes, 1978. 515(4): p. 395-436.

14. Carlsson, A., *Chapter 5 - Physical properties of phospholipids*, in *Phospholipid Technology and Applications*, F.D. Gunstone, Editor. 2012, Woodhead Publishing. p. 95-139.

15. Chapman, D., R.M. Williams, and B.D. Ladbrooke, *Physical studies of phospholipids. VI. Thermotropic and lyotropic mesomorphism of some 1,2-diacyl-phosphatidylcholines (lecithins).* Chemistry and Physics of Lipids, 1967. 1(5): p. 445-475.

16. Chapman, D. and A. Morrison, *Physical Studies of Phospholipids: IV. High resolution nuclear magnetic resonance spectra of phospholipids and related substances.* Journal of Biological Chemistry, 1966. 241(21): p. 5044-5052.

17. Cevc, G., T.M. Allen, and S.L. Neidleman, *Phospholipids handbook*. 1993.

18. Bangham, A.D., *Membrane models with phospholipids.* Progress in Biophysics and Molecular Biology, 1968. 18: p. 29-95.

19. Willumeit, R., A. Schuster, P. Iliev, S. Linser, and F. Feyerabend, *Phospholipids as implant coatings.* Journal of Materials Science: Materials in Medicine, 2007. 18(2): p. 367-380.

20. Singh, H., *Nanotechnology Applications in Functional Foods; Opportunities and Challenges.* Preventive nutrition and food science, 2016. 21(1): p. 1-8.

21. Mashaghi, S., T. Jadidi, G. Koenderink, and A. Mashaghi, *Lipid Nanotechnology.* International Journal of Molecular Sciences, 2013. 14(2).

22. Ahmad, M.U., *Nanotechnology: emerging interest, opportunities, and challenges*, in *Lipids in Nanotechnology*, M.U. Ahmad, Editor. 2012, AOCS Press. p. 1-14.

23. Li, J., X. Wang, T. Zhang, C. Wang, Z. Huang, X. Luo, and Y. Deng, *A review on phospholipids and their main applications in drug delivery systems.* Asian Journal of Pharmaceutical Sciences, 2015. 10(2): p. 81-98.

24. van Hoogevest, P. and A. Fahr, *Phospholipids in Cosmetic Carriers*, in *Nanocosmetics: From Ideas to Products*, J. Cornier, C.M. Keck, and M. Van de Voorde, Editors. 2019, Springer International Publishing: Cham. p. 95-140.

25. Mazur, F., M. Bally, B. Städler, and R. Chandrawati, *Liposomes and lipid bilayers in biosensors.* Advances in Colloid and Interface Science, 2017. 249: p. 88-99.

26. Vasdekis, A.E., E.A. Scott, S. Roke, J.A. Hubbell, and D. Psaltis, *Vesicle Photonics.* Annual Review of Materials Research, 2013. 43(1): p. 283-305.

27. Fahy, E., S. Subramaniam, H.A. Brown, C.K. Glass, A.H. Merrill, R.C. Murphy, C.R.H. Raetz, D.W. Russell, Y. Seyama, W. Shaw, T. Shimizu, F. Spener, G. van Meer, M.S. VanNieuwenhze, S.H. White, J.L. Witztum, and E.A. Dennis, *A comprehensive classification system for lipids.* Journal of Lipid Research, 2005. 46(5): p. 839-862.

28. Fahy, E., S. Subramaniam, R.C. Murphy, M. Nishijima, C.R.H. Raetz, T. Shimizu, F. Spener, G. van Meer, M.J.O. Wakelam, and E.A. Dennis, *Update of the LIPID MAPS comprehensive classification system for lipids.* Journal of lipid research, 2009. 50 Suppl(Suppl): p. S9-S14.

29. Coleman, R.A. and D.P. Lee, *Enzymes of triacylglycerol synthesis and their regulation.* Progress in Lipid Research, 2004. 43(2): p. 134-176.

30. Gorter, E. and F. Grendel, *On biomolecular layers of lipoids on the chromocytes of the blood.* Journal of Experimental Medicine, 1925. 41(4): p. 439-443.

31. Danielli, J.F. and H. Davson, *A contribution to the theory of permeability of thin films.* Journal of Cellular and Comparative Physiology, 1935. 5(4): p. 495-508.

32. Yeagle, P.L., *The structure of biological membranes.* 2012.

33. Cullis, P.R. and B. De Kruijff, *Lipid polymorphism and the functional roles of lipids in biological membranes.* Biochimica et Biophysica Acta (BBA) - Reviews on Biomembranes, 1979. 559(4): p. 399-420.

34. Sezgin, E., I. Levental, S. Mayor, and C. Eggeling, *The mystery of membrane organization: composition, regulation and roles of lipid rafts.* Nature Reviews Molecular Cell Biology, 2017. 18(6): p. 361-374.

35. Jackson, J.C., *46 - Respiratory Disorders in the Preterm Infant*, in *Avery's Diseases of the Newborn (Tenth Edition)*, C.A. Gleason and S.E. Juul, Editors. 2018, Content Repository Only!: Philadelphia. p. 653-667.e2.

36. Hope, M.J., M.B. Bally, L.D. Mayer, A.S. Janoff, and P.R. Cullis, *Generation of multilamellar and unilamellar phospholipid vesicles.* Chemistry and Physics of Lipids, 1986. 40(2): p. 89-107.

37. Talsma, H., H. Jousma, K. Nicolay, and D.J.A. Crommelin, *Multilamellar or multivesicular vesicles?* International Journal of Pharmaceutics, 1987. 37(1): p. 171-173.

38. Barenholz, Y., D. Gibbes, B.J. Litman, J. Goll, T.E. Thompson, and F.D. Carlson, *A simple method for the preparation of homogeneous phospholipid vesicles.* Biochemistry, 1977. 16(12): p. 2806-2810.

39. Saunders, L., J. Perrin, and D. Gammack, *Ultrasonic irradiation of some phospholipid sols.* Journal of Pharmacy and Pharmacology, 1962. 14(1): p. 567-572.

40. Hamilton, R.L., J. Goerke, L.S. Guo, M.C. Williams, and R.J. Havel, *Unilamellar liposomes made with the French pressure cell: a simple preparative and semiquantitative technique.* Journal of Lipid Research, 1980. 21(8): p. 981-992.

41. Barenholzt, Y., S. Amselem, and L. D, *A new method for preparation of phospholipid vesicles (liposomes) - french press.* FEBS Letters, 1979. 99(1): p. 210-214.

42. Olson, F., C.A. Hunt, F.C. Szoka, W.J. Vail, and D. Papahadjopoulos, *Preparation of liposomes of defined size distribution by extrusion through polycarbonate membranes.* Biochimica et Biophysica Acta (BBA) - Biomembranes, 1979. 557(1): p. 9-23.

43. Hauser, H.O., *The effect of ultrasonic irradiation on the chemical structure of egg lecithin.* Biochemical and Biophysical Research Communications, 1971. 45(4): p. 1049-1055.

44. Langmuir, I., *The mechanism of the surface phenomena of flotation.* Transactions of the Faraday Society, 1920. 15(June): p. 62-74.

45. Rayleigh, *Surface Tension.* Nature, 1891. 43(1115): p. 437-439.

46. Mueller, P., D.O. Rudin, H. Ti Tien, and W.C. Wescott, *Reconstitution of Cell Membrane Structure in vitro and its Transformation into an Excitable System.* Nature, 1962. 194(4832): p. 979-980.

47. Tamm, L.K. and H.M. McConnell, *Supported phospholipid bilayers.* Biophysical Journal, 1985. 47(1): p. 105-113.

48. Kalb, E., S. Frey, and L.K. Tamm, *Formation of supported planar bilayers by fusion of vesicles to supported phospholipid monolayers.* Biochimica et Biophysica Acta (BBA) - Biomembranes, 1992. 1103(2): p. 307-316.

49. Reviakine, I. and A. Brisson, *Formation of Supported Phospholipid Bilayers from Unilamellar Vesicles Investigated by Atomic Force Microscopy.* Langmuir, 2000. 16(4): p. 1806-1815.

50. Richter, R.P., R. Bérat, and A.R. Brisson, *Formation of Solid-Supported Lipid Bilayers: An Integrated View.* Langmuir, 2006. 22(8): p. 3497-3505.

51. Blodgett, K.B., *Films Built by Depositing Successive Monomolecular Layers on a Solid Surface.* Journal of the American Chemical Society, 1935. 57(6): p. 1007-1022.

52. Kim, J., G. Kim, and P.S. Cremer, *Investigations of Water Structure at the Solid/Liquid Interface in the Presence of Supported Lipid Bilayers by Vibrational Sum Frequency Spectroscopy.* Langmuir, 2001. 17(23): p. 7255-7260.

53. Castellana, E.T. and P.S. Cremer, *Solid supported lipid bilayers: From biophysical studies to sensor design.* Surface Science Reports, 2006. 61(10): p. 429-444.

54. McConnell, H.M., T.H. Watts, R.M. Weis, and A.A. Brian, *Supported planar membranes in studies of cell-cell recognition in the immune system.* Biochimica et Biophysica Acta (BBA) - Reviews on Biomembranes, 1986. 864(1): p. 95-106.

55. Ollivon, M., S. Lesieur, C. Grabielle-Madelmont, and M.t. Paternostre, *Vesicle reconstitution from lipid–detergent mixed micelles.* Biochimica et Biophysica Acta (BBA) - Biomembranes, 2000. 1508(1): p. 34-50.

56. Vacklin, H.P., F. Tiberg, and R.K. Thomas, *Formation of supported phospholipid bilayers via co-adsorption with β-d-dodecyl maltoside.* Biochimica et Biophysica Acta (BBA) - Biomembranes, 2005. 1668(1): p. 17-24.

57. Nagle, J.F. and S. Tristram-Nagle, *Structure of lipid bilayers.* Biochimica et Biophysica Acta (BBA) - Reviews on Biomembranes, 2000. 1469(3): p. 159-195.

58. Keller, C.A. and B. Kasemo, *Surface specific kinetics of lipid vesicle adsorption measured with a quartz crystal microbalance.* Biophysical journal, 1998. 75(3): p. 1397-1402.

59. Hamai, C., T. Yang, S. Kataoka, P.S. Cremer, and S.M. Musser, *Effect of Average Phospholipid Curvature on Supported Bilayer Formation on Glass by Vesicle Fusion.* Biophysical Journal, 2006. 90(4): p. 1241-1248.

60. Reimhult, E., F. Höök, and B. Kasemo, *Intact Vesicle Adsorption and Supported Biomembrane Formation from Vesicles in Solution: Influence of Surface Chemistry, Vesicle Size, Temperature, and Osmotic Pressure.* Langmuir, 2003. 19(5): p. 1681-1691.

61. Johnson, J.M., T. Ha, S. Chu, and S.G. Boxer, *Early steps of supported bilayer formation probed by single vesicle fluorescence assays.* Biophys J, 2002. 83(6): p. 3371-9.

62. Gregoriadis, G., *Liposome technology.* 1984.

63. Pecora, R., *Dynamic light scattering : applications of photon correlation spectroscopy*. 1985, New York; London: Plenum Press.

64. Tredgold, R.H., *The physics of Langmuir-Blodgett films.* Reports on Progress in Physics, 1987. 50(12): p. 1609.

65. Roberts, G., *Langmuir-Blodgett Films*. 1990: Springer, Boston, MA.

66. Ulman, A., *Langmuir-Blodgett films*, in *An Introduction to Ultrathin Organic Films*, A. Ulman, Editor. 1991, Academic Press: San Diego. p. 101-236.

67. Johansson, L.B.Å. and G. Lindblom, *Orientation and mobility of molecules in membranes studied by polarized light spectroscopy.* Quarterly Reviews of Biophysics, 1980. 13(1): p. 63-118.

68. Göppert, M., *Über die Wahrscheinlichkeit des Zusammenwirkens zweier Lichtquanten in einem Elementarakt.* Naturwissenschaften, 1929. 17(48): p. 932-932.

69. Kaiser, W. and C.G.B. Garrett, *Two-Photon Excitation in CaF2: Er2+*. Physical Review Letters, 1961. 7(6): p. 229-231.

70. Denk, W., J.H. Strickler, and W.W. Webb, *Two-photon laser scanning fluorescence microscopy.* Science, 1990. 248(4951): p. 73.

71. Bagatolli, L.A. and E. Gratton, *Two Photon Fluorescence Microscopy of Coexisting Lipid Domains in Giant Unilamellar Vesicles of Binary Phospholipid Mixtures.* Biophysical Journal, 2000. 78(1): p. 290-305.

72. Schwille, P. and P. Schwille, *Fluorescence techniques to study lipid dynamics.* Cold Spring Harbor Perspectives in Biology, 2011. 3(11).

73. Korlach, J., P. Schwille, W.W. Webb, and G.W. Feigenson, *Characterization of lipid bilayer phases by confocal microscopy and fluorescence correlation spectroscopy.* Proceedings of the National Academy of Sciences, 1999. 96(15): p. 8461.

74. Thompson, N.L., A.M. Lieto, and N.W. Allen, *Recent advances in fluorescence correlation spectroscopy.* Current Opinion in Structural Biology, 2002. 12(5): p. 634-641.

75. Sánchez, S.A. and E. Gratton, *Lipid−Protein Interactions Revealed by Two-Photon Microscopy and Fluorescence Correlation Spectroscopy.* Accounts of Chemical Research, 2005. 38(6): p. 469-477.

76. Bacia, K. and P. Schwille, *Fluorescence Correlation Spectroscopy*, in *Lipid Rafts*, T.J. McIntosh, Editor. 2007, Humana Press: Totowa, NJ. p. 73-84.

77. Perrin, F., *Polarisation de la lumière de fluorescence. Vie moyenne des molécules dans l'etat excité.* J. Phys. Radium, 1926. 7(12): p. 390-401.

78. Weber, G., *Rotational Brownian Motion and Polarization of the Fluorescence of Solutions*, in *Advances in Protein Chemistry*, M.L. Anson, K. Bailey, and J.T. Edsall, Editors. 1953, Academic Press. p. 415-459.

79. Best, L., E. John, and F. Jähnig, *Order and fluidity of lipid membranes as determined by fluorescence anisotropy decay.* European Biophysics Journal, 1987. 15(2): p. 87-102.

80. Gasecka, A., T.-J. Han, C. Favard, B.R. Cho, and S. Brasselet, *Quantitative Imaging of Molecular Order in Lipid Membranes Using Two-Photon Fluorescence Polarimetry.* Biophysical Journal, 2009. 97(10): p. 2854-2862.

81. Liu, J. and J.C. Conboy, *1,2-diacyl-phosphatidylcholine flip-flop measured directly by sum-frequency vibrational spectroscopy.* Biophysical journal, 2005. 89(4): p. 2522-2532.

82. D.Marsh, E.b.G., Ernst), *Electron Spin Resonance: Spin Labels, D.Marsh, (Edited by Ernst Grell), Membrane Spectroscopy.* 1981.

83. Seelig, J., *Deuterium magnetic resonance: theory and application to lipid membranes.* Quarterly Reviews of Biophysics, 1977. 10(3): p. 353-418.

84. Hauser, H., W. Guyer, M. Spiess, I. Pascher, and S. Sundell, *The polar group conformation of a lysophosphatidylcholine analogue in solution: A high-resolution nuclear magnetic resonance study.* Journal of Molecular Biology, 1980. 137(3): p. 265-282.

85. Forbes, J., C. Husted, and E. Oldfield, *High-field, high-resolution proton "magic-angle" sample-spinning nuclear magnetic resonance spectroscopic studies of gel and liquid crystalline lipid bilayers and the effects of cholesterol.* Journal of the American Chemical Society, 1988. 110(4): p. 1059-1065.

86. Pascher, I. and S. Sundell, *Membrane lipids: preferred conformational states and their interplay. The crystal structure of dilauroylphosphatidyl-N,N-dimethylethanolamine.* Biochimica et Biophysica Acta (BBA) - Biomembranes, 1986. 855(1): p. 68-78.

87. Hitchcock, P.B., R. Mason, K.M. Thomas, and G.G. Shipley, *Structural Chemistry of 1,2 Dilauroyl-DL-phosphatidylethanolamine: Molecular Conformation and Intermolecular Packing of Phospholipids.* Proceedings of the National Academy of Sciences, 1974. 71(8): p. 3036.

88. Büldt, G., H.U. Gally, A. Seelig, J. Seelig, and G. Zaccai, *Neutron diffraction studies on selectively deuterated phospholipid bilayers.* Nature, 1978. 271(5641): p. 182-184.

89. Büldt, G., H.U. Gally, J. Seelig, and G. Zaccai, *Neutron diffraction studies on phosphatidylcholine model membranes: I. Head group conformation.* Journal of Molecular Biology, 1979. 134(4): p. 673-691.

90. Zaccai, G., G. Büldt, A. Seelig, and J. Seelig, *Neutron diffraction studies on phosphatidylcholine model membranes: II. Chain conformation and segmental disorder.* Journal of Molecular Biology, 1979. 134(4): p. 693-706.

91. Cevc, G., W. Fenzl, and L. Sigl, *Surface-Induced X-Ray Reflection Visualization of Membrane Orientation and Fusion into Multibilayers.* Science, 1990. 249(4973): p. 1161.

92. Krbecek, R., C. Gebhardt, H. Gruler, and E. Sackmann, *Three dimensional microscopic surface profiles of membranes reconstructed from freeze etching electron micrographs.* Biochimica et Biophysica Acta (BBA) - Biomembranes, 1979. 554(1): p. 1-22.

93. Zasadzinski, J.A., J. Schneir, J. Gurley, V. Elings, and P.K. Hansma, *Scanning tunneling microscopy of freeze-fracture replicas of biomembranes.* Science, 1988. 239(4843): p. 1013.

94. Weisenhorn, A.L., M. Egger, F. Ohnesorge, S.A.C. Gould, S.P. Heyn, H.G. Hansma, R.L. Sinsheimer, H.E. Gaub, and P.K. Hansma, *Molecular-resolution images of Langmuir-Blodgett films and DNA by atomic force microscopy.* Langmuir, 1991. 7(1): p. 8-12.

95. Hoenig, D. and D. Moebius, *Direct visualization of monolayers at the air-water interface by Brewster angle microscopy.* The Journal of Physical Chemistry, 1991. 95(12): p. 4590-4592.

96. Hönig, D. and D. Möbius, *Reflectometry at the Brewster angle and Brewster angle microscopy at the air-water interface.* Thin Solid Films, 1992. 210-211: p. 64-68.

97. Lautz, C. and T.M. Fischer, *Brewster angle autocorrelation spectroscopy a new method for precise determination of the tilt angle of amphiphiles in Langmuir monolayers.* Materials Science and Engineering: C, 1998. 5(3): p. 271-274.

98. Lautz, C., T.M. Fischer, M. Weygand, M. Lösche, P.B. Howes, and K. Kjaer, *Determination of alkyl chain tilt angles in Langmuir monolayers: A comparison of Brewster angle autocorrelation spectroscopy and x-ray diffraction.* The Journal of Chemical Physics, 1998. 108(11): p. 4640-4646.

99. Hosoi, K., T. Ishikawa, A. Tomioka, and K. Miyano, *Quantitative Image Analysis in Brewster Angle Microscopy: Molecular Tilt of a Stearic Acid Monolayer on Water.* Japanese Journal of Applied Physics, 1993. 32(Part 2, No.1A/B): p. L135-L137.

100. Tsao, M.-W., T.M. Fischer, and C.M. Knobler, *Quantitative Analysis of Brewster-Angle Microscope Images of Tilt Order in Langmuir Monolayer Domains.* Langmuir, 1995. 11(8): p. 3184-3188.

101. Chapman, D., *Infrared spectroscopy of lipids.* Journal of the American Oil Chemists Society, 1965. 42(5): p. 353-371.

102. Arrondo, J.L.R., F.M. Goñi, and J.M. Macarulla, *Infrared spectroscopy of phosphatidylcholines in aqueous suspension a study of the phosphate group vibrations.* Biochimica et Biophysica Acta (BBA) - Lipids and Lipid Metabolism, 1984. 794(1): p. 165-168.

103. Casal, H.L. and H.H. Mantsch, *Polymorphic phase behaviour of phospholipid membranes studied by infrared spectroscopy.* Biochimica et Biophysica Acta (BBA) - Reviews on Biomembranes, 1984. 779(4): p. 381-401.

104. Naumann, D., *FT-infrared and FT-Raman spectroscopy in biomedical research.* Applied Spectroscopy Reviews, 2001. 36(2-3): p. 239-298.

105. Chung, J.B., R.E. Hannemann, and E.I. Franses, *Surface analysis of lipid layers at air/water interfaces.* Langmuir, 1990. 6(11): p. 1647-1655.

106. Fringeli, U.P., *The Structure of Lipids and Proteins Studied by Attenuated Total Reflection (ATR) Infrared Spectroscopy II. Oriented Layers of a Homologous Series: Phosphatidylethanolamine to Phosphatidylcholine*, in *Zeitschrift für Naturforschung C*. 1977. p. 20.

107. Saccani, J., S. Castano, F. Beaurain, M. Laguerre, and B. Desbat, *Stabilization of Phospholipid Multilayers at the Air−Water Interface by Compression beyond the Collapse: A BAM, PM-IRRAS, and Molecular Dynamics Study.* Langmuir, 2004. 20(21): p. 9190-9197.

108. Kycia, A.H., M. Vezvaie, V. Zamlynny, J. Lipkowski, and M.W.P. Petryk, *Non-contact detection of chemical warfare simulant triethyl phosphate using PM-IRRAS.* Analytica Chimica Acta, 2012. 737: p. 45-54.

109. Zaborowska, M., M. Broniatowski, P. Wydro, D. Matyszewska, and R. Bilewicz, *Structural modifications of lipid membranes exposed to statins – Langmuir monolayer and PM-IRRAS study.* Journal of Molecular Liquids, 2020. 313: p. 113570.

110. Huth, F., A. Govyadinov, S. Amarie, W. Nuansing, F. Keilmann, and R. Hillenbrand, *Nano-FTIR Absorption Spectroscopy of Molecular Fingerprints at 20 nm Spatial Resolution.* Nano Letters, 2012. 12(8): p. 3973-3978.

111. Hermann, P., B. Kästner, A. Hoehl, V. Kashcheyevs, P. Patoka, G. Ulrich, J. Feikes, M. Ries, T. Tydecks, B. Beckhoff, E. Rühl, and G. Ulm, *Enhancing the sensitivity of nano-FTIR spectroscopy.* Optics Express, 2017. 25(14): p. 16574-16588.

112. Mester, L., A.A. Govyadinov, S. Chen, M. Goikoetxea, and R. Hillenbrand, *Subsurface chemical nanoidentification by nano-FTIR spectroscopy.* Nature Communications, 2020. 11(1): p. 3359.

113. Donaldson, P.M., C.S. Kelley, M.D. Frogley, J. Filik, K. Wehbe, and G. Cinque, *Broadband near-field infrared spectromicroscopy using photothermal probes and synchrotron radiation.* Optics Express, 2016. 24(3): p. 1852-1864.

114. Smekal, A., *Zur Quantentheorie der Dispersion.* Naturwissenschaften, 1923. 11(43): p. 873-875.

115. Raman, C.V., *A new radiation.* Indian J. Phys., 1928. 2: p. 387-398.

116. Raman, C.V. and K.S. Krishnan, *A New Type of Secondary Radiation.* Nature, 1928. 121(3048): p. 501-502.

117. *Eine neue Erscheinung bei der Lichtzerstreuung in Krystallen.* Naturwissenschaften, 1928. 16(28): p. 557-558.

118. Brown, K.G., W.L. Peticolos, and E. Brown, *Raman studies of conformational changes in model membrane systems.* Biochemical and Biophysical Research Communications, 1973. 54(1): p. 358-364.

119. Spiker, R.C. and I.W. Levin, *Raman spectra and vibrational assignments for dipalmitoyl phosphatidylcholine and structurally related molecules.* Biochimica et Biophysica Acta (BBA) - Lipids and Lipid Metabolism, 1975. 388(3): p. 361-373.

120. Bunow, M.R. and I.W. Levin, *Raman spectra and vibrational assignments for deuterated membrane lipids: 1,2-Dipalmitoyl phosphatidylcholine-d9 and -d62.* Biochimica et Biophysica Acta (BBA) - Lipids and Lipid Metabolism, 1977. 489(2): p. 191-206.

121. Smith, R., K.L. Wright, and L. Ashton, *Raman spectroscopy: an evolving technique for live cell studies.* Analyst, 2016. 141(12): p. 3590-3600.

122. Creighton, J.A., *Surface raman electromagnetic enhancement factors for molecules at the surface of small isolated metal spheres: The determination of adsorbate orientation from sers relative intensities.* Surface Science, 1983. 124(1): p. 209-219.

123. Hines, M.A., T.D. Harris, A.L. Harris, and Y.J. Chabal, *Looking up the down staircase: Surface Raman spectroscopy as a probe of adsorbate orientation.* Journal of Electron Spectroscopy and Related Phenomena, 1993. 64-65: p. 183-191.

124. Živanović, V., Z. Kochovski, C. Arenz, Y. Lu, and J. Kneipp, *SERS and Cryo-EM Directly Reveal Different Liposome Structures during Interaction with Gold Nanoparticles.* The Journal of Physical Chemistry Letters, 2018. 9(23): p. 6767-6772.

125. Freudiger, C.W., W. Min, B.G. Saar, S. Lu, G.R. Holtom, C. He, J.C. Tsai, J.X. Kang, and X.S. Xie, *Label-free biomedical imaging with high sensitivity by stimulated Raman scattering microscopy.* Science, 2008. 322(5909): p. 1857-61.

126. Begley, R.F., A.B. Harvey, and R.L. Byer, *Coherent anti-Stokes Raman spectroscopy.* Applied Physics Letters, 1974. 25(7): p. 387-390.

127. Prince, R.C., R.R. Frontiera, and E.O. Potma, *Stimulated Raman Scattering: From Bulk to Nano.* Chemical Reviews, 2017. 117(7): p. 5070-5094.

128. Hu, F., L. Shi, and W. Min, *Biological imaging of chemical bonds by stimulated Raman scattering microscopy.* Nature Methods, 2019. 16(9): p. 830-842.

129. Day, J.P.R., K.F. Domke, G. Rago, H. Kano, H.-o. Hamaguchi, E.M. Vartiainen, and M. Bonn, *Quantitative Coherent Anti-Stokes Raman Scattering (CARS) Microscopy.* The Journal of Physical Chemistry B, 2011. 115(24): p. 7713-7725.

130. Cheng, J.-X., S. Pautot, D.A. Weitz, and X.S. Xie, *Ordering of water molecules between phospholipid bilayers visualized by coherent anti-Stokes Raman scattering microscopy.* Proceedings of the National Academy of Sciences, 2003. 100(17): p. 9826.

131. Débarre, D., W. Supatto, A.-M. Pena, A. Fabre, T. Tordjmann, L. Combettes, M.-C. Schanne-Klein, and E. Beaurepaire, *Imaging lipid bodies in cells and tissues using third-harmonic generation microscopy.* Nature Methods, 2006. 3(1): p. 47-53.

132. Olivier, N., F. Aptel, K. Plamann, M.-C. Schanne-Klein, and E. Beaurepaire, *Harmonic microscopy of isotropic and anisotropic microstructure of the human cornea.* Optics Express, 2010. 18(5): p. 5028-5040.

133. Zimmerley, M., P. Mahou, D. Débarre, M.-C. Schanne-Klein, and E. Beaurepaire, *Probing Ordered Lipid Assemblies with Polarized Third-Harmonic-Generation Microscopy.* Physical Review X, 2013. 3(1): p. 011002.

134. Brasselet, S., *Polarization-resolved nonlinear microscopy: application to structural molecular and biological imaging.* Advances in Optics and Photonics, 2011. 3(3): p. 205.

135. Bioud, F.-Z., P. Gasecka, P. Ferrand, H. Rigneault, J. Duboisset, and S. Brasselet, *Structure of molecular packing probed by polarization-resolved nonlinear four-wave mixing and coherent anti-Stokes Raman-scattering microscopy.* Physical Review A, 2014. 89(1): p. 013836.

136. Tom, H.W.K., C.M. Mate, X.D. Zhu, J.E. Crowell, T.F. Heinz, G.A. Somorjai, and Y.R. Shen, *Surface Studies by Optical Second-Harmonic Generation: The Adsorption of O2, CO, and Sodium on the Rh(111) Surface.* Physical Review Letters, 1984. 52(5): p. 348-351.

137. Bain, C.D., *Sum-frequency vibrational spectroscopy of the solid/liquid interface.* Journal of the Chemical Society, Faraday Transactions, 1995. 91(9): p. 1281-1296.

138. Eisenthal, K.B., *Liquid Interfaces Probed by Second-Harmonic and Sum-Frequency Spectroscopy.* Chemical Reviews, 1996. 96(4): p. 1343-1360.

139. Gragson, D.E., B.M. Mc Carty, G.L. Richmond, and D.S. Alavi, *High-power broadly tunable picosecond IR laser system for use in nonlinear spectroscopic applications.* Journal of the Optical Society of America B, 1996. 13(9): p. 2075-2083.

140. Shen, Y.R., *Surfaces probed by nonlinear optics.* Surface Science, 1994. 299-300: p. 551-562.

141. Tadjeddine, A. and A. Peremans, *Vibrational spectroscopy of the electrochemical interface by visible infrared sum-frequency generation.* Surface Science, 1996. 368(1): p. 377-383.

142. ChungBoik, C.-Y. and E.O. Potma, *Biomolecular Imaging with Coherent Nonlinear Vibrational Microscopy.* Annual Review of Physical Chemistry, 2013. 64(1): p. 77-99.

143. Dynarowicz-Łątka, P., A. Dhanabalan, and O.N. Oliveira, *Modern physicochemical research on Langmuir monolayers.* Advances in Colloid and Interface Science, 2001. 91(2): p. 221-293.

144. Parodi, V., E. Jacchetti, R. Osellame, G. Cerullo, D. Polli, and M.T. Raimondi, *Nonlinear Optical Microscopy: From Fundamentals to Applications in Live Bioimaging.* Frontiers in Bioengineering and Biotechnology, 2020. 8(1174).

145. Colthup, N.B., L.H. Daly, and S.E. Wiberley, *PREFACE*, in *Introduction to Infrared and Raman Spectroscopy (Third Edition)*, N.B. Colthup, L.H. Daly, and S.E. Wiberley, Editors. 1990, Academic Press: San Diego. p. xi-xii.

146. Bloembergen, N. and P.S. Pershan, *Light Waves at the Boundary of Nonlinear Media.* Physical Review, 1962. 128(2): p. 606-622.

147. Armstrong, J.A., N. Bloembergen, J. Ducuing, and P.S. Pershan, *Interactions between Light Waves in a Nonlinear Dielectric.* Physical Review, 1962. 127(6): p. 1918-1939.

148. Zhu, X.D., H. Suhr, and Y.R. Shen, *Surface vibrational spectroscopy by infrared-visible sum frequency generation.* Physical Review B, 1987. 35(6): p. 3047-3050.

149. Tom, H.W.K., *Studies of surfaces using optical second harmonic generation.* Ph.D. Thesis, 1984.

150. Wang, H.-F., W. Gan, R. Lu, Y. Rao, and B.-H. Wu *Quantitative spectral and orientational analysis in surface sum frequency generation vibrational spectroscopy (SFG-VS).* International Reviews in Physical Chemistry, 2005. 24(2): p. 191-256.

151. Wang, H.-F., L. Velarde, W. Gan, and L. Fu, *Quantitative Sum-Frequency Generation Vibrational Spectroscopy of Molecular Surfaces and Interfaces: Lineshape, Polarization, and Orientation.* Annual Review of Physical Chemistry, 2015. 66(1): p. 189-216.

152. Ward, R.N., D.C. Duffy, P.B. Davies, and C.D. Bain, *Sum-Frequency Spectroscopy of Surfactants Adsorbed at a Flat Hydrophobic Surface.* The Journal of Physical Chemistry, 1994. 98(34): p. 8536-8542.

153. Roke, S., A.W. Kleyn, and M. Bonn, *Time- vs. frequency-domain femtosecond surface sum frequency generation.* Chemical Physics Letters, 2003. 370(1): p. 227-232.

154. Hommel, E.L., G. Ma, and H.C. Allen, *Broadband Vibrational Sum Frequency Generation Spectroscopy of a Liquid Surface.* Analytical Sciences, 2001. 17(11): p. 1325-1329.

155. Ma, G., J. Liu, L. Fu, and E.C.Y. Yan, *Probing Water and Biomolecules at the Air–Water Interface with a Broad Bandwidth Vibrational Sum Frequency Generation Spectrometer from 3800 to 900 cm−1.* Applied Spectroscopy, 2009. 63(5): p. 528-537.

156. Zhuang, X., P.B. Miranda, D. Kim, and Y.R. Shen, *Mapping molecular orientation and conformation at interfaces by surface nonlinear optics.* Physical Review B, 1999. 59(19): p. 12632-12640.

157. Lambert, A.G., P.B. Davies, and D.J. Neivandt, *Implementing the Theory of Sum Frequency Generation Vibrational Spectroscopy: A Tutorial Review.* Applied Spectroscopy Reviews, 2005. 40(2): p. 103-145.

158. Wang, J., C. Chen, S.M. Buck, and Z. Chen, *Molecular Chemical Structure on Poly(methyl methacrylate) (PMMA) Surface Studied by Sum Frequency Generation (SFG) Vibrational Spectroscopy.* The Journal of Physical Chemistry B, 2001. 105(48): p. 12118-12125.

159. Butcher, P.N. and D. Cotter, *The elements of nonlinear optics*. 1991: Cambridge University Press.

160. Shen, Y.R., *The principles of nonlinear optics*. New York. 1984.

161. Shalhout, F.Y., S. Malyk, and A.V. Benderskii, *Relative Phase Change of Nearby Resonances in Temporally Delayed Sum Frequency Spectra.* The Journal of Physical Chemistry Letters, 2012. 3(23): p. 3493-3497.

162. Laaser, J.E., W. Xiong, and M.T. Zanni, *Time-Domain SFG Spectroscopy Using Mid-IR Pulse Shaping: Practical and Intrinsic Advantages.* The Journal of Physical Chemistry B, 2011. 115(11): p. 2536-2546.

163. Velarde, L. and H.-F. Wang, *Unified treatment and measurement of the spectral resolution and temporal effects in frequency-resolved sum-frequency generation vibrational spectroscopy (SFG-VS).* Physical Chemistry Chemical Physics, 2013. 15(46): p. 19970-19984.

164. Curtis, A.D., S.B. Reynolds, A.R. Calchera, and J.E. Patterson, *Understanding the Role of Nonresonant Sum-Frequency Generation from Polystyrene Thin Films.* The Journal of Physical Chemistry Letters, 2010. 1(16): p. 2435-2439.

165. Curtis, A.D., S.R. Burt, A.R. Calchera, and J.E. Patterson, *Limitations in the Analysis of Vibrational Sum-Frequency Spectra Arising from the Nonresonant Contribution.* The Journal of Physical Chemistry C, 2011. 115(23): p. 11550-11559.

166. Lagutchev, A., S.A. Hambir, and D.D. Dlott, *Nonresonant Background Suppression in Broadband Vibrational Sum-Frequency Generation Spectroscopy.* The Journal of Physical Chemistry C, 2007. 111(37): p. 13645-13647.

167. Stiopkin, I.V., H.D. Jayathilake, C. Weeraman, and A.V. Benderskii, *Temporal effects on spectroscopic line shapes, resolution, and sensitivity of the broad-band sum frequency generation.* The Journal of Chemical Physics, 2010. 132(23): p. 234503.

168. Shen, Y.R., *Surface properties probed by second-harmonic and sum-frequency generation.* Nature, 1989. 337(6207): p. 519-525.

169. Hore, D.K., J.L. King, F.G. Moore, D.S. Alavi, M.Y. Hamamoto, and G.L. Richmond, *Ti:Sapphire-Based Picosecond Visible-Infrared Sum-Frequency Spectroscopy from 900–3100 cm−1.* Applied Spectroscopy, 2004. 58(12): p. 1377-1384.

170. Schrödle, S. and G.L. Richmond, *Sequential Wavelength Tuning: Dynamics at Interfaces Investigated by Vibrational Sum-Frequency Spectroscopy.* Applied Spectroscopy, 2008. 62(4): p. 389-393.

171. van der Ham, E.W.M., Q.H.F. Vrehen, and E.R. Eliel, *Self-dispersive sum-frequency generation at interfaces.* Optics Letters, 1996. 21(18): p. 1448-1450.

172. van der Ham, E.W.M., Q.H.F. Vrehen, and E.R. Eliel, *High-resolution sum-frequency spectra using broadband laser sources.* Surface Science, 1996. 368(1): p. 96-101.

173. Richter, L.J., T.P. Petralli-Mallow, and J.C. Stephenson, *Vibrationally resolved sum-frequency generation with broad-bandwidth infrared pulses.* Optics Letters, 1998. 23(20): p. 1594-1596.

174. Tian, C.S. and Y.R. Shen, *Recent progress on sum-frequency spectroscopy.* Surface Science Reports, 2014. 69(2): p. 105-131.

175. Liu, J. and J.C. Conboy, *Phase Behavior of Planar Supported Lipid Membranes Composed of Cholesterol and 1,2-Distearoyl-sn-Glycerol-3-Phosphocholine Examined by Sum-Frequency Vibrational Spectroscopy.* Vibrational Spectroscopy, 2009. 50(1): p. 106-115.

176. Wu, H.-L., Y. Tong, Q. Peng, N. Li, and S. Ye, *Phase transition behaviors of the supported DPPC bilayer investigated by sum frequency generation (SFG) vibrational spectroscopy and atomic force microscopy (AFM).* Physical Chemistry Chemical Physics, 2016. 18(3): p. 1411-1421.

177. Liu, J. and J.C. Conboy, *Phase Transition of a Single Lipid Bilayer Measured by Sum-Frequency Vibrational Spectroscopy.* Journal of the American Chemical Society, 2004. 126(29): p. 8894-8895.

178. Eisenthal, K.B., *Second Harmonic Spectroscopy of Aqueous Nano- and Microparticle Interfaces.* Chemical Reviews, 2006. 106(4): p. 1462-1477.

179. Liu, Y., E.C.Y. Yan, X. Zhao, and K.B. Eisenthal, *Surface Potential of Charged Liposomes Determined by Second Harmonic Generation.* Langmuir, 2001. 17(7): p. 2063-2066.

180. Troiano, J.M., L.L. Olenick, T.R. Kuech, E.S. Melby, D. Hu, S.E. Lohse, A.C. Mensch, M. Dogangun, A.M. Vartanian, M.D. Torelli, E. Ehimiaghe, S.R. Walter, L. Fu, C.R. Anderton, Z. Zhu, H. Wang, G. Orr, C.J. Murphy, R.J. Hamers, J.A. Pedersen, and F.M. Geiger, *Direct Probes of 4 nm Diameter Gold Nanoparticles Interacting with Supported Lipid Bilayers.* The Journal of Physical Chemistry C, 2015. 119(1): p. 534-546.

181. Anglin, T.C. and J.C. Conboy, *Kinetics and Thermodynamics of Flip-Flop in Binary Phospholipid Membranes Measured by Sum-Frequency Vibrational Spectroscopy.* Biochemistry, 2009. 48(43): p. 10220-10234.

182. Anglin, T.C., M.P. Cooper, H. Li, K. Chandler, and J.C. Conboy, *Free Energy and Entropy of Activation for Phospholipid Flip-Flop in Planar Supported Lipid Bilayers.* The Journal of Physical Chemistry B, 2010. 114(5): p. 1903-1914.

183. Olenick, L.L., H.M. Chase, L. Fu, Y. Zhang, A.C. McGeachy, M. Dogangun, S.R. Walter, H.-f. Wang, and F.M. Geiger, *Single-component supported lipid bilayers probed using broadband nonlinear optics.* Physical Chemistry Chemical Physics, 2017.

184. Ries, R.S., H. Choi, R. Blunck, F. Bezanilla, and J.R. Heath, *Black Lipid Membranes: Visualizing the Structure, Dynamics, and Substrate Dependence of Membranes.* The Journal of Physical Chemistry B, 2004. 108(41): p. 16040-16049.

185. Wang, T., D. Li, X. Lu, A. Khmaladze, X. Han, S. Ye, P. Yang, G. Xue, N. He, and Z. Chen, *Single Lipid Bilayers Constructed on Polymer Cushion Studied by Sum Frequency Generation Vibrational Spectroscopy.* The Journal of Physical Chemistry C, 2011. 115(15): p. 7613-7620.

186. Kett, P.J.N., M.T.L. Casford, and P.B. Davies, *Sum Frequency Generation (SFG) Vibrational Spectroscopy of Planar Phosphatidylethanolamine Hybrid Bilayer Membranes under Water.* Langmuir, 2010. 26(12): p. 9710-9719.

187. Kett, P.J.N., M.T.L. Casford, and P.B. Davies, *Structure of Mixed Phosphatidylethanolamine and Cholesterol Monolayers in a Supported Hybrid Bilayer*

Membrane Studied by Sum Frequency Generation Vibrational Spectroscopy. The Journal of Physical Chemistry B, 2011. 115(20): p. 6465-6473.

188. Liu, J., K.L. Brown, and J.C. Conboy, *The effect of cholesterol on the intrinsic rate of lipid flip–flop as measured by sum-frequency vibrational spectroscopy.* Faraday Discussions, 2013. 161(0): p. 45-61.

189. Doğangün, M., M.N. Hang, J.M. Troiano, A.C. McGeachy, E.S. Melby, J.A. Pedersen, R.J. Hamers, and F.M. Geiger, *Alteration of Membrane Compositional Asymmetry by LiCoO2 Nanosheets.* ACS Nano, 2015. 9(9): p. 8755-8765.

190. McGeachy, A.C., L.L. Olenick, J.M. Troiano, R.S. Lankone, E.S. Melby, T.R. Kuech, E. Ehimiaghe, D.H. Fairbrother, J.A. Pedersen, and F.M. Geiger, *Resonantly Enhanced Nonlinear Optical Probes of Oxidized Multiwalled Carbon Nanotubes at Supported Lipid Bilayers.* The Journal of Physical Chemistry B, 2017. 121(6): p. 1321-1329.

191. Toledo-Fuentes, X., D. Lis, and F. Cecchet, *Structural Changes to Lipid Bilayers and Their Surrounding Water upon Interaction with Functionalized Gold Nanoparticles.* The Journal of Physical Chemistry C, 2016. 120(38): p. 21399-21409.

192. Hu, P., X. Zhang, C. Zhang, and Z. Chen, *Molecular interactions between gold nanoparticles and model cell membranes.* Physical Chemistry Chemical Physics, 2015. 17(15): p. 9873-9884.

193. Roke, S., J. Schins, M. Müller, and M. Bonn, *Vibrational Spectroscopic Investigation of the Phase Diagram of a Biomimetic Lipid Monolayer.* Physical Review Letters, 2003. 90(12): p. 128101.

194. Li, B., X. Li, Y.-H. Ma, X. Han, F.-G. Wu, Z. Guo, Z. Chen, and X. Lu, *Sum Frequency Generation of Interfacial Lipid Monolayers Shows Polarization Dependence on Experimental Geometries.* Langmuir, 2016. 32(28): p. 7086-7095.

195. Chen, X., J. Wang, C.B. Kristalyn, and Z. Chen, *Real-Time Structural Investigation of a Lipid Bilayer during Its Interaction with Melittin Using Sum Frequency Generation Vibrational Spectroscopy.* Biophysical Journal, 2007. 93(3): p. 866-875.

196. Yan, E.C.Y., L. Fu, Z. Wang, and W. Liu, *Biological Macromolecules at Interfaces Probed by Chiral Vibrational Sum Frequency Generation Spectroscopy.* Chemical Reviews, 2014. 114(17): p. 8471-8498.

197. Li, B., X. Lu, X. Han, F.-G. Wu, J.N. Myers, and Z. Chen, *Interfacial Fresnel Coefficients and Molecular Structures of Model Cell Membranes: From a Lipid Monolayer to a Lipid Bilayer.* The Journal of Physical Chemistry C, 2014. 118(49): p. 28631-28639.

198. Liu, J. and J.C. Conboy, *Structure of a Gel Phase Lipid Bilayer Prepared by the Langmuir−Blodgett/Langmuir-Schaefer Method Characterized by Sum-Frequency Vibrational Spectroscopy.* Langmuir, 2005. 21(20): p. 9091-9097.

199. Zhang, X., X. Wang, and J.D. Miller, *Wetting of selected fluorite surfaces by water.* Surface Innovations, 2015. 3(1): p. 39-48.

200. Hope, M.J., M.B. Bally, G. Webb, and P.R. Cullis, *Production of large unilamellar vesicles by a rapid extrusion procedure. Characterization of size distribution, trapped volume and ability to maintain a membrane potential.* Biochimica et Biophysica Acta (BBA) - Biomembranes, 1985. 812(1): p. 55-65.

201. Raoult, F., A.C.L. Boscheron, D. Husson, C. Sauteret, A. Modena, V. Malka, F. Dorchies, and A. Migus, *Efficient generation of narrow-bandwidth picosecond pulses*

by frequency doubling of femtosecond chirped pulses. Optics Letters, 1998. 23(14): p. 1117-1119.

202. Nejbauer, M. and C. Radzewicz, *Efficient spectral shift and compression of femtosecond pulses by parametric amplification of chirped light.* Optics Express, 2012. 20(3): p. 2136-2142.

203. Hanssen, L.M. and C. Zhu, *Wavenumber Standards for Mid-infrared Spectrometry*, in *Handbook of Vibrational Spectroscopy*. 2001.

204. Gaber, B.P., P. Yager, and W.L. Peticolas, *Interpretation of biomembrane structure by Raman difference spectroscopy. Nature of the endothermic transitions in phosphatidylcholines.* Biophysical journal, 1978. 21(2): p. 161-176.

205. Weeraman, C., S.A. Mitchell, R. Lausten, L.J. Johnston, and A. Stolow, *Vibrational sum frequency generation spectroscopy using inverted visible pulses.* Optics Express, 2010. 18(11): p. 11483-11494.

206. Isaienko, O. and E. Borguet, *Ultra-broadband sum-frequency vibrational spectrometer of aqueous interfaces based on a non-collinear optical parametric amplifier.* Optics Express, 2012. 20(1): p. 547-561.

207. Pool, R.E., J. Versluis, E.H.G. Backus, and M. Bonn, *Comparative Study of Direct and Phase-Specific Vibrational Sum-Frequency Generation Spectroscopy: Advantages and Limitations.* The Journal of Physical Chemistry B, 2011. 115(51): p. 15362-15369.

208. König, K., T.W. Becker, P. Fischer, I. Riemann, and K.J. Halbhuber, *Pulse-length dependence of cellular response to intense near-infrared laser pulses in multiphoton microscopes.* Optics Letters, 1999. 24(2): p. 113-115.

209. Hopt, A. and E. Neher, *Highly Nonlinear Photodamage in Two-Photon Fluorescence Microscopy.* Biophysical Journal, 2001. 80(4): p. 2029-2036.

210. Koester, H.J., D. Baur, R. Uhl, and S.W. Hell, *Ca2+ Fluorescence Imaging with Pico- and Femtosecond Two-Photon Excitation: Signal and Photodamage.* Biophysical Journal, 1999. 77(4): p. 2226-2236.

211. König, K., *Laser tweezers and multiphoton microscopes in life sciences.* Histochemistry and Cell Biology, 2000. 114(2): p. 79-92.

212. Alfred, V., N. Joachim, H. Gereon, and P. Guenther. *Femtosecond-laser-produced low-density plasmas in transparent biological media: a tool for the creation of chemical, thermal, and thermomechanical effects below the optical breakdown threshold*. in *Proc.SPIE*. 2002.

213. Sengupta, S., L. Bromley Iii, and L. Velarde, *Aggregated States of Chalcogenorhodamine Dyes on Nanocrystalline Titania Revealed by Doubly Resonant Sum Frequency Spectroscopy.* The Journal of Physical Chemistry C, 2017. 121(6): p. 3424-3436.

214. Riaz, S. and G. Friedrichs, *Vibrational sum-frequency generation study of molecular structure, sterical constraints and nonlinear optical switching contrast of mixed alkyl-azobenzene self-assembled monolayers.* Zeitschrift für Physikalische Chemie, 2020. 234(7-9): p. 1427-1452.

215. Wang, C.-y., H. Groenzin, and M.J. Shultz, *Molecular Species on Nanoparticulate Anatase TiO2 Film Detected by Sum Frequency Generation: Trace Hydrocarbons and Hydroxyl Groups.* Langmuir, 2003. 19(18): p. 7330-7334.

216. Hunt, J.H., P. Guyot-Sionnest, and Y.R. Shen, *Observation of C-H stretch vibrations of monolayers of molecules optical sum-frequency generation.* Chemical Physics Letters, 1987. 133(3): p. 189-192.

217. Stiopkin, I.V., H.D. Jayathilake, A.N. Bordenyuk, and A.V. Benderskii, *Heterodyne-Detected Vibrational Sum Frequency Generation Spectroscopy.* Journal of the American Chemical Society, 2008. 130(7): p. 2271-2275.

218. Liljeblad, J.F.D., V. Bulone, E. Tyrode, M.W. Rutland, and C.M. Johnson, *Phospholipid monolayers probed by vibrational sum frequency spectroscopy: instability of unsaturated phospholipids.* Biophysical journal, 2010. 98(10): p. L50-L52.

219. Backus, E.H.G., D. Bonn, S. Cantin, S. Roke, and M. Bonn, *Laser-Heating-Induced Displacement of Surfactants on the Water Surface.* The Journal of Physical Chemistry B, 2012. 116(9): p. 2703-2712.

220. Wang, Z., J.A. Carter, A. Lagutchev, Y.K. Koh, N.-H. Seong, D.G. Cahill, and D.D. Dlott, *Ultrafast Flash Thermal Conductance of Molecular Chains.* Science, 2007. 317(5839): p. 787.

221. Yesudas, F., M. Mero, J. Kneipp, and Z. Heiner, *Vibrational sum-frequency generation spectroscopy of lipid bilayers at repetition rates up to 100 kHz.* The Journal of Chemical Physics, 2018. 148(10): p. 104702.

222. Lu, R., W. Gan, B.-h. Wu, H. Chen, and H.-f. Wang, *Vibrational Polarization Spectroscopy of CH Stretching Modes of the Methylene Group at the Vapor/Liquid Interfaces with Sum Frequency Generation.* The Journal of Physical Chemistry B, 2004. 108(22): p. 7297-7306.

223. Lu, R., W. Gan, B.-h. Wu, Z. Zhang, Y. Guo, and H.-f. Wang, *C−H Stretching Vibrations of Methyl, Methylene and Methine Groups at the Vapor/Alcohol (n = 1−8) Interfaces.* The Journal of Physical Chemistry B, 2005. 109(29): p. 14118-14129.

224. Watry, M.R., T.L. Tarbuck, and G.L. Richmond, *Vibrational Sum-Frequency Studies of a Series of Phospholipid Monolayers and the Associated Water Structure at the Vapor/Water Interface.* The Journal of Physical Chemistry B, 2003. 107(2): p. 512-518.

225. MacPhail, R.A., H.L. Strauss, R.G. Snyder, and C.A. Elliger, *Carbon-hydrogen stretching modes and the structure of n-alkyl chains. 2. Long, all-trans chains.* The Journal of Physical Chemistry, 1984. 88(3): p. 334-341.

226. Feng, R.-J., X. Li, Z. Zhang, Z. Lu, and Y. Guo, *Spectral assignment and orientational analysis in a vibrational sum frequency generation study of DPPC monolayers at the air/water interface.* The Journal of Chemical Physics, 2016. 145(24): p. 244707.

227. Okur, H.I., Y. Chen, N. Smolentsev, E. Zdrali, and S. Roke, *Interfacial Structure and Hydration of 3D Lipid Monolayers in Aqueous Solution.* The Journal of Physical Chemistry B, 2017. 121(13): p. 2808-2813.

228. Snyder, R.G., H.L. Strauss, and C.A. Elliger, *Carbon-hydrogen stretching modes and the structure of n-alkyl chains. 1. Long, disordered chains.* The Journal of Physical Chemistry, 1982. 86(26): p. 5145-5150.

229. Pullanchery, S., T. Yang, and P.S. Cremer, *Introduction of Positive Charges into Zwitterionic Phospholipid Monolayers Disrupts Water Structure Whereas Negative Charges Enhances It.* The Journal of Physical Chemistry B, 2018. 122(51): p. 12260-12270.

230. Saha, A., S. SenGupta, A. Kumar, and P.D. Naik, *Interaction of l-Phenylalanine with Lipid Monolayers at Air–Water Interface at Different pHs: Sum-Frequency Generation Spectroscopy and Surface Pressure Studies.* The Journal of Physical Chemistry C, 2018. 122(7): p. 3875-3884.

231. Goerke, J., *Pulmonary surfactant: functions and molecular composition.* Biochimica et Biophysica Acta (BBA) - Molecular Basis of Disease, 1998. 1408(2): p. 79-89.

232. Wüstneck, R., J. Perez-Gil, N. Wüstneck, A. Cruz, V.B. Fainerman, and U. Pison, *Interfacial properties of pulmonary surfactant layers.* Advances in Colloid and Interface Science, 2005. 117(1): p. 33-58.

233. Hubert Motschmann and H. Mohwald, *Langmuir–Blodgett Films*, in *Handbook of Applied Surface and Colloid Chemistry*, K. Holmberg, Editor. 2001, John Wiley & Sons, Ltd.

234. Qiao, L., A. Ge, Y. Liang, and S. Ye, *Oxidative Degradation of the Monolayer of 1-Palmitoyl-2-Oleoyl-sn-Glycero-3-Phosphocholine (POPC) in Low-Level Ozone.* The Journal of Physical Chemistry B, 2015. 119(44): p. 14188-14199.

235. Li, Y., R. Feng, L. Lin, M. Liu, Y. Guo, and Z. Zhang, *Ordering effects of cholesterol on sphingomyelin monolayers investigated by high-resolution broadband sum-frequency generation vibrational spectroscopy.* Chinese Chemical Letters, 2018. 29(3): p. 357-360.

236. Velarde, L. and H.-f. Wang, *Capturing inhomogeneous broadening of the –CN stretch vibration in a Langmuir monolayer with high-resolution spectra and ultrafast vibrational dynamics in sum-frequency generation vibrational spectroscopy (SFG-VS).* The Journal of Chemical Physics, 2013. 139(8): p. 084204.

237. Velarde, L., X.-y. Zhang, Z. Lu, A.G. Joly, Z. Wang, and H.-f. Wang, *Communication: Spectroscopic phase and lineshapes in high-resolution broadband sum frequency vibrational spectroscopy: Resolving interfacial inhomogeneities of "identical" molecular groups.* The Journal of Chemical Physics, 2011. 135(24): p. 241102.

238. Feng, R.-j., L. Lin, Y.-y. Li, M.-h. Liu, Y. Guo, and Z. Zhang, *Effect of Ca2+ to Sphingomyelin Investigated by Sum Frequency Generation Vibrational Spectroscopy.* Biophysical Journal, 2017. 112(10): p. 2173-2183.

239. Fu, L., S.-L. Chen, and H.-F. Wang, *Validation of Spectra and Phase in Sub-1 cm–1 Resolution Sum-Frequency Generation Vibrational Spectroscopy through Internal Heterodyne Phase-Resolved Measurement.* The Journal of Physical Chemistry B, 2016. 120(8): p. 1579-1589.

240. Mifflin, A.L., L. Velarde, J. Ho, B.T. Psciuk, C.F.A. Negre, C.J. Ebben, M.A. Upshur, Z. Lu, B.L. Strick, R.J. Thomson, V.S. Batista, H.-F. Wang, and F.M. Geiger, *Accurate Line Shapes from Sub-1 cm–1 Resolution Sum Frequency Generation Vibrational Spectroscopy of α-Pinene at Room Temperature.* The Journal of Physical Chemistry A, 2015. 119(8): p. 1292-1302.

241. O'Leary, T.J. and I.W. Levin, *Raman spectroscopic study of the melting behavior of anhydrous dipalmitoylphosphatidylcholine bilayers.* The Journal of Physical Chemistry, 1984. 88(9): p. 1790-1796.

242. Conboy, J.C., M.C. Messmer, and G.L. Richmond, *Investigation of Surfactant Conformation and Order at the Liquid−Liquid Interface by Total Internal Reflection Sum-Frequency Vibrational Spectroscopy.* The Journal of Physical Chemistry, 1996. 100(18): p. 7617-7622.

243. Tamm, L.K. and S.A. Tatulian, *Infrared spectroscopy of proteins and peptides in lipid bilayers.* Quarterly Reviews of Biophysics, 1997. 30(4): p. 365-429.

244. Miranda, P.B., V. Pflumio, H. Saijo, and Y.R. Shen, *Chain−Chain Interaction between Surfactant Monolayers and Alkanes or Alcohols at Solid/Liquid Interfaces.* Journal of the American Chemical Society, 1998. 120(46): p. 12092-12099.

245. Krishnamurty, S., M. Stefanov, T. Mineva, S. Bégu, J.M. Devoisselle, A. Goursot, R. Zhu, and D.R. Salahub, *Density Functional Theory-Based Conformational Analysis of a Phospholipid Molecule (Dimyristoyl Phosphatidylcholine).* The Journal of Physical Chemistry B, 2008. 112(42): p. 13433-13442.

246. Yesudas, F., M. Mero, J. Kneipp, and Z. Heiner, *High-resolution and high-repetition-rate vibrational sum-frequency generation spectroscopy of one- and two-component phosphatidylcholine monolayers.* Analytical and Bioanalytical Chemistry, 2019. 411(19): p. 4861-4871.

247. Larsson, K. and R.P. Rand, *Detection of changes in the environment of hydrocarbon chains by raman spectroscopy and its application to lipid-protein systems.* Biochimica et Biophysica Acta (BBA) - Lipids and Lipid Metabolism, 1973. 326(2): p. 245-255.

248. Gaber, B.P. and W.L. Peticolas, *On the quantitative interpretation of biomembrane structure by Raman spectroscopy.* Biochimica et Biophysica Acta (BBA) - Biomembranes, 1977. 465(2): p. 260-274.

249. Snyder, R.G., S.L. Hsu, and S. Krimm, *Vibrational spectra in the C□H stretching region and the structure of the polymethylene chain.* Spectrochimica Acta Part A: Molecular Spectroscopy, 1978. 34(4): p. 395-406.

250. Maroncelli, M., H.L. Strauss, and R.G. Snyder, *On the methylene-d2(CD2) probe infrared method for determining polymethylene chain conformation.* The Journal of Physical Chemistry, 1985. 89(20): p. 4390-4395.

251. Shannon, V.L., H.L. Strauss, R.G. Snyder, C.A. Elliger, and W.L. Mattice, *Conformation of the cycloalkanes C14H28, C16H32, and C22H44 in the liquid and high-temperature crystalline phases by vibrational spectroscopy.* Journal of the American Chemical Society, 1989. 111(6): p. 1947-1958.

252. Snyder, R.G. and M.W. Poore, *Conformational Structure of Polyethylene Chains from the Infrared Spectrum of the Partially Deuterated Polymer.* Macromolecules, 1973. 6(5): p. 708-715.

253. Mondal, J.A., S. Nihonyanagi, S. Yamaguchi, and T. Tahara, *Three Distinct Water Structures at a Zwitterionic Lipid/Water Interface Revealed by Heterodyne-Detected Vibrational Sum Frequency Generation.* Journal of the American Chemical Society, 2012. 134(18): p. 7842-7850.

254. Ishiyama, T., D. Terada, and A. Morita, *Hydrogen-Bonding Structure at Zwitterionic Lipid/Water Interface.* The Journal of Physical Chemistry Letters, 2016. 7(2): p. 216-220.

255. Doğangün, M., P.E. Ohno, D. Liang, A.C. McGeachy, A.G. Bé, N. Dalchand, T. Li, Q. Cui, and F.M. Geiger, *Hydrogen-Bond Networks near Supported Lipid Bilayers from Vibrational Sum Frequency Generation Experiments and Atomistic Simulations.* The Journal of Physical Chemistry B, 2018. 122(18): p. 4870-4879.

256. Mondal, J.A., S. Nihonyanagi, S. Yamaguchi, and T. Tahara, *Structure and Orientation of Water at Charged Lipid Monolayer/Water Interfaces Probed by Heterodyne-*

Detected Vibrational Sum Frequency Generation Spectroscopy. Journal of the American Chemical Society, 2010. 132(31): p. 10656-10657.

257. Sovago, M., E. Vartiainen, and M. Bonn, *Observation of buried water molecules in phospholipid membranes by surface sum-frequency generation spectroscopy.* The Journal of Chemical Physics, 2009. 131(16): p. 161107.

258. Bonn, M., Y. Nagata, and E.H.G. Backus, *Molecular Structure and Dynamics of Water at the Water–Air Interface Studied with Surface-Specific Vibrational Spectroscopy.* Angewandte Chemie International Edition, 2015. 54(19): p. 5560-5576.

259. Bellamy, L.J., *The infra-red spectra of complex molecules : dy L.J. Bellamy*. 1958, London; New York: Methuen ; Wiley.

260. de Beer, A.G.F., J.-S. Samson, W. Hua, Z. Huang, X. Chen, H.C. Allen, and S. Roke, *Direct comparison of phase-sensitive vibrational sum frequency generation with maximum entropy method: Case study of water.* The Journal of Chemical Physics, 2011. 135(22): p. 224701.

261. Verreault, D., W. Hua, and H.C. Allen, *From Conventional to Phase-Sensitive Vibrational Sum Frequency Generation Spectroscopy: Probing Water Organization at Aqueous Interfaces.* The Journal of Physical Chemistry Letters, 2012. 3(20): p. 3012-3028.

262. Takeshita, N., M. Okuno, and T.-a. Ishibashi, *Molecular conformation of DPPC phospholipid Langmuir and Langmuir–Blodgett monolayers studied by heterodyne-detected vibrational sum frequency generation spectroscopy.* Physical Chemistry Chemical Physics, 2017. 19(3): p. 2060-2066.

263. Yamaguchi, S., *Development of single-channel heterodyne-detected sum frequency generation spectroscopy and its application to the water/vapor interface.* The Journal of Chemical Physics, 2015. 143(3): p. 034202.

264. Hishida, M., Y. Kaneko, M. Okuno, Y. Yamamura, T.-a. Ishibashi, and K. Saito, *Communication: Salt-induced water orientation at a surface of non-ionic surfactant in relation to a mechanism of Hofmeister effect.* The Journal of Chemical Physics, 2015. 142(17): p. 171101.

265. Notter, R.H., S.A. Tabak, S. Holcomb, and R.D. Mavis, *Postcollapse dynamic surface pressure relaxation in binary surface films containing dipalmitoyl phosphatidylcholine.* Journal of Colloid and Interface Science, 1980. 74(2): p. 370-377.

266. Olżyńska, A., M. Zubek, M. Roeselova, J. Korchowiec, and L. Cwiklik, *Mixed DPPC/POPC Monolayers: All-atom Molecular Dynamics Simulations and Langmuir Monolayer Experiments.* Biochimica et Biophysica Acta (BBA) - Biomembranes, 2016. 1858(12): p. 3120-3130.

267. Cevc, G., *Effect of Lipid Headgroups and (Nonelectrolyte) Solution on the Structural and Phase Properties of Bilayer Membranes.* Berichte der Bunsengesellschaft für physikalische Chemie, 1988. 92(9): p. 953A-961.

268. Lotta, T.I., I.S. Salonen, J.A. Virtanen, K.K. Eklund, and P.K.J. Kinnunen, *Fourier transform infrared study of fully hydrated dimyristoylphosphatidylglycerol. Effects of sodium on the sn-1' and sn-3' headgroup stereoisomers.* Biochemistry, 1988. 27(21): p. 8158-8169.

269. Salonen, I.S., K.K. Eklund, J.A. Virtanen, and P.K.J. Kinnunen, *Comparison of the effects of NaCl on the thermotropic behaviour of sn-1' and sn-3' stereoisomers of 1,2-*

dimyristoyl-sn-glycero-3-phosphatidylglycerol. Biochimica et Biophysica Acta (BBA) - Biomembranes, 1989. 982(2): p. 205-215.

270. Rand, R.P., N. Fuller, V.A. Parsegian, and D.C. Rau, *Variation in hydration forces between neutral phospholipid bilayers: evidence for hydration attraction.* Biochemistry, 1988. 27(20): p. 7711-7722.

271. Javanainen, M., W. Hua, O. Tichacek, P. Delcroix, L. Cwiklik, and H.C. Allen, *Structural Effects of Cation Binding to DPPC Monolayers.* Langmuir, 2020. 36(50): p. 15258-15269.

272. Zhang, T., M.G. Cathcart, A.S. Vidalis, and H.C. Allen, *Cation effects on phosphatidic acid monolayers at various pH conditions.* Chemistry and Physics of Lipids, 2016. 200: p. 24-31.

273. Rock, W., B. Qiao, T. Zhou, A.E. Clark, and A. Uysal, *Heavy Anionic Complex Creates a Unique Water Structure at a Soft Charged Interface.* The Journal of Physical Chemistry C, 2018. 122(51): p. 29228-29236.

274. Nagata, Y. and S. Mukamel, *Vibrational Sum-Frequency Generation Spectroscopy at the Water/Lipid Interface: Molecular Dynamics Simulation Study.* Journal of the American Chemical Society, 2010. 132(18): p. 6434-6442.

275. Ma, G. and H.C. Allen, *New Insights into Lung Surfactant Monolayers Using Vibrational Sum Frequency Generation Spectroscopy.* Photochemistry and Photobiology, 2006. 82(6): p. 1517-1529.

276. Szekeres, G.P., S. Krekic, R.L. Miller, M. Mero, K. Pagel, and Z. Heiner, *The interaction of chondroitin sulfate with a lipid monolayer observed by using nonlinear vibrational spectroscopy.* Physical Chemistry Chemical Physics, 2021. 23(23): p. 13389-13395.

277. Fringeli, U.P., H.G. Müldner, H.H. Günthard, W. Gasche, and W. Leuzinger, *The Structure of Lipids and Proteins Studied by Attenuated Total-Reflection (ATR) Infrared Spectroscopy.* Zeitschrift für Naturforschung B, 1972. 27(7): p. 780-796.

278. Casal, H.L., H.H. Mantsch, F. Paltauf, and H. Hauser, *Infrared and 31P-NMR studies of the effect of Li+ and Ca2+ on phosphatidylserines.* Biochimica et Biophysica Acta (BBA) - Lipids and Lipid Metabolism, 1987. 919(3): p. 275-286.

279. Tsuboi, M., Y. Kyogoku, and T. Shimanouchi, *Infrared absorption spectra of protonated and deprotonated nucleosides.* Biochimica et Biophysica Acta, 1962. 55(1): p. 1-12.

280. Shimanouchi, T., M. Tsuboi, and Y. Kyogoku, *Infrared Spectra of Nucleic Acids and Related Compounds*, in *Advances in Chemical Physics*. 1964. p. 435-498.

281. Lippert, J.L. and W.L. Peticolas, *Raman active vibrations in long-chain fatty acids and phospholipid sonicates.* Biochimica et Biophysica Acta (BBA) - Biomembranes, 1972. 282: p. 8-17.

282. Hübner, W. and H.H. Mantsch, *Orientation of specifically 13C=O labeled phosphatidylcholine multilayers from polarized attenuated total reflection FT-IR spectroscopy.* Biophysical Journal, 1991. 59(6): p. 1261-1272.

283. Volkov, V.V., Y. Takaoka, and R. Righini, *What are the Sites Water Occupies at the Interface of a Phospholipid Membrane?* The Journal of Physical Chemistry B, 2009. 113(13): p. 4119-4124.

284. Mrázková, E., P. Hobza, M. Bohl, D.R. Gauger, and W. Pohle, *Hydration-Induced Changes of Structure and Vibrational Frequencies of Methylphosphocholine Studied as a Model of Biomembrane Lipids.* The Journal of Physical Chemistry B, 2005. 109(31): p. 15126-15134.

285. Costard, R., C. Greve, I.A. Heisler, and T. Elsaesser, *Ultrafast Energy Redistribution in Local Hydration Shells of Phospholipids: A Two-Dimensional Infrared Study.* The Journal of Physical Chemistry Letters, 2012. 3(23): p. 3646-3651.

286. Costard, R., N.E. Levinger, E.T.J. Nibbering, and T. Elsaesser, *Ultrafast Vibrational Dynamics of Water Confined in Phospholipid Reverse Micelles.* The Journal of Physical Chemistry B, 2012. 116(19): p. 5752-5759.

287. Fookson, J.E. and D.F.H. Wallach, *Structural differences among phosphatidylcholine, phosphatidylethanolamine, and mixed phosphatidylcholine/ phosphatidylethanolamine multilayers: An infrared absorption study.* Archives of Biochemistry and Biophysics, 1978. 189(1): p. 195-204.

288. Costard, R., I.A. Heisler, and T. Elsaesser, *Structural Dynamics of Hydrated Phospholipid Surfaces Probed by Ultrafast 2D Spectroscopy of Phosphate Vibrations.* The Journal of Physical Chemistry Letters, 2014. 5(3): p. 506-511.

289. Falk, M., K.A. Hartman, and R.C. Lord, *Hydration of Deoxyribonucleic Acid. II. An Infrared Study.* Journal of the American Chemical Society, 1963. 85(4): p. 387-391.

290. Laage, D., T. Elsaesser, and J.T. Hynes, *Water Dynamics in the Hydration Shells of Biomolecules.* Chemical Reviews, 2017. 117(16): p. 10694-10725.

291. Mortimer, F.S., *Vibrational assignment and rotational isomerism in some simple organic phosphates.* Spectrochimica Acta, 1957. 9(4): p. 270-281.

292. Michael, W.P.P. *The noncontact detection of nerve agent simulants on U.S. military CARC*. in *Proc.SPIE*. 2009.

293. Snyder, R.G. and J.H. Schachtschneider, *Vibrational analysis of the n-paraffins—I: Assignments of infrared bands in the spectra of C3H8 through n-C19H40.* Spectrochimica Acta, 1963. 19(1): p. 85-116.

294. Snyder, R.G., *Vibrational Study of the Chain Conformation of the Liquid n-Paraffins and Molten Polyethylene.* The Journal of Chemical Physics, 1967. 47(4): p. 1316-1360.

295. Cernescu, A., M. Szuwarzyński, U. Kwolek, P. Wydro, M. Kepczynski, S. Zapotoczny, M. Nowakowska, and L. Quaroni, *Label-Free Infrared Spectroscopy and Imaging of Single Phospholipid Bilayers with Nanoscale Resolution.* Analytical Chemistry, 2018. 90(17): p. 10179-10186.

296. Mendelsohn, R., J.W. Brauner, and A. Gericke, *External Infrared Reflection Absorption Spectrometry of Monolayer Films at the Air-Water Interface.* Annual Review of Physical Chemistry, 1995. 46(1): p. 305-334.

297. Meiklejohn, R.A., R.J. Meyer, S.M. Aronovic, H.A. Schuette, and V.W. Meloche, *Characterization of Long-Chain Fatty Acids by Infrared Spectroscopy.* Analytical Chemistry, 1957. 29(3): p. 329-334.

298. Goñi, F.M. and J.L.R. Arrondo, *A study of phospholipid phosphate groups in model membranes by Fourier transform infrared spectroscopy.* Faraday Discussions of the Chemical Society, 1986. 81(0): p. 117-126.

299. Shinoda, K., W. Shinoda, T. Baba, and M. Mikami, *Comparative molecular dynamics study of ether- and ester-linked phospholipid bilayers.* The Journal of Chemical Physics, 2004. 121(19): p. 9648-9654.

300. Yin, J. and Y.-P. Zhao, *Hybrid QM/MM simulation of the hydration phenomena of dipalmitoylphosphatidylcholine headgroup.* Journal of Colloid and Interface Science, 2009. 329(2): p. 410-415.

301. Yellin, N. and I.W. Levin, *Hydrocarbon chain trans-gauche isomerization in phospholipid bilayer gel assemblies.* Biochemistry, 1977. 16(4): p. 642-647.

302. Czamara, K., K. Majzner, M.Z. Pacia, K. Kochan, A. Kaczor, and M. Baranska, *Raman spectroscopy of lipids: a review.* Journal of Raman Spectroscopy, 2015. 46(1): p. 4-20.

303. Pohle, W., C. Selle, H. Fritzsche, and M. Bohl, *Comparative FTIR spectroscopic study upon the hydration of lecithins and cephalins.* Journal of Molecular Structure, 1997. 408-409: p. 273-277.

304. Sun, S., A.M. Sendecki, S. Pullanchery, D. Huang, T. Yang, and P.S. Cremer, *Multistep Interactions between Ibuprofen and Lipid Membranes.* Langmuir, 2018. 34(36): p. 10782-10792.

305. Saha, A., S. SenGupta, A. Kumar, and P.D. Naik, *Interaction of Sodium Dodecyl Sulfate with Lipid Monolayer Studied by Sum-Frequency Generation Spectroscopy at Air–Water Interface.* The Journal of Physical Chemistry C, 2017. 121(24): p. 13175-13182.

306. Yan, E.C.Y., Z. Wang, and L. Fu, *Proteins at Interfaces Probed by Chiral Vibrational Sum Frequency Generation Spectroscopy.* The Journal of Physical Chemistry B, 2015. 119(7): p. 2769-2785.

307. Nguyen, K.T., R. Soong, S.-C. lm, L. Waskell, A. Ramamoorthy, and Z. Chen, *Probing the Spontaneous Membrane Insertion of a Tail-Anchored Membrane Protein by Sum Frequency Generation Spectroscopy.* Journal of the American Chemical Society, 2010. 132(43): p. 15112-15115.

308. Meister, K., S.J. Roeters, A. Paananen, S. Woutersen, J. Versluis, G.R. Szilvay, and H.J. Bakker, *Observation of pH-Induced Protein Reorientation at the Water Surface.* The Journal of Physical Chemistry Letters, 2017. 8(8): p. 1772-1776.

309. Hosseinpour, S., S.J. Roeters, M. Bonn, W. Peukert, S. Woutersen, and T. Weidner, *Structure and Dynamics of Interfacial Peptides and Proteins from Vibrational Sum-Frequency Generation Spectroscopy.* Chemical Reviews, 2020. 120(7): p. 3420-3465.

310. Goussous, S.A., M.T.L. Casford, A.C. Murphy, G.P.C. Salmond, F.J. Leeper, and P.B. Davies, *Structure of the Fundamental Lipopeptide Surfactin at the Air/Water Interface Investigated by Sum Frequency Generation Spectroscopy.* The Journal of Physical Chemistry B, 2017. 121(19): p. 5072-5077.

311. Ding, B., A. Panahi, J.-J. Ho, J.E. Laaser, C.L. Brooks, M.T. Zanni, and Z. Chen, *Probing Site-Specific Structural Information of Peptides at Model Membrane Interface In Situ.* Journal of the American Chemical Society, 2015. 137(32): p. 10190-10198.

312. Roeters, S.J., C.N. van Dijk, A. Torres-Knoop, E.H.G. Backus, R.K. Campen, M. Bonn, and S. Woutersen, *Determining In Situ Protein Conformation and Orientation from the Amide-I Sum-Frequency Generation Spectrum: Theory and Experiment.* The Journal of Physical Chemistry A, 2013. 117(29): p. 6311-6322.

List of figures

List of tables

List of abbreviations

AFM	atomic force microscopy
ATR-FTIR	attenuated total internal reflection infrared
BB-VSFG	broadband sum-frequency generation spectroscopy
BLM	black lipid membrane
CaF_2	calcium fluoride
CARS	coherent-anti-stokes Raman spectroscopy
CCD	charge-coupled device
DOPC	1,2-dioleoyl-sn-glycero-3-phosphocholine
DPPC	1,2-dipalmitoyl-sn-glycero-3-phosphocholine
DPPC-d62	1,2-dipalmitoyl-d62-sn-glycero-3-phosphocholine
Egg-PC	1,2-Dialkyl-sn-glycero-3-phosphocholine
f	focal length
FWHM	full width at half maximum
G	gas phase
G-LE	gas-liquid expanded phase
HRR-BB-VSFG	high repetition-rate broadband sum-frequency generation spectroscopy
iCCD	intensified charge-coupled device
iEMCCD	intensified electron-multiplying charge-coupled device
IR	infrared
kHz	kilo Hertz
LB	Langmuir-Blodgett
LC	liquid-crystalline
LE	liquid-expanded
LE-LC	liquid expanded-liquid crystalline
LS	Langmuir-Schaeffer
LSPR	localized surface plasmon resonance
µm	micrometer
min	minutes
MIR	mid-infrared
NRB	non-resonant background
PA	phosphatidic acid
PBS	phosphate-buffered saline

PC	phosphatidylcholines
PE	phosphoethanolamine
PG	phosphoglycerol
PI	phosphoinositol
PS	phosphoserine
ps	picosecond
QCM	quartz crystal microbalance
RMS	root-mean-square
s	seconds
SERS	surface-enhanced Raman spectroscopy
SFG	sum-frequency generation
SHG	second-harmonic generation
SLB	supported lipid bilayer
SNR	Signal to noise ratio
SPR	surface plasmon resonance
SUV	small unilamellar vesicles
UV-VIS	ultraviolet-visible
VIS	visible
VSFG	vibrational sum frequency generation spectroscopy
XRD	x-ray diffraction
π-A	surface pressure-area
2D	2-dimensional

List of publications

Journal articles discussed in this thesis

1. **F. Yesudas**, M. Mero, J. Kneipp, Z. Heiner. High-resolution and high-repetition-rate vibrational sum-frequency generation spectroscopy of one- and two-component phosphatidylcholine monolayers. *Analytical and Bioanalytical Chemistry.* **2019**, 411, 4861.

2. **F. Yesudas**, M. Mero, J. Kneipp, Z. Heiner. Vibrational sum-frequency generation spectroscopy of lipid bilayers at repetition rates up to 100 kHz. *The Journal of Chemical*

Declaration

I declare that I have completed the thesis independently using only the aids and tools specified. I have not applied for a doctor's degree in the doctoral subject elsewhere and do not hold a corresponding doctor's degree. I have taken due note of the Faculty of Mathematics and Natural Sciences PhD Regulations, published in the Official Gazette of Humboldt-Universitaet zu Berlin no. 42/2018 on 11/07/2018.